Method for in vitro Cell Irradiation with Low Energy Protons

–

On the Relative Biological Effectiveness of protons for human glioblastoma cells

Anne Marit Rykkelid

Thesis for the Degree of

Master of Science

Department of Physics

Faculty of Mathematics and Natural Sciences

University of Oslo

November 2017

Acknowledgements

The work presented in this thesis was carried out at the Department of Physics, University of Oslo as a cooperation between the Biophysics and Medical Physics Group, and the Nuclear and Energy Physics Group. I would like to thank the groups for the good cooperation, and the engineers at Oslo Cyclotron Laboratory for the help setting up the cyclotron.

First of I would like to express my gratitude to my supervisors Eirik Malinen, Nina F. Edin, Erik O. Pettersen and Sunniva Siem for their guidance, help and support throughout my thesis. Special thanks goes to Nina F. Edin, who has cooperated with me on all the experiments performed at OCL, and been patient and inspiring in her tutoring throughout the project.

I would also like to thank:

Joe A. Sandvik for his instructions in Laboratory techniques and technical assistance.

Efim Brondz for equipment designs and technical assistance.

Tordis Dahle and Kristian Ytre-Hauge for their cooperation and for providing Monte Carlo simulations.

Agnes Baker for practical assistance and good company during experiments.

I am very grateful for my time at the Biophysics and Medical Physics group, for the collective support, the discussions over lunch, and the positive atmosphere.

Blindern, 2017

Anne Marit Rykkelid

Abstract

Proton therapy has become more and more established in the last decade due to its beneficial energy deposition, and a proton therapy unit will be built in Norway within the next years. With a peak in energy deposition towards the end of the proton track (the Bragg-Peak) followed by a steep fall to zero dose when the protons come to a halt, proton irradiation is of great advantage for spearing the healthy tissue, in particular when treating tumour close to organs at risk (OAR). The common way of planning radiotherapy is to place the end of the radiation field at the edge of the tumour, but for proton irradiation this will lead to a risk for a small positional displacement of the patient causing the end of the proton track to reach organs at risk. Today, the applied value of Relative Biological Effectiveness (RBE) in proton therapy planning is an average value of 1.1 (with x-rays or ^{60}Co as a reference) for practical use. It is commonly accepted that this may not be a good estimate, particularly at the end of the treatment fields where the largest increase in Linear Energy Transfer (LET) occurs. It is therefore important to investigate the biological effect of high LET protons in order to avoid underestimation of the posed risk. One can imagine mapping the effects of LET for different proton energies and cell types to act as an extra degree of freedom in radiotherapy in the future to achieve larger tumour control probability.

Presented in this thesis is a setup developed in order to irradiate human cells *in vitro* with 16 MeV protons at Oslo Cyclotron Laboratory (OCL). The main goal of the project was to produce cell survival curves for both low and high LET values by irradiation at different positions in the depth-dose Bragg-Peak (BP), and consequently find the corresponding RBE for the T98G human glioblastoma cell line.

The setup developed for dosimetry and cell irradiation included a scattering filter for proton beam homogeneity, a Monitor Chamber (MC) for relative dose measurements, an Ionization Chamber (IC) for absolute dose measurements, and a heated container in order to keep the cells at a stable temperature during irradiation. Gafchromic EBT3 dosimetry films were irradiated and used as a measure of proton beam homogeneity. The MC was in the beam line during cell survival experiments after being calibrated to absolute dose using the IC in the initial dosimetry measurements. The calibration was performed separately for the different depths of cell irradiations.

Several cell survival experiments were conducted with average LET values of 7.5 keV/µm in front of the Bragg-Peak, and 41 keV/µm in the distal edge. For the high LET values, the survival curves appeared to have a strange shape with a curvature opposite of the expected as the dose increased, ending in a "tail" that converged towards a constant fraction. The scattering of the protons caused small variations in proton range. At the end of their track, this resulted in a dose-distribution highly sensitive to small absorber depth variations, compared to the distribution in front of the BP. The measured dose-distribution by the Gafchromic EBT3 dosimetry films were used to correct the dose measurements from the IC for inhomogeneous dose distribution. However, this was not sufficient to explain our measured surviving fractions for the high doses.

Just before the deadline of this thesis, additional experiments were conducted, which suggested that the dose distribution problem could, at least in part, originate from inhomogeneity in the structure of the Parafilm. The initial proton energy was limited to 16 MeV, and as the lids of the cell dishes were of a thickness that would make irradiations in front of the Bragg-Peak impossible, it was replaced with a thin layer of Parafilm during irradiation. Parafilm also functioned as a depth component to position the cell in the distal edge of the Bragg-Peak. However, the latest data showed that the elasticity of the Parafilm resulted in an inhomogeneous structure a bit like an accordion, leaving stripes receiving lower doses. For the cell irradiations conducted at the distal edge of the BP, only a very small additional thickness in the Parafilm may have resulted in some cells being positioned behind the BP and left them completely shielded. Another explanation of the "tail" with damage saturation as an effect of the high LET values was discussed, but what stood out as the most probable cause was the variation in Parafilm thickness that caused shielded areas were the protons could not reach.

Using the assumption that some cells were shielded from radiation, a correction was made to eliminate the un-irradiated cells from the curve fitting. The RBE values found at a 0.1 survival level were 5.8 for cells irradiated in the distal edge of the BP (high LET), and 2.3 in front of the BP (low LET). All RBE values were calculated compared to 220 keV x-rays. These values suggest that the conventionally used RBE value of 1.1 for proton therapy dose planning is too low. The use of more correct and LET-dependent RBE-values may be used to optimize the dose planning leading to better tumour control and less irradiation of normal tissue.

Sammendrag

Protonterapi er blitt mer og mer etablert det siste tiåret på grunn av sin fordelaktige energiavsetning, og i løpet av de neste årene vil det også komme et senter for protonterapi i Norge. Det aller meste av energien til protonene avsettes rett før de stanser, hvilket fører til en lav doseavsetning inntil en dramatisk øking etterfulgt av et skarpt fall i dose i det protonene stopper helt opp (Bragg-Peaken). Denne karakteristikken er en stor fordel når man ønsker å beskytte normalvev, spesielt ved behandling av en tumor som ligger tett inntil risikoorganer. Den vanligste måten å planlegge strålebehandling på er ved å legge slutten på strålefeltet i ytterkant av tumor, men ved bruk av protoner vil små posisjonelle endringer kunne føre til at slutten av strålefeltet med den høye doseavsetningen treffer risikoorganer. I dag brukes en gjennomsnittlig RBE på 1.1 i planlegging av behandling med protoner (med røntgen eller ^{60}Co som referanse), men det er allment godtatt at dette ikke nødvendigvis er et godt estimat i alle tilfeller, spesielt i slutten på strålefeltet hvor den største økningen av LET (Linear Energy Transfer) skjer. Det er derfor viktig å undersøke sammenhengen mellom den relative biologiske effekten (RBE) og høy-LET protoner, for å være sikker på at man ikke undervurderer risikoen ved at slutten av strålefeltet treffer normalvev eller risikoorganer. Ved å kartlegge den biologiske effekten av økninger i LET for forskjellige protonenergier og celletyper, kan dette potensielt brukes til optimalisering av behandlingsplaner.

I denne oppgaven blir det presentert et oppsett utviklet for å bestråle humanceller *in vitro* med 16 MeV protoner ved Syklotronlaboratoriet, Universitetet i Oslo. Prosjektets hovedmål var å bestråle celler med både høy og lav LET ved å endre posisjoneringen i forhold til dybde-dose Bragg-toppen og kartlegge resulterende overlevelseskurver for T98G human glioblastom cellelinjen.

Oppsettet inkluderte et spredningsfilter for homogenitet i strålefeltet, et transmisjonskammer for relativ dose måling, et ionisasjonskammer for absolutt dose måling og en oppvarmet beholder for stabil celletemperatur under bestråling. I tillegg ble Gafchromic EBT3 dosimetrifilmer bestrålt og brukt som et mål på felthomogenitet. Under eksperimentene for celleoverlevelse ble transmisjonskammeret brukt for å overvåke den akkumulerte protonfluksen, kalibrert til absolutt dose ved hjelp av ionisasjonskammeret fra initiale dosimetrimålinger. Kalibreringen ble utført separat for de ulike bestrålingsdypene i Bragg-toppen.

Det ble utført flere eksperimenter for celleoverlevelse, med gjennomsnittlige LET-verdier på 7.5 keV/µm foran Bragg-toppen og 41 keV/µm i bakkant. For de høye LET-verdiene fikk overlevelseskurvene en motsatt krumming enn det som var forventet etter hvert som dosen økte, før den endte i en «hale» som konvergerte mot en konstant fraksjon. Spredningen i protonene forårsaket små variasjoner i rekkevidden til protonene. Dette førte til at homogeniteten i enden av Bragg-toppen ble svært følsom for små dybdevariasjoner sammenliknet med foran Bragg-toppen. Dosedistribusjonen målt av Gafchromic EBT3 i bakkant av Bragg-toppen ble brukt for å korrigere dosen målt av ionisasjonskammeret, men dette var ikke nok til å forklare den rare formen på overlevelseskurvene.

Få dager før innlevering av masteroppgaven ble det uført nye eksperimenter, som antydet at den observerte inhomogeniteten i dose oppsto på grunn av strukturen i Parafilm. Under cellebestråling ble lokket på petriskålene erstattet med tynn Parafilm, fordi den lave energien på 16 MeV ville gjøre bestråling foran Bragg-toppen umulig ved bruk av lokket. Parafilmen ble også brukt som absorbator for posisjonering i Bragg-toppen. Resultatene antydet at den elastiske strukturen til Parafilmen forårsaket en inhomogen dosefordeling, litt som et trekkspill, slik at noen stripete områder fikk lavere doser. Ved bestrålinger i bakkant av Bragg-toppen kan svært små tillegg i tykkelse ha hindret protonene i å rekke frem, og ført til at noen celler ble skjermet fra strålingen. Dette kan forklare at celleoverlevelsen vi observerer går mot en konstant fraksjon. Muligheten for at høye LET verdier førte til en metning i inaktivering av celler ble også diskutert, men at variasjonene i Parafilm tykkelse førte til områder hvor cellene ble skjermet fra stråling, fremstod som den mest sannsynlige forklaringen.

Basert på denne antagelsen ble det gjort korreksjoner på overlevelsesdataene for å eliminere effekten av dose-distribusjon og ubestrålte områder fra kurvetilpasningene. Ved et overlevelsesnivå på 0.1 ble RBE verdier på 2.3 funnet i forkant av Bragg-toppen (lav LET), og hele 5.8 ble funnet i bakkant (høy LET). Alle RBE verdier ble funnet med 220 keV røntgen stråling som referanse. Disse verdiene antyder at den gjennomsnittlige RBE verdien på 1.1 brukt i protonterapi doseplanlegging er for lav. Ved å innføre mere korrekte og LET-avhengige RBE-verdier vil man kunne optimere doseplanene og oppnå bedre tumorkontroll og mindre bestråling av normalvevet.

Abbrevations

Abbreviation	Explanation
OAR	Organs at Risk
LET	Linear Energy Transfer
HCP	Heavy Charged Particles
RBE	Relative Biological Effectiveness
Linac	Linear Accelerator
OD	Optical Density
LSF	Least Squares Fitting
C60	Radioactive isotope of Cobalt. Cobalt 60.
CP	Charged Particle
PE	Photoelectric Effect
PP	Pair Production
LQ-model	Linear Quadratic Model
SSB	Single Strand Break
DSB	Double Strand Break
UV	Ultraviolet (radiation)
BER	Base Excision Repair
NER	Nucleotide Excision Repair
HRR	Homologous Recombination Repair
NHEJ	Nonhomologous End-Joining
LDR	Low Dose-Rate
HDR	High Dose-Rate
IC	Ionization Chamber
MC	Monitor Chamber
UiO	University of Oslo
NRH	The Norwegian Radium Hospital
BP	Depth-dose Bragg Peak
G1	Group 1: results from cell survival experiments in front of the Bragg-Peak
G2	Group 2: results from cell survival experiments in distal edge of the Bragg-Peak
SF	Surviving Fraction

Table of Contents

1 Introduction

Radiotherapy is widely used in cancer treatment, both with curative or palliative intent. As ionizing radiation deposit its energy continuously from entering the skin to reaching the tumour, the radiation given in treatment will not be able to cover just the tumour, there will always be dose deposited in surrounding healthy tissue as well. In cases where the tumour is located close to organs at risk (OAR), the dose to the normal tissue can cause severe side-effects.

Normally the type of radiation used in radiotherapy is high energy x-rays, produced by accelerated electrons hitting a target in a linear accelerator. The energy deposition of these x-rays causes ionizations along the entire track throughout the body, with maximum dose given near the surface. For accelerated protons however, the range is well defined, and they deposit most of their energy at the end of the track, known as the Bragg-peak. In radiotherapy this characteristic can be of a great advantage as it is possible to select an energy span to target the tumour with high doses, and at the same time reduce the amount of dose to the normal tissue compared to standard radiotherapy.

Different types of radiation have different Linear Energy Transfer (LET) characteristics that describe the density of energy deposition along the track of the radiation particle. A higher LET means a denser deposition that may cause damages that are more difficult to repair. For x-rays, and γ-rays the LET is approximately constant along the track, while for heavy charged particles (HCP) the LET is high to begin with, as well as increasing as the particle reaches the end of its track. The effect of high LET radiation on biological tissue is of great interest when it comes to radiotherapy. The variation in the effect of cell inactivation along a charged particle track may influence how the treatment should be planned, and the treatment beams positioned. The effectiveness is commonly measured by the Relative Biological Effect (RBE) which is ratio of the doses resulting in a certain effect comparing the investigated type of radiation and a standard radiation reference such as x-rays.

The commonly used RBE value in radiation treatment with protons is a constant value of 1.1. There is discussion whether this a generalization that may cause non-optimal treatment plans with over-treatment in areas of the normal tissue and organs at risk. Especially at the

boarders between the treatment volume and the normal tissue, where radiation particles reach the end of their tracks from overlapping fields, the dose is in danger of being underestimated. This can have significant consequences for radiation caused side-effects (Sorensen et al., 2017), which are important aspects in reviewing a treatment plan. By knowing more about the effects high LET radiation and its connection to RBE, one may also imagine the possibility of aiming the high LET areas of the treatment beams at the most resistant cells in the tumour, to optimize the treatment.

Different experiments have given various results as to how RBE depends on radiation type and quality. While there seem to be a consensus that the RBE is higher than 1.1 at the end of a proton track, results have varied to such an extent that this constant value is still applied (Paganetti, 2014). The variations in results may be caused by uncertainties in dosimetry, radiation quality or positioning of irradiated cells. It is also an issue of biological material, and differences between in vivo and in vitro effects. Developing a precise way to do in vitro cell survival irradiation experiments is therefore important to be able to know more about the effects occurring in the Bragg peak. Especially at the end of the track, when the LET is increasing the most, it is important to know more about the impact on the RBE.

The most available HCP is protons, which is the lightest HCP used in radiotherapy. Using low initial energy, one can still achieve high LET values. Low-energy protons also deliver a clean energy spectrum and thereby one can avoid some of the distribution effects that occur during overlapping fields of high energy protons. To understand the effects of the LET, it is important to investigate the clean spectrum as well as the more broad and clinical spectrum. The aim of this thesis was to develop a precise method for irradiating cells with protons at points in front of and in the distal edge of the Bragg-Peak in order to study if the difference in LET has any effect on the cell survival and RBE for the T98G human glioblastoma cell line.

2 Theory

2.1 Radiation Physics in Radiotherapy

2.1.1 Ionizing Radiation and Radioactive decay

In radiotherapy several kinds of external radiation can be applied. Most commonly used are high energy x-rays, but electrons, protons and heavier ions such as α-particles and carbon ions are also in clinical use.

X-rays and γ-rays are both electromagnetic radiation, and at the same quantum energy they have identical properties. The only difference is in their mode of origin. γ-rays are emitted from radioactive nuclei, or from annihilation processes between matter and antimatter. X-rays, however, are emitted by charged particles in two ways: By particles changing atomic electron energy levels by de-excitation, or by particles interacting with and being deaccelerated in a Coulomb force field.

The quantum energy of electromagnetic radiation follows in equation 1.

$$E_\gamma = \frac{hc}{\lambda} \tag{1}$$

Fast electrons, or positrons if positively charged, can be a result of several processes. They can be a product of radioactive β-decay, then called β-rays, or a result of charged particle collisions, then known as δ-rays. Van der Graaf generators are able to deliver continuous high intensity electron beams with energies up to 12 MeV, while pulsed beams at much larger energies can be produced by linear accelerators, betatrons and microtrons.

Heavy charged particles (HCP) can be obtained by modification of available particles, such as stripping of electrons, or as fission fragments from nuclear processes, either naturally or artificially produced (Lyman et al., 1986). When the particle of interest is directly accelerated it is called a primary beam. A secondary beam is when accelerated particles have nuclear interactions with a target material, producing the desired particle beam.

Acceleration is normally done by a cyclotron, but a specially designed linear accelerator for HCP or a Van der Graaf generator are also possible accelerators.

The different types of radiation has different qualities and different ways of depositing energy, as will be discussed below, resulting in the depth-dose curves shown in Figure 1. It can be seen from the plot that electrons deposit their energy very close to the surface of the traversing medium and x-rays deposit most of their energy close to the surface, but has a long "tail" inwards in the medium. Where most of the energy is deposited is referred to as the build-up region. If the energy of the x-rays is increased, the build-up region moves to increasing depths. At the same time the percentage dose deposition after the build-up region will be higher. For protons, and other HCPs, the shape of the depth-dose curve stands out, as most of the energy is deposited at the end of their track. This characteristic peak is commonly known as the *Bragg-peak* (Attix, 1986).

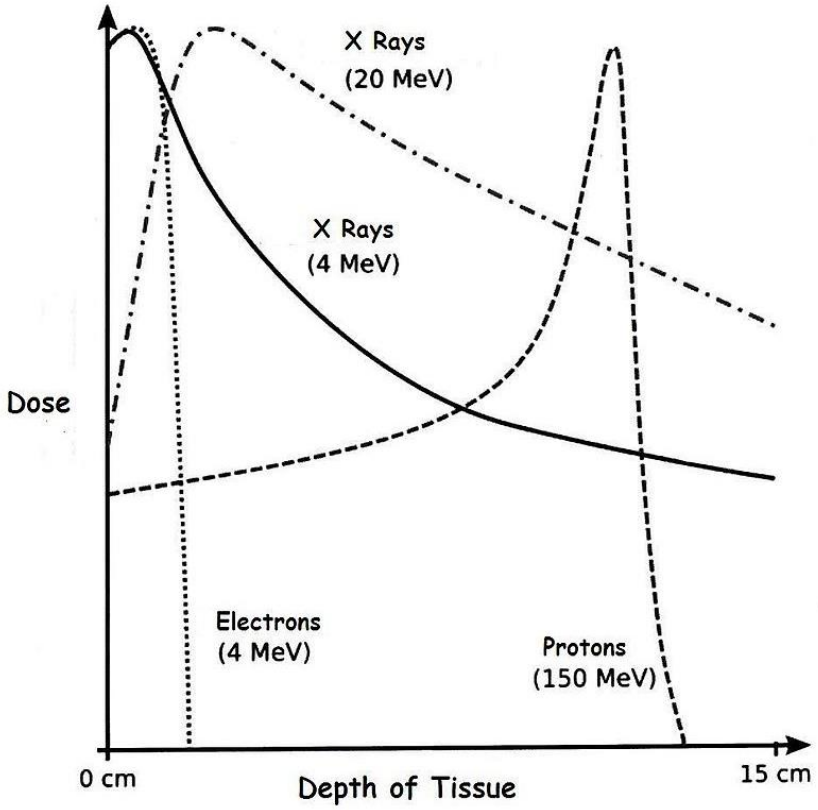

FIGURE 1. DEPTH DOSE CURVES FOR DIFFERENT TYPES OF IONIZING RADIATION (PAUL, 2009). 4 MEV ELECTRONS, 4 MEV X-RAYS, 20 MEV X-RAYS AND 150 MEV PROTONS.

Interaction of Ionizing Radiation with Matter

When working with different types of irradiation it is important to operate with a common quantity, a measure of how much irradiation is received by the matter in question. This quantity is the *dose (D)*, and reflects how much energy is absorbed per mass unit exposed to ionizing irradiation. The following chapter is based upon chapter 2, 7 and 8 in "Introduction to Radiological Physics and Radiation Dosimetry" (Attix, 1986).

Energy imparted as shown in equation 2 is a theoretical description of the energy deposited by ionizing radiation inside a finite volume *V* of mass *m*. The absorbed dose is then defined as the energy imparted at point *P* per unit mass inside the volume *V* as seen in equation 3.

$$\epsilon = (R_{in})_u - (R_{out})_u + (R_{in})_c - (R_{out})_c + \sum Q \tag{2}$$

Where $(R_{in})_u =$ radiant energy of uncharged particles entering V,

$(R_{out})_u =$ radiant energy of uncharged particles escaping V,

$(R_{in})_c =$ radiant energy of charged particles entering V,

$(R_{out})_c =$ radiant energy of charged particles escaping V,

$\sum Q$ = net energy derived from rest mass in V.

$$D = \frac{d\epsilon}{dm} \tag{3}$$

Where ϵ is the energy imparted, and *dm* is the infinitesimal mass at point *P* in *V*.

There are different types of ionizing radiation and differences in the energy deposition in different materials that needs to be taken this into account when calculating the absorbed dose. The two main types of radiation are directly and indirectly ionizing radiation. Directly ionizing radiation is charged particles such as electrons, protons and ions, while indirectly ionizing radiation is particles without charge, such as photons and neutrons.

Photons

To be able to find an expression for the absorbed dose in a medium, we must look at the ways photons interact with it. Ionizing radiation transfer its energy by interacting with

charged particles in the medium. For photons, the most commonly used indirectly ionizing radiation in radiotherapy, there are several different ways energy can be transferred to charged particles. The four ways this can happen is by photoelectric effect (PE), Compton scattering, Pair Production (PP), and photonuclear interactions. From a dosimetric point of view, Rayleigh scattering can be ignored as the event is close to elastic and the only energy transferred is the recoil of the particle it scatters off. Photonuclear interactions need to be addressed in x-ray production for shielding purposes, but the contribution to dose is negligible. By focusing on the three processes that result in an energy transfer to electrons, it is possible to deduct coefficients for attenuation, energy transfer and energy absorption.

The mass energy-transfer coefficient describes how much energy equivalent mass is transferred to the absorbing medium, and a total coefficient can be found as a sum of the coefficients of the three processes as shown in equation 4.

$$\frac{\mu_{tr}}{\rho} = \frac{\tau_{tr}}{\rho} + \frac{\sigma_{tr}}{\rho} + \frac{\kappa_{tr}}{\rho} \quad (cm^2/g) \tag{4}$$

Where $\frac{\mu_{tr}}{\rho}$ is the total energy-transferred coefficient, and $\frac{\tau_{tr}}{\rho}$, $\frac{\sigma_{tr}}{\rho}$ and $\frac{\kappa_{tr}}{\rho}$ is the energy-transferred coefficients for PE, Compton and PP interactions.

When removing the average energy lost to radiative interactions by secondary electrons, the quantity reduces to the mass energy-absorption coefficient as given in equation 5. This is achieved by multiplying with the factor $(1 - g)$ where g represent this average energy fraction.

$$\frac{\mu_{en}}{\rho} = \frac{\mu_{tr}}{\rho}(1 - g) \quad (cm^2/g) \tag{5}$$

These mass energy coefficients and the *g* fractions are tabulated for different photon energies and absorbing materials. As our goal is to find an expression for the absorbed dose by photons, we need to take one more step. To find the dose deposited at a point *P* from a monoenergetic photon beam, it is necessary to know the number of photons passing through the point, and the energy of the photons. The flux, φ, is defined as the number of particles passing through the area *A*. By multiplying by the energy *E,* we get the energy

fluence Ψ. By multiplying the energy fluence with the mass energy-transfer coefficient we arrive at an expression resulting in the absorbed dose as shown in equation 6.

$$D = \left(\frac{\mu_{en}}{\rho}\right)\Psi \quad (MeV/g) = 1.602 \cdot 10^{-10}\left(\frac{\mu_{en}}{\rho}\right)\Psi \quad (Gy) \tag{6}$$

Often the quantity Kerma is useful in dosimetry as a quantity closely knit to the absorbed dose. It is defined as the total energy transferred to the absorbing material, *including* the radiative loss as seen in equation 7. It then follows that the part of the Kerma causing ionization, noted K_c, is equal to the absorbed dose as shown in equation 8.

$$K = \left(\frac{\mu_{tr}}{\rho}\right)\Psi = D + \frac{\mu_{tr}}{\rho}g = D + K_r \tag{7}$$

$$K = K_c + K_r \implies D = K_c \tag{8}$$

Charged Particles

Moving to charged particles, we need to take a look at how the incoming charged particles can interact with the particles in the absorbing material. The incoming particles can interact in four ways; soft collisions, hard collisions, interaction with the nuclear field and inelastic interaction with the nucleus. The latter is only relevant for heavy charged particles (HCP) with high energies. For electrons, only 2-3% of the interactions are inelastic, and the rest is elastic scattering where the energy transfer is so small it is not enough to emit an x-ray or for excitation of the nucleus. It is just enough for conservation of momentum in the collision. For HCPs the kinetic energy needs to be about 100MeV or higher and the impact parameter needs to be less than the nuclear radius (high Z material) for inelastic interactions with the nucleus to occur. In the present study, we operate with energies well below this, so it is not necessary to include this interaction for HCPs.

The impact parameter b is the smallest distance from the centre of the nucleus, to the trajectory of the incoming particle, as shown in Figure 2.

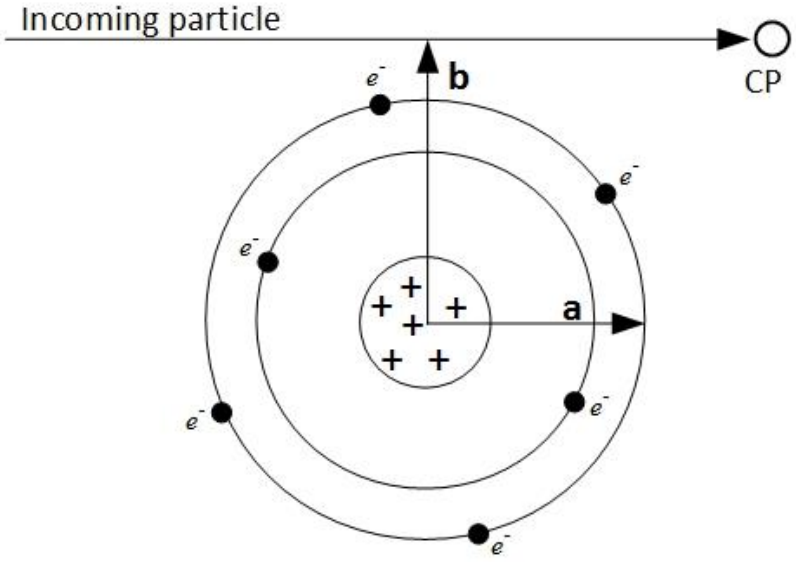

FIGURE 2. ILLUSTRATION OF THE IMPACT PARAMETER, b. THE SHORTEST DISTANCE BETWEEN THE TRAJECTORY OF AN INCOMING CP TO CENTRE OF NUCLEUS IN TRAVERSED MATERIAL IS CALLED THE IMPACT PARAMETER. THE ATOMIC RADIUS IS DENOTED AS a.

When incoming CPs pass close to a nucleus, or $b \ll a$, the incoming particle will experience a Coulomb force interaction with the atomic nucleus. As mentioned previously only 2-3% of these interactions are inelastic and contributes to the energy loss in the case of electrons. In this case the electrons will be defected and significantly slowed down, releasing x-rays known as bremsstrahlung. For HCPs this case can be neglected.

Collisions are the interactions causing most of the energy deposition. Soft collisions occur when the incoming particles pass the atoms at a considerable distance, in other words, $b \gg a$. When the particle passes the atom, the Coulomb field of the incoming particle will interact with the atom causing the atom to be excited to a higher energy level, and sometimes making the atom eject a valence electron. These collisions will only cause small amounts of energy to be transferred, but they are at the same time the most probable and therefore the most numerous interaction.

Hard collision happens when the incoming particle “hits” the atom, or $b \sim a$. When this happens, the interaction with one single electron becomes more likely, and the electron will be ejected from the atom with a large kinetic energy. These electrons are often called δ-

rays. Even though these interactions are less probable, the amount of energy deposited in matter from hard collisions will be much greater. It is therefore considered that the energy deposited from hard and soft collisions is approximately the same.

When we want to know something about the dose deposited by CPs, the most important quantity is the *mass collision stopping power (SP)*. The *SP* is the expectation value of energy loss per unit pathlength *x* by an incoming charged particle. It is dependent on kinetic energy *T*, the particle type, *Y*, and the atomic number *Z* of the absorbing material. As mentioned, the collisions are the main interactions causing energy loss of the incoming particles, and the *SP* is therefore split into two parts, energy loss by hard and soft collisions. This can be seen in equation 9.

$$\left(\frac{dT}{\rho dx}\right)_c = \left(\frac{dT_s}{\rho dx}\right)_c + \left(\frac{dT_h}{\rho dx}\right)_c \quad (MeV/cm) \tag{9}$$

By making a series of assumptions, adding the two terms and making a few corrections, it can be shown that the *mass collision stopping power* for HCP follows equation 10.

$$\left(\frac{dT}{\rho dx}\right)_c = 0.3071\ \frac{Zz^2}{A\beta^2}\left[13.8373 + \ln\left(\frac{\beta^2}{1-\beta^2}\right) - \beta^2 - \ln I - \frac{C}{Z}\right] \tag{10}$$

Where *Z* and *A* is the atomic number and mass number of the stopping medium, I is the mean excitation potential of the stopping material, C/Z is the shell correction for the material, *z* is the charge of the traversing particle, $\beta = v/c$ and is related to the kinetic energy of the incoming particle.

For HCP we can approximate the total stopping power with the mass collision stopping power, shown in equation 11, as the mass radiative stopping power gives no significant energy loss. For electrons and positrons, however, this needs to be included as shown in equation 12. The mass collision stopping power for electrons will look slightly different as well. The hard-collision term is based on the Møller cross section and the Bhabha cross section for electrons and positrons, and the polarization effect needs to be taken into account. I will not go into further details on this.

$$HCP\text{:}\ \left(\frac{dT}{\rho dx}\right) \approx \left(\frac{dT}{\rho dx}\right)_c \tag{11}$$

$$e^- \; and \; e^+ : \left(\frac{dT}{\rho dx}\right) = \left(\frac{dT}{\rho dx}\right)_c + \left(\frac{dT}{\rho dx}\right)_r \tag{12}$$

Often your stopping medium will be a mixture of different elements, and then it can be useful to remember Bragg's Rule. By the assumptions made in Bragg's Rule, it can be shown that the total stopping power for the medium can be approximated with a sum of the stopping powers in the different elements or chemical compounds. With weight fractions, fz_1, fz_2 …, of elements z_1, z_2 …, the stopping power can be written as in equation 13.

$$\left(\frac{dT}{\rho dx}\right)_{mix} = fz_1 \left(\frac{dT}{\rho dx}\right)_{z_1} + fz_2 \left(\frac{dT}{\rho dx}\right)_{z_2} + \cdots \tag{13}$$

Finally, we can connect the stopping power to the dose. This can be done by the simple expression:

$$D = \varphi \times \left(\frac{dT}{\rho dx}\right) \tag{14}$$

Where φ is the fluence, as described previously.

Closely related to the mass collision stopping power is the *restricted stopping power* and the *linear energy transfer*, which are important quantities in radiotherapy. When calculating the dose in a small object, the dose can be overestimated as some δ-rays from hard collisions may have high enough energies to escape the object. The restricted stopping power is useful in this case and includes the soft collisions and the part of the hard collisions resulting in δ-rays with lower energies than a limit Δ. This quantity has the same units as the stopping power and is denoted as $\left(\frac{dT}{\rho dx}\right)_\Delta$. The *linear energy transfer* (LET) differs from the restricted stopping power only by a constant and a factor of stopping medium density. It usually is denoted as L_Δ and has the units $keV/\mu m$. The relation between restricted stopping power and LET is shown in equation 15.

$$L_\Delta = \frac{\rho}{10}\left(\frac{dT}{\rho dx}\right)_\Delta \tag{15}$$

2.1.2 Ionizing Radiation Devices

X-ray tube

In an x-ray tube the production of x-rays are done by accelerating electrons and having them hit a metallic target, an anode. A high potential difference is applied between the anode (target) and the cathode in order to accelerate the electrons. The electrons are released at the cathode, creating a beam of electrons towards the anode. When the electrons hit the anode, which is a high Z material, the electrons are deaccelerated by interacting with the nucleus and release radiation called Bremsstrahlung. This process is illustrated Figure 3. In addition to Bremsstrahlung production, excitations and ionizations occur. Most of the electron energy will be deposited by these interactions, which will produce a great deal of heat. Cooling of the anode is therefore needed (Attix, 1986). A schematic drawing of an x-ray tube is given in Figure 4.

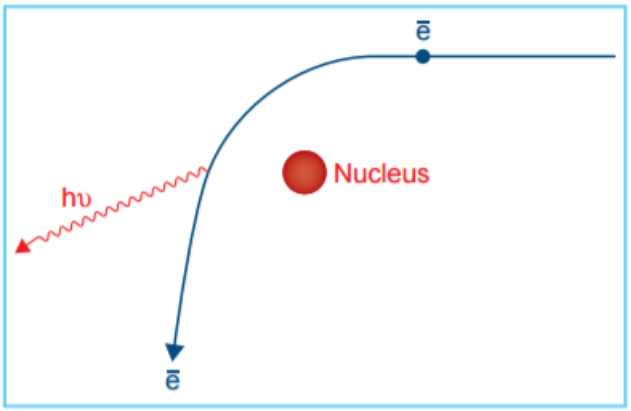

FIGURE 3. ILLUSTRATION OF THE BREMSSTRAHLUNG PROCESS. AN INCOMING ELECTRON IS DEACCELERATED BY INTERACTION WITH THE NUCLEUS, AND RELEASES ENERGY AS A PHOTON. (KHAN ET AL., 2014, FIGURE 3.8)

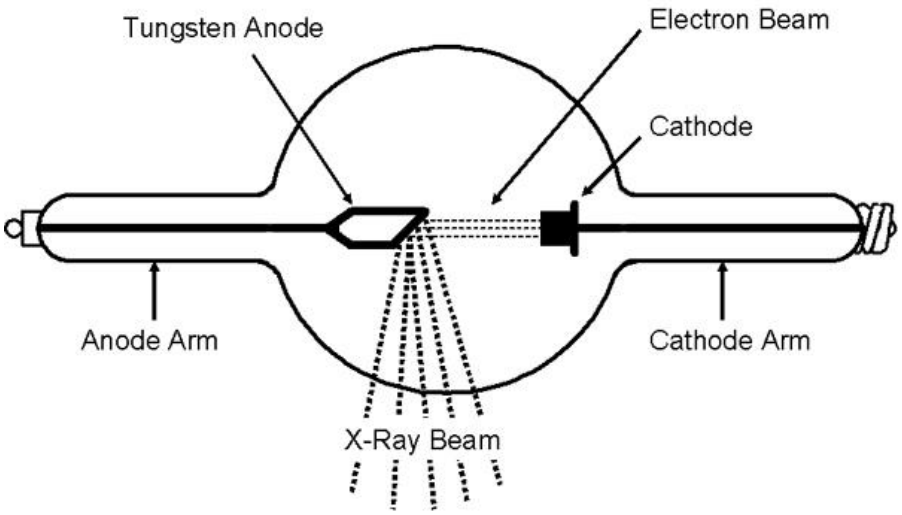

FIGURE 4. ILLUSTRATION OF A COOLIDGE X-RAY TUBE. ELECTRONS ARE RELEASED FROM THE CATHODE AND ACCELERATED TOWARDS THE ANODE BY A POTENTIAL DIFFERENCE BETWEEN THE ANODE AND THE CATHODE. THE ELECTRONS HITTING THE ANODE WILL CAUSE X-RAY RADIATION. (FRAME, 1999).

The unfiltered x-ray spectrum from a 150 kV electron beam is plotted in Figure 5. The Bremsstrahlung spectrum is continuous, and the average energy is about one third of the maximum energy. The two peaks in the spectrum are characteristic x-rays. If an electron has enough energy, it can hit one of the orbital electrons in the inner shells and knock it out. When this happens, one of the electrons in the higher energy levels will fall back into the place of the ejected electron, releasing its excessive energy as a photon. The energy of the photon will be the energy difference between the two energy levels, and the characteristic lines in the spectrum will reflect the difference in energy for different levels. Usually when working with x-rays, a homogenous energy is desired, or at least as close to that as possible. It is common to use filters like aluminium or cobber, to remove the low energies and the characteristic x-rays. This will result in a lower intensity, but a “cleaner” beam.

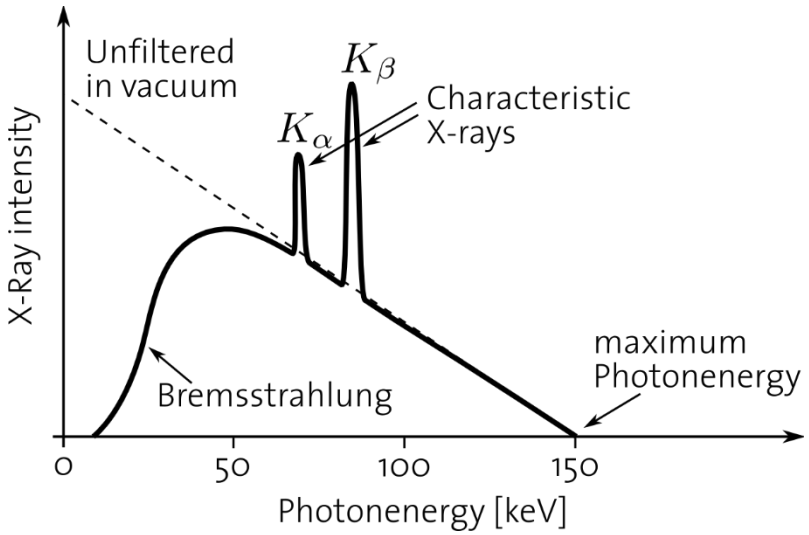

FIGURE 5.TYPICAL X-RAY SPECTRUM SHOWING BREMSSTRAHLUNG AND THE CHARACTERISTIC LINES K_α, K_β (CATTIN, 2016, FIG 1.16).

Linear Accelerator

A linear accelerator (linac) is used for accelerating charged particles, usually electrons, to energies in the range of several MeV. The electrons are accelerated by high frequency electromagnetic waves through a linear tube with cavities (Khan et al., 2014). An electron gun supplies pulses of electrons that "surf" on the electromagnetic waves, gaining energy very efficiently. Linear accelerators are commonly used for radiation therapy, and are normally operated in energy ranges between 2-12MeV. An illustration of the typical composition of a linac for medical use is shown in Figure 6. After acceleration of the electrons, due to practicalities in radiotherapy, bending magnets will bend the electron beam 90 degrees where they will hit a target, or they will be used directly for irradiation.

The medical linac is able to deliver both high energy electrons and x-rays as they usually have a removable target. When the target is present the electrons will hit the anode and produce x-rays as described in the previous section. Because the electrons can obtain a much larger energies in a linac compared to an x-ray tube, the electrons hitting the target will cause the high energetic x-rays to be released in the same direction as the incoming electrons, and not in an angle as is the case for the x-ray tube. This makes changing between treatment with electrons and high energy x-rays quite easy, as the target can simply be

removed for treatment with electrons, and no additional directional change of the beam is necessary.

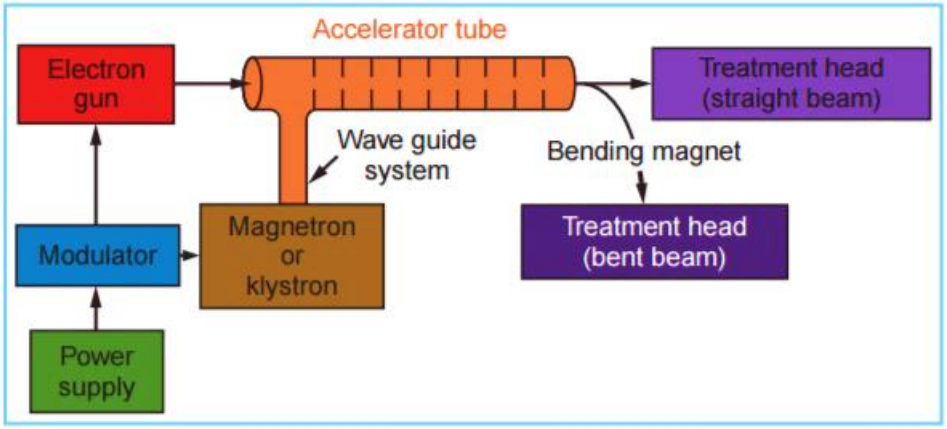

FIGURE 6. BLOCK DIAGRAM OF A MEDICAL LINAC (KHAN ET AL., 2014, FIGURE 4.5). THE ELECTRONS ARE PROVIDED BY AN ELECTRON GUN AND ACCELERATED BY HIGH FREQUENCY ELECTROMAGNETIC WAVES (PRODUCED BY A MAGNETRON OR KLYSTRON) THROUGH THE ACCELERATOR TUBE, BEFORE A BENDING MAGNETS STEER THE BEAM IN DESIRED DIRECTION. THE ELECTRON BEAM MAY BE USED DIRECTLY, OR HIT A TARGET AND PRODUCE HIGH ENERGY X-RAYS.

In linacs for medical use, collimators are used to shape the beam as wanted, and they are equipped with a moving arm, making it possible to irradiate from different angels, optimizing the dose distribution to the treatment volume. In some cases the collimators and the arm can move while the beam is on, giving even more optimization possibilities.

Cyclotron accelerator

A cyclotron is a particle accelerator where the particles cycles in an orbital motion, receiving a small voltage increment in each orbit. A magnetic field bends the particle beam into a circular path inside two semi-circular chambers with a small gap between them. These metal chambers are called “D’s” because of their shape. Schematic illustration of this in Figure 7. The two “D’s” are connected to an alternating voltage source, accelerating the particles when they are in the gap. The acceleration only occurs in this gap, so while the particles are in the chambers they only experience the magnetic field keeping them in an orbital track. When the beam has reached the wanted energy, usually in the MeV range, it is extracted for further tuning and use.

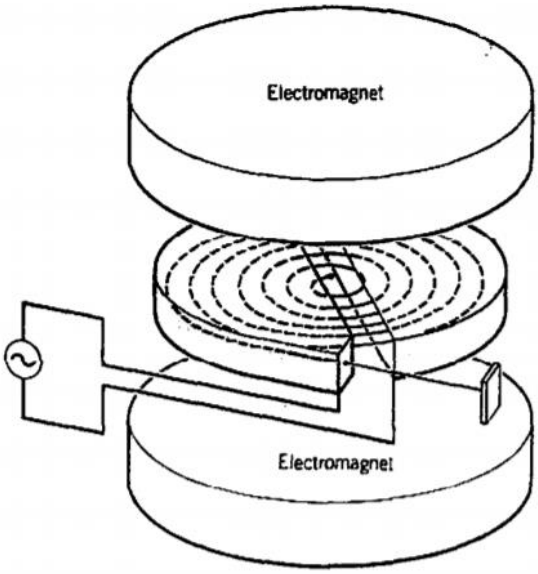

FIGURE 7. A SIMPLIFIED DIAGRAM OF A CYCLOTRON ACCELERATOR. PARTICLE BEAM SPIRALS OUTWARDS FROM THE CENTRE, AND RECEIVES ENERGY WHEN IT CROSSES THE GAP (KRANE AND HALLIDAY, 1988, FIGURE 15.11).

The path of the particles is determined by the applied magnetic field and the particle speed. By Lorenz force law in the circular orbit with a perpendicular magnetic field, the force experienced by the particle is (equation 16 and 17):

$$F = qvB = \frac{mv^2}{r} \Rightarrow v = \frac{rqB}{m} \tag{16}$$

Giving that, the time for a semi-circular orbit is:

$$t = \frac{\pi r}{v} = \frac{\pi m}{qB} \tag{17}$$

As the particles are accelerated, the radii of the circular orbit will increase. This happens at a rate so that the orbital time is independent of the radius and the orbital speed. The frequency ends up being only dependent of the particle mass and charge, and the external magnetic field. Thus the frequency of the ac voltage needed to accelerate the particles in each gap is (equation 18):

$$v = \frac{1}{2t} = \frac{qB}{2\pi m} \tag{18}$$

The particle beam is delivered by an Ion-source, and accelerated before they are “steered” by steering coils in the desired direction. Though the idea is simple, the system requires to be operated in vacuum, a lot of space and cooling is needed, and the extraction of the particle beam can be somewhat complicated.

^{60}Co

^{60}Co is a radioactive isotope of ^{59}Co (stable Cobalt atom) with one extra neutron, and a half-life of $5{,}27$ years. The radionuclei decays to ^{60}Ni by β^-emission with an energy of 0.31 MeV, which further goes to a stable state by emitting two γ-rays of 1.17 MeV. This path to a stable state has a probability of 99.88%. In rare cases (probability of 0.12%) the electron emitted has an energy of 1.48 MeV, and goes to the stable Nickel nuclei by releasing a γ-ray of 1.33 MeV. The isotope is produced artificially by neutron activation in nuclear reactors (Podgoršak, 2005). Radioactive nuclei such as ^{60}Co can be incorporated in machines and used for external beam therapy, known as teletherapy. Teletherapy machines store the source in what is called “the head”, where it is well shielded, and has a mechanism that brings it to the front of the treatment arm. There it is collimated, as the nuclei will release radiation in all directions, and shaped to a treatment beam (Podgoršak, 2005).

Because ^{60}Co has quite a long half-life, a simple energy spectra with high energies, a high specific activity and it is easy to produce, it is the most well suited isotope for teletherapy.

2.2 Dosimetry

2.2.1 Ionization chambers

Ionization chambers are dosimeters used for determining dose from ionizing radiation. They can vary greatly in shape and size, but the concept is the same. An ionization chamber consists of a cavity filled with gas, surrounded by a conducting material and with a central collecting electrode. As the gas is ionized by radiation, the resulting charged particles will create a small current that can be related to a dose (Podgoršak, 2005). To be able to connect the response of the chamber to dose, it needs to be calibrated. This is usually done by exposing it to a C60 source which emits two distinct and known gamma energies. (Ma et

al., 2001). It is important that the dosimeter is properly calibrated by a certified calibration laboratory, to reduce uncertainties to a minimum. The same goes for the electrometer responsible for measuring the resulting current from the ionization chamber. The chamber can be air-kerma calibrated, or dose calibrated depending on the type of radiation in question.

For x-rays the only calibration available is the air-kerma calibration. The dose to air is proportional to the signal from the ionization chamber, but usually it is not the dose to air that is interesting. In this case it is possible to arrive at the dose to water by applying Bragg-Gray cavity theory (Attix, 1986). By adding correction and perturbation factors, the dose to water from x-rays can be written as in equation 19 (Waldeland et al., 2010).

$$D_{water} = M_u N_k k_u p_u \left(\frac{\mu_{en}}{\rho}\right)_{water,air} \tag{19}$$

Where M_u is the chamber reading corrected for temperature and pressure, N_k is the air-kerma calibration factor, k_u is a response correction factor at a reference depth(close to unity), p_u is the perturbation correction factor, and $(\mu_{en}/\rho)_{water,air}$ is the ratio between the mass energy absorption coefficients for a given energy at the reference depth. Both k_u and $(\mu_{en}/\rho)_{water,air}$ are tabulated.

2.2.2 Gafchromic EBT3 Radiochromic Dosimetry Films

Gafchromic EBT3 radiochromic dosimetry films are used for measuring the absorbed dose from ionizing radiation. The films come in sheets of dimensions 8''x10'' and consist of an active layer in between two equal layers of polyester as shown in Figure 8. The active layer contains an active component, marker dye and stabilizers (Casanova Borca et al., 2013). The atomic composition of the layers can be seen in Table 1. When ionizing radiation enters the active layer the film is dyed, making it possible to measure the optical density of the film and correlate it to a dose. This a very useful tool for visualizing dose distributions in the 2D-plane.

To be able to correlate OD to a dose, a calibrated and homogenous beam is needed in order to make a calibration curve. Approximately 6-10 different dose points, depending on

wanted dose range, is sufficient (Gafchromic, 2014). The OD function takes the form shown in equation 20. Individual calibration is needed for each type of ionizing radiation.

$$\bar{d}_x = -log\left(\frac{a + bD}{c + D}\right) \tag{20}$$

Where D is the delivered dose, $\bar{d}_x$ is the measured optical density, a, b and c are independent parameters.

TABLE 1. ATOMIC COMPOSITION OF THE GAFCHROMIC EBT3 DOSIMETRY FILM (TECHNICAL SUPPORT SPECIALIST AT GAFCHROMIC FILMS AND SOFTWARE MR R. AYDIN II 2016, PERS.COMM., 12 OCTOBER). THE COMPOSITION OF THESE LAYERS IS A GOOD FAITH ESTIMATE BASED ON THE MANUFACTURER'S IDENTIFICATION OF THE CONSTITUENTS.

Layer	**Thickness microns**	**Approx. density g/cm2**	**Composition (ATOM %)**								
			H	**Li**	**C**	**N**	**O**	**Na**	**S**	**Al**	**Cl**
Polyester film base	125	1.35	36.4	0.0	45.5	0.0	18.2	0.0	0.0	0.0	0.0
Active layer (assumes 7.5% moisture)	30	1.2	56.3	0.7	28.5	0.3	12.4	0.1	0.1	1.4	0.2
Polyester film base	125	1.35	36.4	0.0	45.5	0.0	18.2	0.0	0.0	0.0	0.0
Overall composition	280	1.33	43.0	0.2	39.8	0.1	16.2	0.0	0.0	0.5	0.1

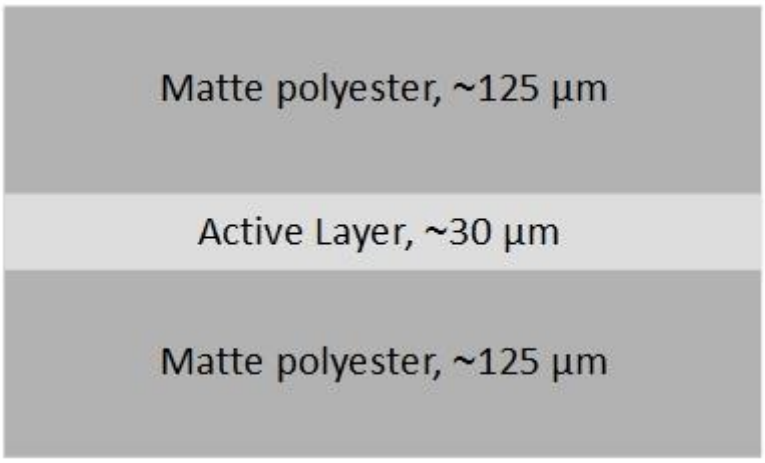

FIGURE 8. ILLUSTRATION OF THE COMPOSITION OF THE GAFCHROMIC EBT3 DOSIMETRY FILM. BASED ON INFORMATION IN TABLE 1.

To measure the optical density, the films need to be scanned and analysed. The scanning can be done by using a flatbed RGB scanner that measures the transparency of the irradiated film. It is important to turn off all colour and image corrections in order to not lose any information. It is recommended to place the film close to the centre of the scanner in landscape orientation, and always in the same orientation (Gafchromic, 2014).

The EBT3 films are symmetrical, making the OD the same if irradiated from either side, but it is still important to be consistent and always use the same orientation because there can be up to 4.5% difference in OD between landscape and portrait orientation (Casanova Borca et al., 2013).

2.3 Radiobiology

2.3.1 Direct and Indirect Action of Radiation

The following section is based on chapter 1 in "Radiobiology for the Radiologist" (Hall and Giaccia, 2012).

Ionizing radiation can be split into two main groups: directly and indirectly ionization radiation. *Independent* of the type of ionizing radiation, charged or uncharged particles, the radiation can interact with critical targets in the cell directly or indirectly. The critical target of a cell is the deoxyribonucleic acid (DNA), and the cause of damage is referred to as *direct* and *indirect action* or *effect* of radiation, see Figure 9.

A direct action is when a primary charged particle or a secondary electron acts directly on the DNA-molecule and causes damage. An indirect action is when the charged particles first interacts with a molecule in the DNA's surroundings, creating free radicals. Then these highly reactive free radicals cause damage on the DNA. For this to happen the radicals must be created close to the DNA, typically inside a radius of 2nm of the central axis of the DNA molecule.

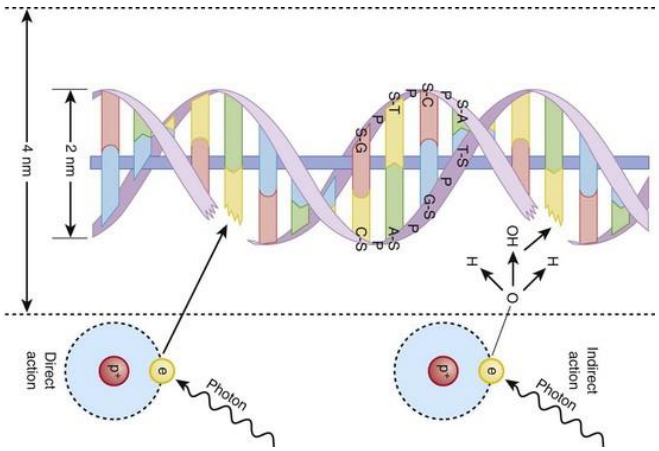

FIGURE 9. DIRECT AND INDIRECT ACTIONS OF RADIATION ON DNA SHOWN SCHEMATICALLY. DIRECT ACTION IS FOR EXAMPLE WHEN AN ATOM ABSORBS A PHOTON AND RELEASES A SECONDARY ELECTRON THEREBY CAUSING DAMAGE ON THE DNA MOLECULE. INDIRECT ACTION IS WHEN A PHOTON INTERACTS WITH A MOLECULE (USUALLY A WATER MOLECULE) SURROUNDING THE DNA, CREATING A FREE RADICAL THAT CAUSES DAMAGE ON THE DNA. THIS NEEDS TO OCCUR CLOSE TO THE DNA-HELIX, APPROXIMATELY WITHIN A RADIUS OF $2\ nm$. FIGURE ACQUIRED FROM (COLEY AND CAFFEY, 2013, FIGURE 1-3).

A cell consists of 80% water, so the assumption that the ionizing radiation will interact with a water molecule is fair. When a water molecule is ionized by radiation, chemical reactions may occur as shown in equation 21, resulting in the free radicals $OH^{\cdot}$ and $H^{\cdot}$ marked in red. These can further react with biomolecules, where an undamaged molecule is denoted as BMH, where BM indicates biomolecule and the H is a hydrogen atom. The reactions shown in equation 22 result in damaged biomolecules (e.g. DNA) also marked in red.

$$\begin{array}{l} H_2O + Ionizing\ radiation \rightarrow \quad H_2O^+ \quad + \quad e^- \\ \qquad\qquad\qquad\qquad\qquad\quad \downarrow \qquad\qquad \searrow \\ \qquad\qquad\qquad\qquad\qquad\quad H^+ + OH^{\cdot} \qquad\quad e^- + H_2O \rightarrow OH^- + H^{\cdot} \end{array} \tag{21}$$

$$\left| \begin{array}{l} BMH + H^{\cdot} \rightarrow \quad BMH_2 \\ \qquad\qquad\quad \searrow \\ \qquad\qquad\quad BM^{\cdot} + H_2 \end{array} \right| \quad \left| \begin{array}{l} BMH + OH^{\cdot} \rightarrow \quad BMHOH^{\cdot} \\ \qquad\qquad\quad \searrow \\ \qquad\qquad\quad BM^{\cdot} + H_2O \end{array} \right| \tag{22}$$

2.3.2 Radiation Damage

The following section is based on chapter 2 in “Radiobiology for the Radiologist” (Hall and Giaccia, 2012), and chapter 5 in “Molecular Biology of the Cell” (Alberts, 2008).

It is commonly accepted that the sensitive target for biological effects caused by radiation in a cell, is the DNA. The DNA-molecule is large with the shape of a double helix, and has a chemical composition as shown in Figure 10. The sugar and phosphate works as a backbone, and attached to this is the four different bases; Adenine (A), Thymine (T), Cytosine (C) and Guanine (G). Two and two bases are complementary (A and T, C and G), and are connected by a hydrogen binding. Damages in DNA caused by radiation may result in mutations, cell inactivation or cell death.

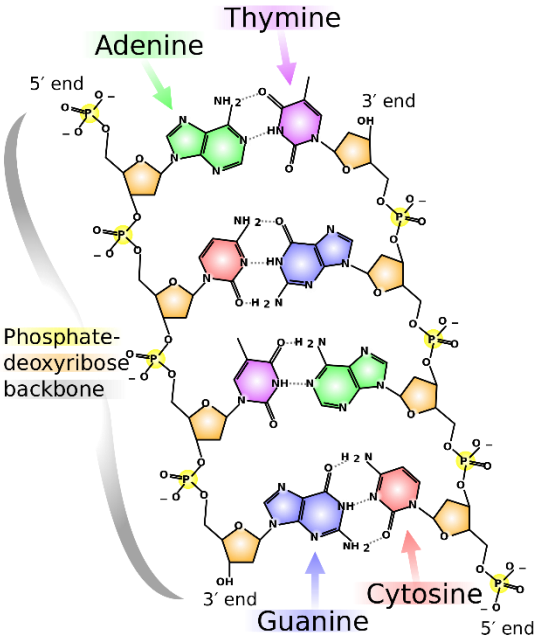

FIGURE 10. CHEMICAL STRUCTURE OF DNA (BALL, 2016). THE DNA MOLECULE CONSIST OF A BACKBONE OF SUGAR AND PHOSPHATE WITH FOUR DIFFERENT BASES ATTACHED TO IT: ADENINE, THYMINE, CYTOSINE AND GUANINE.

The three types of damage that may occur on the DNA-helix as a result of radiation are single-strand breaks (SSBs), double-strand breaks (DSBs) and base damage. Most types of damages are easily repaired and have small biological consequences as each strand in the DNA contains all the information needed to repair the damages correctly. The problems arise when information about the base sequencing is entirely lost. The different types of DNA-strand breaks can be seen in Figure 11. The most important types of damages in radiotherapy are the DNA strand breaks, as these are most likely to cause chromosome

abbreviations and cell inactivation. Single-strand breaks occur when one or more bases are lost from one of the DNA-strands, or when the sugar-phosphate structure is damaged. If two SSBs occur on opposite strands at the same place they are treated as a double-strand break. DSBs may therefore be a result of one or more damages. High LET radiation such as neutrons and heavy charged particles are often linked to a high density of DSBs.

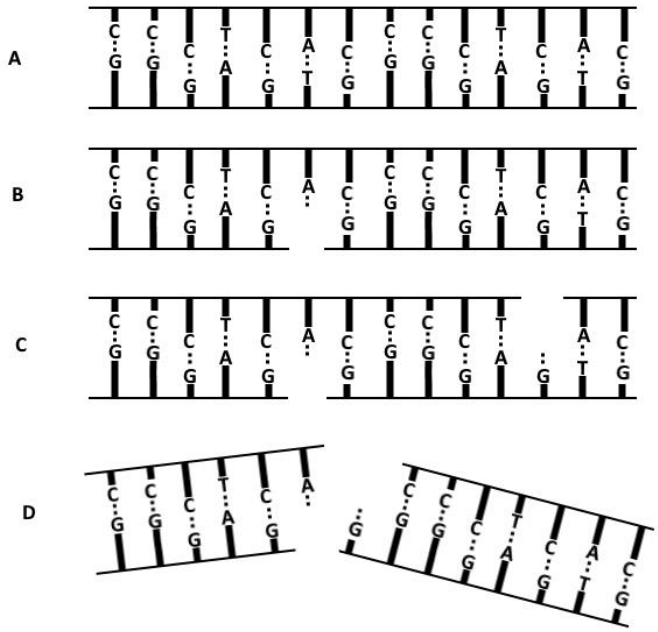

FIGURE 11. ILLUSTRATION OF DNA-BREAKS CAUSED BY RADIATION. A: 2D REPRESENTATION OF A SEQUENCE OF UNDAMAGED DNA WITH COMPLEMENTARY BASE-PAIRS (ADENINE PAIRED WITH THYMINE, CYTOSINE PAIRED WITH GUANINE). DOTTED LINES INDICATE HYDROGEN-BINDINGS. B: A SINGLE STRAND BREAK WITH NO LOSS OF INFORMATION AS IT CAN BE REPAIRED USING THE OTHER STRAND AS TEMPLATE. C: TWO SINGLE-STRAND BREAKS WELL SEPARATED IS TREATED AS INDIVIDUAL SSBS. D: BREAKS IN TWO STRANDS CLOSE TO EACH OTHER MAY LEAD TO A DOUBLE-STRAND BREAK CAUSING THE CHROMATIN TO SNAP INTO TWO PIECES. FIGURE BASED UPON (HALL AND GIACCIA, 2012, FIGURE 2.2)

Base damages may occur not only as a consequence of radiation, but also under normal cell conditions. The type of base damages is closely related to the structure of the base. The bases are categorized in purines and pyrimidines, where the purines; adenine and guanine are double-ring groups, and the pyrimidines; cytosine and guanine are single-ring groups. Depurination and deamination is the two most frequent spontaneous damages on the DNA. Depurination is when a purine base loses its linkages to the sugar-phosphate molecule, whereas deamination is when the pyrimidine cytosine spontaneously transforms to uracil, the base replacing thymine in RNA. Deamination may occur on other bases as well, but

happens at the highest rate on cytosine (Alberts, 2008). These reactions are illustrated in Figure 12.

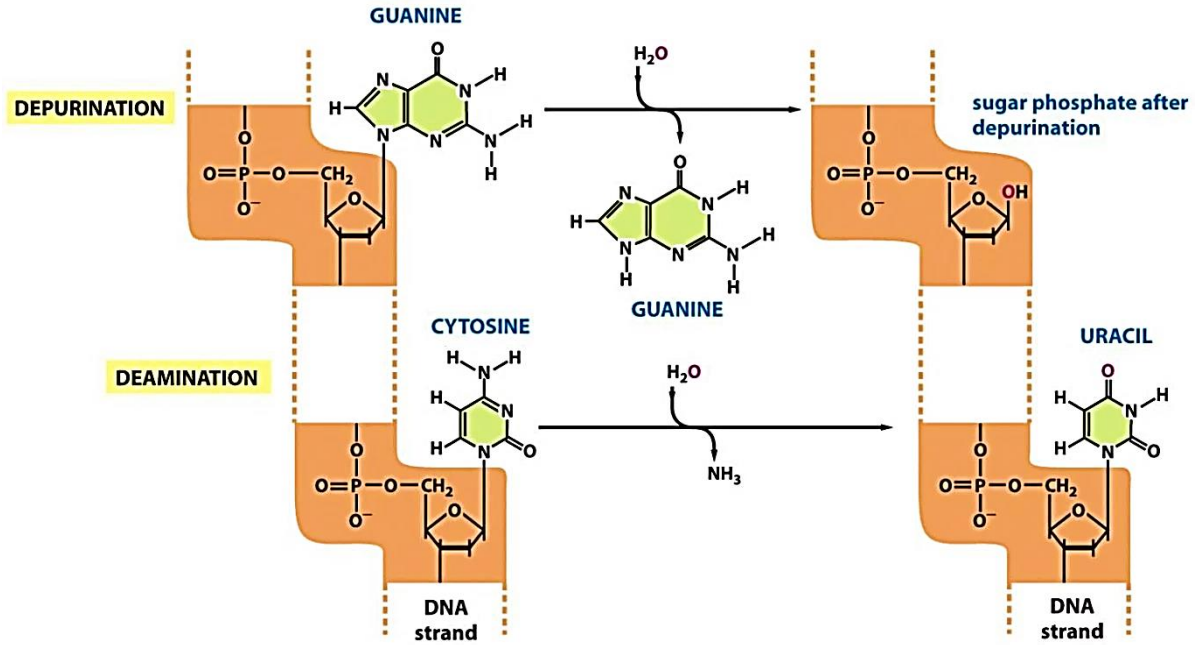

FIGURE 12. ILLUSTRATION OF THE CHEMICAL REACTIONS OF DEPURINATION AND DEAMINATION, THE TWO MOST FREQUENT SPONTANEOUS BASE DAMAGES ON THE DNA IN HUMAN CELLS. DEPURINATION RELEASES THE PURINE FROM THE DNA, HERE IN AN EXAMPLE WITH GUANINE. DEAMINATION CONVERTS A CYTOSINE TO AN ALTERED DNA-BASE, URACIL. DEAMINATION MAY OCCUR ON OTHER BASES AS WELL. SINGLE STRAND DNA SHOWN FOR SIMPLICITY. (ALBERTS, 2008, FIGURE 5-45)

Pyrimidine dimers is the base damage most commonly associated with ultraviolet radiation. Two neighbouring pyrimidine bases may create a link to each other and lose their linkage to their complementary bases. If left unrepaired before replication this may result deletion of one or more base-pairs, or wrongly substituted base pairs in the daughter cells. These mutations would then be permanent. If these damages occur at a high rate and are left

unrepaired, the consequences for the organism would be severe. The most common type of thymine dimer can be seen in Figure 13.

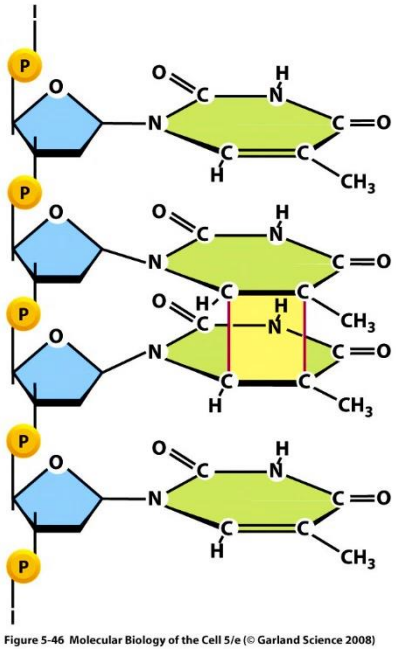

FIGURE 13. THE MOST COMMON TYPE OF THYMINE DIMER. PYRIMIDINE DIMERS OCCUR IN THE DNA WHEN THE CELL IS EXPOSED TO ULTRAVIOLET (UV) RADIATION. SIMILAR DAMAGES MAY FORM BETWEEN ANY TWO NEIGHBOURING PYRIMIDINE BASES IN DNA. (ALBERTS, 2008, FIGURE 5-46)

These types of damages can happen under normal cell conditions and during replication, but the rate of damages increases when the cell is exposed to radiation. DNA-DNA and DNA-protein crosslinks as a result of ionizing radiation are chemical damages to the DNA-bases and –structure and cause unwelcome linkages across the DNA.

2.3.3 Repair

This section is based on chapter 2 in “Radiobiology for the Radiologist” (Hall and Giaccia, 2012) and chapter 5 and 17 in “Molecular Biology of the Cell” (Alberts, 2008).

What type of repair is needed is much dependent on the type of damage, and the stage in the cell cycle. The cell cycle is divided into 4 phases; G1, S, G2 and M. The most critical ones are the S-phase where the DNA is replicated and the M-phase where chromosome segregation and cell division happens (mitosis). To give the cell enough time to grow and duplicate all proteins and organelles, there are two gap phases between the most important

steps: G1 and G2. Before the cell enters the cell cycle it is said to be in G0, where most normal human cells spend most of its life as cell proliferation happens rarely. Stem cells and cancerous cells, however, proliferate at a higher rate. To avoid critical damage during the cell proliferation, and to give time for repair, there are several checkpoints during the cell cycle as shown in Figure 14.

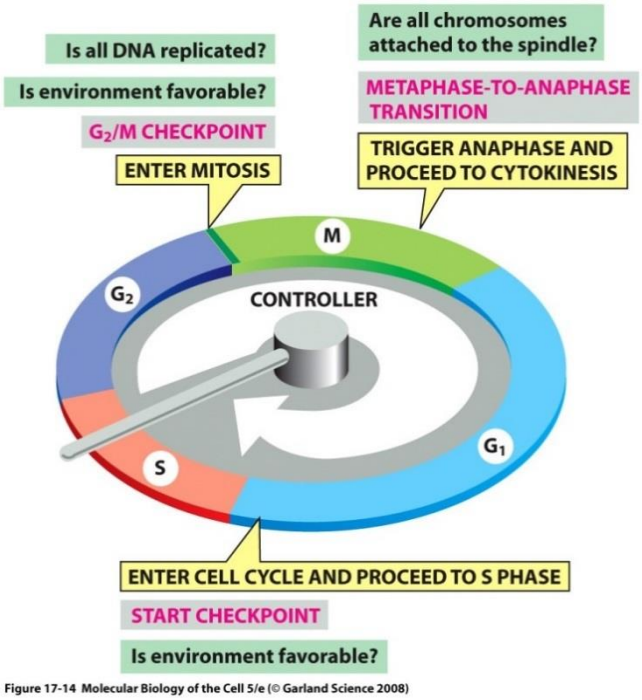

FIGURE 14. ILLUSTRATION OF THE CELL CYCLE AND ITS CHECKPOINTS. A CELL ENTER THE CELL CYCLE IN G1, AND A CELL CYCLE CONTROL SYSTEM TRIGGERS THE IMPORTANT STEPS SUCH AS CHROMOSOME DUPLICATION, MITOSIS AND CYTOKINESIS. THE CONTROL SYSTEM IS INDICATED BY A CENTRAL ARM ROTATING CLOCKWISE. IF PROBLEMS LIKE UNFAVOURABLE ENVIRONMENT, DAMAGES THAT NEED REPAIR OR THE PREVIOUS PROCESS SIMPLY IS NOT DONE YET, THE CONTROLLER CAN TRIGGER A CELL-CYCLE ARREST. THE MOST WELL-KNOWN CHECKPOINTS ARE MARKED WITH YELLOW BOXES. (ALBERTS, 2008, FIGURE 17-14)

These checkpoints are a part of the cell-cycle control system that is to ensure that the division of the cell results in two new viable cells. The control system responds to signals from both the cell itself and the surrounding environment and can stop the cell at different stages throughout the cycle. The first major checkpoint is before the cell enters S-phase and starts the DNA-replication and it makes sure that the cell does not start the process until the environment is safe. The next checkpoint is before mitosis. To start mitosis everything has to be in order; all organelles and proteins must have been duplicated, the cell must be of sufficient size, and most importantly all DNA must have been replicated. This is also the last chance to induce cell-cycle arrest if the environment is unfavourable. Once the cell enters

mitosis, there is no going back. The last major checkpoint is in mitosis, before anaphase and cytokinesis. This is to make sure that all the chromosomes are attached to a spindle, so that both cells will contain a copy of all the DNA after cytokinesis. If this is not the case, or if the environment is not ideal, the cell may be arrested, but repair is not possible at this stage.

The checkpoints give time for repair of damages, but there are many types of damages, and some types are easier to repair than others. The easiest damages to repair are single strand breaks and base damages confined to one of the DNA-strands. This is simply due to the nature of DNA, where the two strands contain all the same information as they are required to have complementary bases.

These damages are repaired through *base excision repair* (BER) and *nucleotide excision repair* (NER). Depurination and deamination on one or several neighbouring bases are repaired through the BER pathway. Enzymes remove the damaged bases, and replace them with the correct bases, before everything is glued back together by ligase. In the case of pyridine dimers and other bulky adducts in the DNA the repair is done by the NER pathway. The initial steps in this pathway can follow two lines, one if the damaged part of the DNA is actively conducting transcription, and another one if not. When a damage occurs on an actively transcribing DNA-strand, the RNA polymerase can block access to the damaged area and prevent repair. The proteins involved to allow repair therefore vary in these cases. The result, however, is the same. The damage is recognized, DNA incisions are made surrounding the damage (usually 24-32 nucleotides in total), these are removed, polymerase synthesises new bases in the gap, and the DNA strands are joint together by ligase.

Double strand breaks are the most complicated damage to repair. In eukaryotic cells however, the repair can be easily done during S or G2 when the sister chromatid can be used as a template for repair. Of course, it is necessary that the sister chromatid is undamaged in the same area as the repair is needed. This is called homologous recombination repair (HRR), and gives a perfect repair without any errors. When the damage occurs in the G1 phase, nonhomologous end-joining (NHEJ) simply glues the ends of the broken strand together. In the case of NHEJ, the repair is prone to errors, as the sequencing of bases may have changed. This is most likely giving rise to most of the

mutations as a consequence of ionizing radiation. The NHEJ can also occur in S and G2 phase if HRR is not possible.

The repair of crosslinks is a process that little still is known about. The assumption is that the repair pathway is a combination of NER and HRR during replication of the DNA. First, the crosslink is removed from one of the strands, resulting in one strand with a SSB and the other with the adduct. Repair then have to be sequenced correctly to avoid loss of information, leaving the crosslink attached to one of the strands until all else is repaired. Translesion synthesis fill the gap left by NER, but this results in a mutation opposite of the adduct. When the other strand is synthesised, a gap is left opposite where the crosslink was removed, resulting in a DBS. This DBS is repaired by homologous recombination, and a new round of NER removes the crosslink adduct completely. The replication fork is then restored, and replication can continue.

The Mismatch Repair pathway removes mismatched bases that may occur during replication. The damage is recognised, the mismatched nucleotides are excised and complementary nucleotides are synthesised and ligated. This repair process also takes part in the homologous recombination pathway if mismatches occur.

Chromosome aberrations are, as mentioned previously, a possible result of DSBs. In the case of DSBs there are three possible scenarios.

1) The ends re-join in their original configuration either by HRR or NHEJ.
2) The ends may fail to re-join and a part of the chromosome is lost after the next mitosis.
3) The ends may re-join with other ends caused by a DSB on the same or another chromosome, causing deformed chromosomes after the next mitosis.

If the result is number 3, the cell is likely to stop dividing or to go to apoptosis as the damages are so severe. This is the reason that cell killing is said to be closely linked to the number of DSBs. Three examples of lethal chromosome aberrations are illustrated in Figure 15. The problem with chromosome aberrations often arises during mitosis. Acentric fragments will be lost, and in some cases such as the anaphase bridge, the chromatid has stuck together causing it to be stretched when it should have been separated.

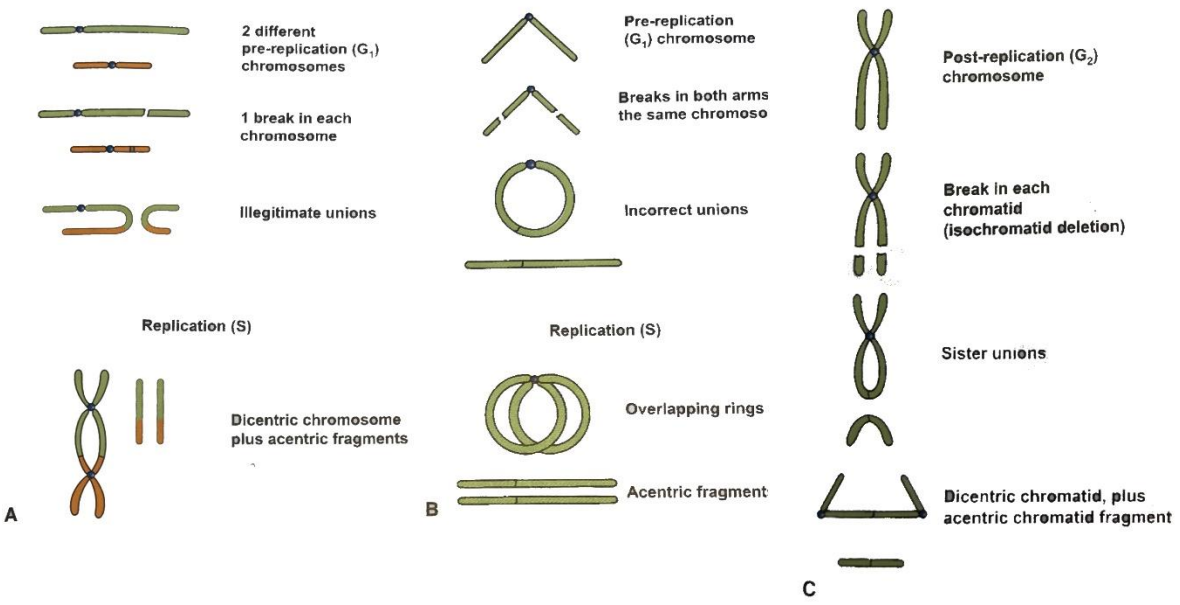

FIGURE 15. EXAMPLES OF THREE LETHAL CHROMOSOME ABERRATIONS. THE ABERRATIONS WILL CAUSE PROBLEMS IN THE NEXT MITOSIS DURING SEPARATION OF THE CHROMOSOMES. IN THE CASES WHERE ACENTRIC FRAGMENTS OCCUR THESE WILL BE LOST IN THE NEXT MITOSIS AS THEY DO NOT HAVE ANY CENTROMERES. A: TWO CHROMOSOMES GET A DSB AND THE WRONG ENDS ARE JOINED TOGETHER. THE RESULT AFTER REPLICATION IS A DICENTRIC CHROMOSOME PLUS ACENTRIC FRAGMENTS. B: TWO DSBS IN BOTH ARMS OF THE SAME CHROMOSOME. THE STICKY ENDS ARE JOINED TOGETHER MAKING A RING. AFTER REPLICATION THERE ARE TWO OVERLAPPING RINGS AND ACENTRIC FRAGMENTS. C: AN ALREADY REPLICATED CHROMOSOME SUFFERS A BREAK IN EACH CHROMATID, AND THE SISTER CHROMOSOMES ENDS STICK TOGETHER. DURING ANAPHASE THE CENTROMERES WILL GO TO EACH POLE AND THE CHROMATID WILL BE STRETCHED. THIS IS CALLED AN ANAPHASE BRIDGE.

All the types of damages can also be split into groups according to the ability to be repaired, such as *lethal damage*, *potentially lethal damage* (PLD) and *sublethal damage* (SLD). When a cell is exposed to radiation, it can obtain damages on its DNA that is either potentially lethal or sublethal. Sublethal damages are possible to repair in less than an hour, such as SSBs and other base damages, under the assumption that they are not exposed to new SLDs. If exposed to new SLD they can turn into potentially lethal damages. Potentially lethal damages are usually lethal and therefore often assumed to include severe damages such as double-strand breaks. The reason for the word potentially however is that by manipulating the environment to induce cell cycle arrest, or by a naturally induced arrest after irradiation, they can be given a chance to be repaired. Such environmental factors can be density-inhibition, or replacing growth medium with a balanced salt solution in post-irradiation incubation. The possible outcomes of radiation damages can be seen in Figure 16.

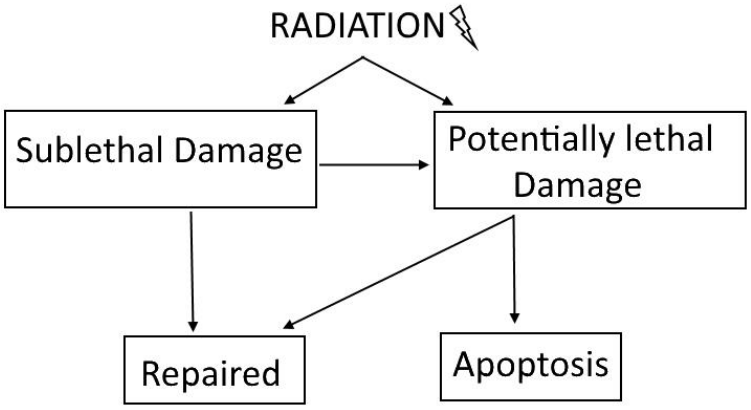

FIGURE 16. POSSIBLE OUTCOMES OF RADIATION DAMAGE. RADIATION DAMAGE CAN CAUSE SUBLETHAL OR POTENTIALLY LETHAL DAMAGE. SUBLETHAL DAMAGE HAS THE ABILITY TO BE REPAIRED IN A SHORT TIME AS LONG AS THEY ARE NOT EXPOSED TO NEW SDLS. IF THEY ARE, THEY CAN BECOME POTENTIALLY LETHAL DAMAGES. POTENTIALLY LETHAL DAMAGE ARE MAINLY LETHAL UNLESS THE ENVIRONMENT POST IRRADIATION IS MANIPULATED TO ALLOW TIME FOR REPAIR. IF NOT REPAIRED THE CELL GOES INTO APOPTOSIS OR NECROSIS.

2.3.4 Cell Survival Curves and the LQ-model

To visualize the survival of cells we plot a survival curve. In radiotherapy, a survival curve shows the relationship between the delivered dose and the surviving fraction of cells. A surviving cell, when operating with proliferating cells such as cancer cells, is characterized as a cell that is able to sustain proliferation (Hall and Giaccia, 2012). Some cells may be able to go through mitosis a few times, but will still be characterized as dead if they have lost their ability to proliferate indefinitely. In practise, in a clonogenic cell survival experiment with such cells, a cell has survived if it has the ability to form a colony of a certain size, usually over 50 cells (Joiner and Kogel, 2009).

To be able to find the *surviving fraction* (S), it is necessary to know the number of cells seeded. However, the number of surviving cells will differ some from the number of cells seeded even if the cells are not exposed to radiation. This is due to many reasons, such as growth conditions and handling with equipment and trypsin. The *plating efficiency* (PE) is a measure of the fraction of seeded cells that survive after this handling and is defined in equation 23. The surviving fraction is defined as the fraction of colonies counted, from cells seeded taking PE into account, as can be seen in equation 24 (Hall and Giaccia, 2012).

$$PE = \frac{\#\ colonies\ counted}{\#\ cells\ seeded} \times 100 \tag{23}$$

$$Surviving\ fraction = \frac{\#\ colonies\ counted}{\#\ cells\ seeded \times (PE/100)} \tag{24}$$

The shape of a cell survival curve is dependent of the type of radiation and the ability to repair for the individual cell or cell line, but some characteristics are similar. The curve usually starts out straight at the low doses in a log-linear plot, and starts to curve towards higher doses. The curvature tends to straighten towards the really high doses again (Hall and Giaccia, 2012). One of the most acknowledged models for surviving fraction is the *linear-quadratic model* (LQ-model).

The LQ-model consist of two components. One component is proportional to the dose, and one is proportional to the square of the dose. These can be interpreted biologically as different sources of damage causing cell inactivation or death. The common interpretation is that the linear term is linked to two chromosome breaks by one electron, and the quadratic term to two chromosome breaks by two separate electrons. This idea is based upon the assumption that chromosome aberrations causes inactivation, and that other types of damage are repairable. Further it is assumed that chromosome aberrations are caused only by double strand breaks, but DSBs can be caused by two SSB very close to each other or by a single DSB. Depending on the stage in the cell cycle, one or two double-strand breaks may lead to chromosome aberrations as discussed above. The LQ-model can be seen in equation 25.

$$S = e^{-(\alpha D + \beta D^2)} \tag{25}$$

Where S is the surviving fraction, D is the dose and α, β are constants and adjustable parameters.

The linear term of the LQ-model can be related to the DSB, and the quadratic term can be related to two close SSBs.

2.3.5 Dose-rate effect

This section is based upon chapter 5 in “Radiobiology for the Radiologist” (Hall and Giaccia, 2012).

The dose-rate effect is the difference in biological consequences of the same dose depending on the rate the dose is delivered with. In other words, the time it takes to deliver a dose impacts the cells possibility to repair damages. The damages in question are the sublethal damages (SLD), as these always can be repaired given enough time before new damages occur (as discussed in section 2.3.3). By lowering the dose-rate, the biological effect will decrease as the cell is given more time to repair SLD before another occur. The characteristic shoulder of the survival curve will also disappear as the dose-rate is lowered. For small doses, the cell will be able to repair a great deal of the SLDs even though the radiation is given acutely, resulting in this shoulder. For LDR the repair is “optimized” for all doses, resulting in a straighter and a less steep line.

The LDR radiation gives more time for repair, but there is also an inverse effect of the dose-rate. For some cell lines there seems to be a point when the dose-rate is lowered below the point where all SLD is repaired, where the slope of the survival curve becomes steeper again. When the dose-rate is very low the cells may be allowed pass through S-phase, but they will still be arrested in the G2-phase. A redistribution of the cell population in the cell cycle happens as the cells are synchronized in this radiosensitive phase, thus increasing the biological effect. If the dose-rate is further lowered the cells may not be arrested at all, but continue through mitosis and cell division. This will again decrease the biological effect, as this tends to prevent cell death. The effects of the dose-rate on the cell survival can be seen in Figure 17.

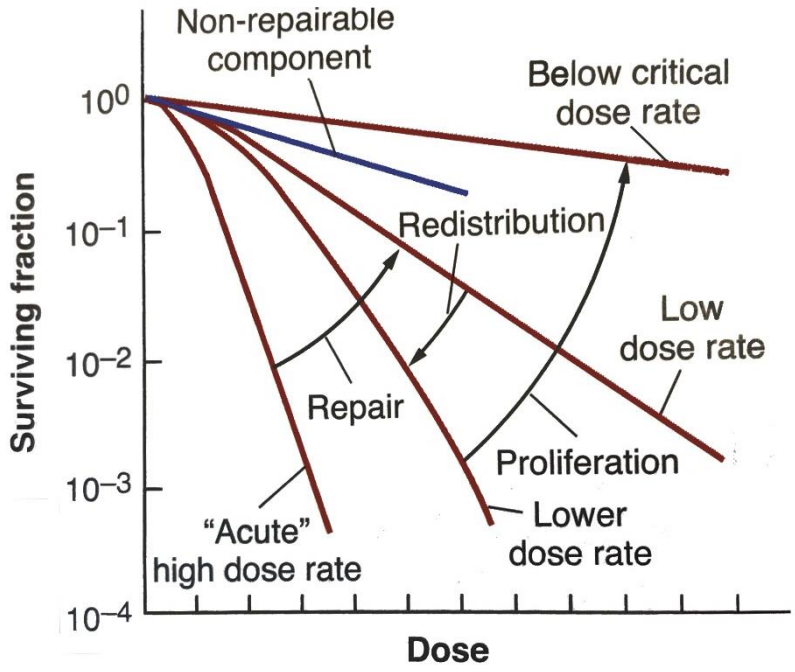

FIGURE 17. THE DOSE-RATE EFFECTS OF SLD REPAIR, REDISTRIBUTION IN THE CELL CYCLE AND PROLIFERATION. WITH LOWER DOSE-RATES THE CELL IS GIVEN MORE TIME TO REPAIR SLD, RESULTING IN A LESS STEEP CURVE WITH LESS CURVATURE. WHEN DOSE-RATE IS LOWERED PAST A CERTAIN LEVEL THE CELLS PASS THROUGH THE CELL CYCLE BUT ARE ARRESTED IN THE G2-PHASE. REDISTRIBUTION IN THIS RADIOSENSITIVE PHASE CAUSES INCREASED BIOLOGICAL EFFECT AND A STEEPER CURVE. WHEN LOWERED FURTHERED CELLS MAY BE ALLOWED TO PASS THROUGH THE WHOLE CELL-CYCLE, AGAIN REDUCING THE BIOLOGICAL EFFECT. (HALL AND GIACCIA, 2012, FIGURE 5.15)

2.3.6 Linear Energy Transfer and Relative biological Effectiveness

This section is based on chapter 7 in "Radiobiology for the Radiologist" (Hall and Giaccia, 2012).

The linear energy transfer (LET) is a measure on the density of the energy deposition of ionizing radiation, and is as described in section 2.1.1 proportional to the restricted stopping power. The unit for LET is keV/µm, reflecting an average energy departed per unit length. As it is a measure of an *average* energy deposition per unit length this value can be calculated in many ways, creating discussion whether or not it is useful to have such a quantity at all. It can however, be useful for comparing the quality of different types of ionizing radiation. Common LET values for different types of radiation is listed in Table 2. When addressing the issue of biological effect of different types of radiation, the LET quantity is especially useful.

TABLE 2. COMMON LET VALUES FOR DIFFERENT TYPES OF RADIATION.

Radiation	LET (keV/µm)
^{60}Co γ-rays	0.2
250 keV x-rays	2.0
10 MeV protons	4.7
150 MeV protons	0.5

The common measure of biological effect is the relative biological effectiveness (RBE). This is a value comparing a type of radiation to a reference type, usually x-rays or ^{60}Co γ-rays. The RBE is a ratio between the dose for the reference radiation and the dose for the radiation you want to measure, corresponding to the same survival level (see equation 26). Survival levels of 0.1 and 0.37 are commonly used.

$$RBE = \frac{Dose(SF)_{reference}}{Dose(SF)_{test\ radiation}} \tag{26}$$

RBE values can vary greatly, not just radiation type, but also tissue and the cell line studied. This is due to the large variations in repair-mechanisms the different cell lines possess, and is especially dependent on their ability to repair sublethal damage.

The variation in LET seem to be one of the reasons the cell survival and RBE differs for different types of radiation. The variation in RBE as a function of LET for survival of a mammalian human cell can be seen in Figure 18. As the LET increases, so does the RBE, but exceeding LET values over 100 keV/µm, it decreases again. It seems like there is an optimal value for maximum biological effect at approximately 100 keV/µm. This ionization density seem to be very close to the average diameter of the DNA double helix, maximizing the probability of double strand breaks (DSB) from a single charged particle. With a further increase in LET the damage efficiency per dose (or energy imparted) is reduced, and the extra energy is wased as it does not cause further damage, only damage to the already struck areas. Thus one achieve a saturation effect, where the additional energy is wasted on areas previouly damaged.

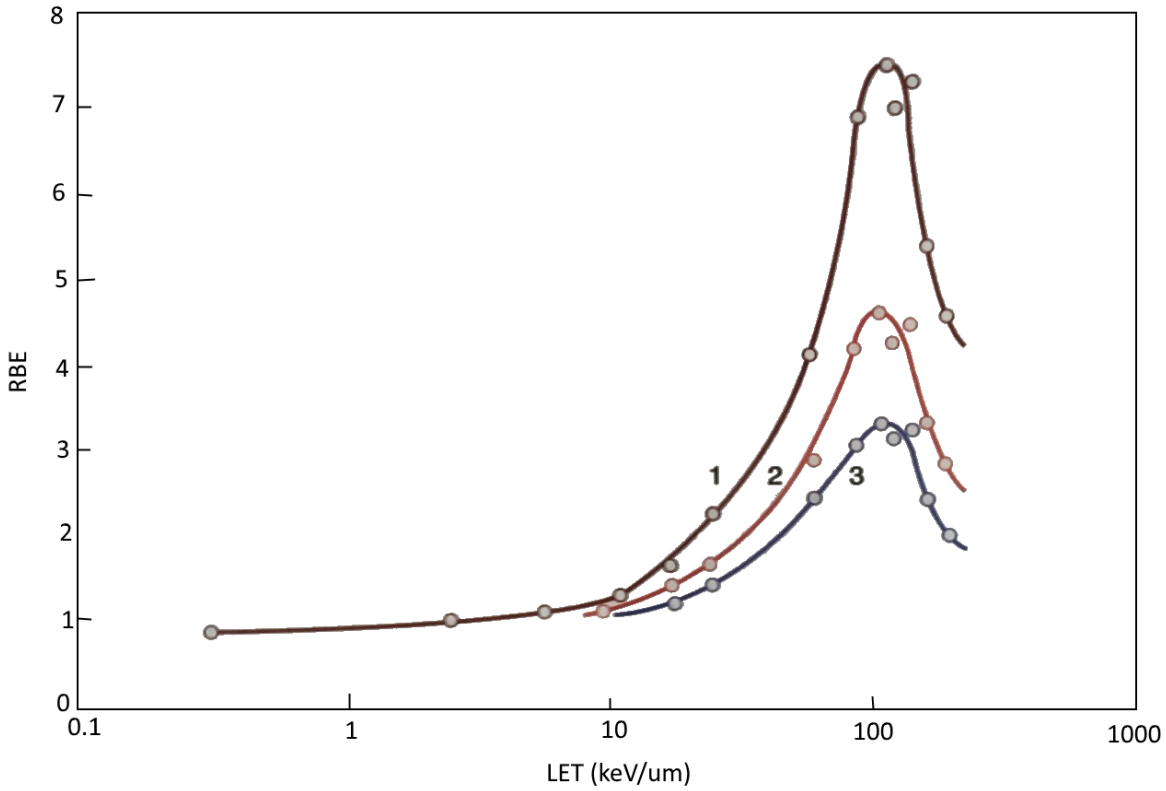

FIGURE 18. THE VARIATION IN RBE AS A FUNCTION OF LET FOR SURVIVAL OF MAMMALIAN CELLS OF HUMAN ORIGIN. 1, 2 AND 3 REFER TO A SURVIVAL LEVEL OF 0.8, 0.1 AND 0.001 RESPECTIVELY. FIGURE BASED UPON FIGURE 7.5 IN (HALL AND GIACCIA, 2012).

2.3.7 Cancer and Particle Therapy

This section is based on chapter 18 in "Radiobiology for the Radiologist" (Hall and Giaccia, 2012), chapter 20 in "Molecular Biology of the Cell" (Alberts, 2008) and chapter 25 in "The Physics of Radiation Therapy" (Khan et al., 2014).

Cancer is what we call the group of diseases where cells divide in an uncontrolled manner. As a consequence of the uncontrolled proliferation and fail of self-elimination, the cells form densely packed groups, tumours. The abnormal cells also may acquire the potential to spread to other parts of the body, known as metastasis. For a cell to become cancerous, the genes controlling cell growth and division, cell-death, and immortalization must be altered in some way. Oncogenes, genes promoting cell growth and cell proliferation, can induce cancer by being overexpressed, while tumour-suppressing genes that act as growth regulators may do the same by being underexpressed. Alterations or loss of genes that are a part of detecting and repairing DNA-damages may result in a weakened control system as

well. Such mutations in the DNA may have originated due to damages to the DNA that have not been repaired or have been repaired incorrectly. An accumulation of several mutations in a cell is necessary for it to become cancerous, but only one single cell is enough to cause progression of the disease.

The reasons that cancerous cells develop are many and complex and are often related to lifestyle and environment. Chemicals, radiation, infections and hormone balance are some of the known causes, and some people are genetically disposed for some types of cancer because of inherited mutations. Cancer may develop very differently depending on the type of cell that has become cancerous, where in the body it is, and what kind of mutation or mutations that are the reason for it. This makes treatment difficult, as the disease behaves differently for all patients. Types of treatment commonly used today are surgery, chemotherapy, radiotherapy and immunotherapy. Often treatment consists of a combination of these.

In modern times, the use of heavy charged particles have entered the area of radiotherapy. Especially protons have become a common tool in cancer treatment. The use of protons for such purposes was first suggested as early as 1946, but it is in the last 15 years this has become widespread across the world. The research towards understanding the effects of linear energy transfer (LET) on the relative biological effect (RBE) is therefore of great essence, as this is still an area of discussion. For practical reasons, an RBE of 1.1 have been used in treatment planning for proton beams, as a constant RBE along the whole proton track makes it easier to compare treatment plans and clinical response with the more commonly used photon beams. As proton beams have a sharp drop in dose at the end of proton track, they are well suited for treating tumours close to organs at risk (OAR). With the positional uncertainties of both patient and tumour, the end of the proton track may be in danger of hitting the OAR, and as this is also the area with the greatest risk of increased RBE values, this may pose additional dangers of side-effects. On the other hand, an increase in RBE may be a benefit as to effectively killing resistant cancer cells. To know more about the effects of the LET on the RBE will be important for improving the radiotherapy with protons, both with the aim to reduce risk and to improve its effectiveness.

3 Materials and Methods

3.1 Process and Setups

In this thesis the aim was to create a setup making it possible to perform cell irradiation experiments at Oslo Cyclotron Laboratory (OCL). This was done using an iterative process. We worked in weekly blocks, where dosimetry and 1-3 cell survival experiments were performed in each block. Positioning in equipment and cell irradiation depths were kept consistent during all experiments in the same block. This will later be referred to as a setup. Further the setups were given numbers chronologically. All setup consistencies from the first block was named "setup 1", etc. The cell survival experiments were named after the setup used during irradiation, and were given a second number after the order they were conducted in. The first cell survival experiment using setup 1, was named setup 1.1 etc. After a block was completed, the data was analysed in order to improve the setup for the next sequence of experiments. An overview of the main differences in the setups for cell irradiations are given in Table 3. A more detailed description of the proton irradiation setup and of changes made along the way can be found in section 3.3.8.

TABLE 3. ROUGH DESCRIPTION OF THE ITERATIVE CHANGES IN THE SETUPS FOR CELL IRRADIATION.

	Monitor Chamber	**Scattering Filter**	**Distance from beam exit window**
Setup 1	Not included	60 µm Fe	88 cm
Setup 2	Included	50 µm W	88 cm
Setup 3	Moved further from beam exit window	50 µm W	78 cm
Setup 4	Same as setup 3	50 µm W	81 cm

This thesis also contain dosimetry and cell survival experiments performed with x-rays and ^{60}C0 gamma rays in order to have references for calculation of the relative biological effect (RBE). As the proton experiments required some additional precautions, such as irradiation without medium, the experiments with these radiation types was attempted to be as similar to the proton experiments as possible to obtain good grounds of comparison.

3.2 Dosimetry

3.2.1 Equipment

Dose measurements

A dose to water calibrated PTW Advanced Markus (PTW-Freiburg, Germany) ionization chamber was used for proton dose measurements. A PTW Monitor Chamber Type 34014 (PTW-Freiburg, Germany) was used for relative radiation flux measurements in the proton beam line. For x-ray and ^{60}Co dosimetry a kerma calibrated ionization chamber IBA FC65-G (IBA Dosimetry, Germany) was used. Gafchromic EBT3 self-developing dosimetry films (Ashland, USA) was used for dose profile measurements in a 2D plane on all modalities investigated in the thesis.

Electrometers

A Standard Imaging electrometer, MAX-4000 (Standard Imaging, USA) was used with the PTW Advanced Markus and the IBA FC65-G ionization chambers. A UNIDOSE E electrometer (PTW-Freiburg, Germany) was used with the PTW Monitor Chamber.

Radiation units

X-ray unit PANTAK PMC 1000 (Pantak, USA) located at Roentgen radiation lab, in the chemistry building, UIO.

Molbatron 80 radiotherapy treatment unit with a ^{60}Co source (T. E. M. Instruments, Crawley, UK) located at The Norwegian Radium Hospital (NRH).

Cyclotron Scanditronix MC-35 (Scanditronix, Uppsala, Sweden) located at Oslo Cyclotron Laboratory.

Linear accelerator, Siemens Artiste (Siemens Medical Solutions, USA) located at the NRH.

For proton beam centration in our irradiation setup, a cylindrical laser holder with a coaxial laser beam was used.

Specially designed items

Holders to keep Markus chamber and monitor chamber vertical on a steel rack during irradiation were made at the instrument workshop at UiO. A slot was made in the holder for the Markus chamber to place rectangles of 60 mm x 65 mm in front of the ionization chamber. This was to be able to place dosimetry films and solid water in the beam line.

Other

An Epson Perfection V850 Pro flatbed scanner was used for scanning dosimetry films.

Slabs of solid water (Nylon6) with thickness 0.5 mm and 1 mm was used as absorbers to reach different depths in the proton beam depth-dose Bragg-Peak.

60 µm Fe and 50 µm W scattering filters were used in order to spread the proton beam and have a homogenous dose covering the cell dish.

3.2.2 Gafchromic EBT3 Film Dosimetry

Gafchromic EBT3 dosimetry films were mainly used as a tool for measuring the homogeneity of the proton beam used for cell irradiation. The films were cut to fit in a film holder, and placed perpendicular to the beam line. When irradiated, an active layer in the middle of the film was dyed. By scanning the films in transparency mode, the amount of light able to pass through the film was measured. This intensity was then related to the optical density (OD) by the equation, $OD = \log_{10} I$, which was possible to correlate to a certain dose. In order to do this, a calibration was needed. All calibrations and dosimetric measurements with films where performed at room temperature (19-23 ^{o}C).

Scanning

An Epson Perfection V850 Pro RGB flatbed scanner in transparency mode was used for scanning Gafchromic EBT3 films. The scanner was on for at least 30 minutes before scanning, and 15 warm-up scans were conducted to stabilize the scanner lamp. Scanning was performed 22-30 hours after irradiation. During scanning, the films where placed in the same position every time, approximately in the centre of the scanner and up-side-down in portrait mode as illustrated in Figure 19. Listed in Appendix A, Table 24 are the settings for scanning of Gafchromic, using an Epson Perfection V850 Pro flatbed scanner.

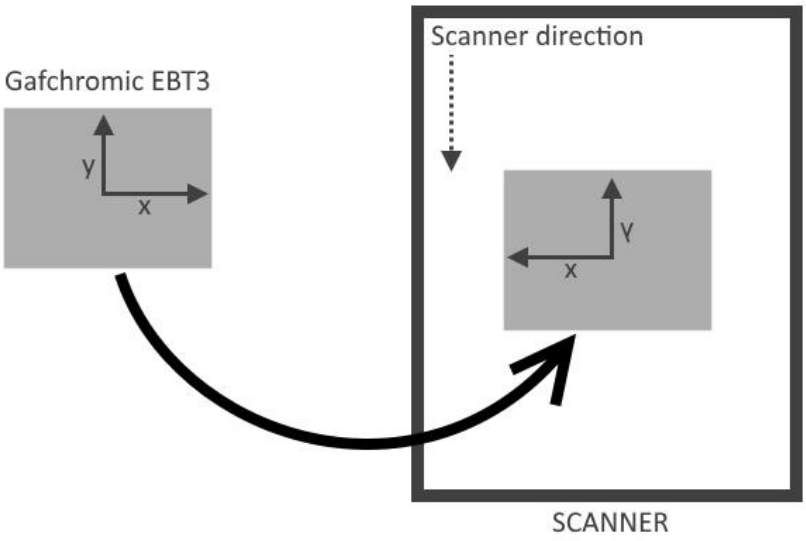

FIGURE 19. FILM ORIENTATION DURING SCANNING OF GAFCHROMIC EB T3 FILMS.

Calibration

To correlate an OD with a dose, a calibration was needed. Films were irradiated with different doses, and the OD was measured. An average over all three colour channels was used as OD. Using the model in equation 27 a best fit of the three independent parameters was found.

$$D = \frac{a\, e^{OD} - c}{1 - b\, e^{OD}} \tag{27}$$

Where D is the delivered dose, OD is the measured optical density, a, b and c are independent parameters.

Electrons

Initial calibration of the Gafchromic EBT3 dosimetry films was performed at the NRH, using 12 MeV electrons produced by a Siemens linear accelerator. The film was placed between two slabs of solid water 100 cm from the source, as shown in Figure 20. The beam was circular with diameter 5 cm. Doses delivered with corresponding Monitor Units (MU) are given in Table 26.

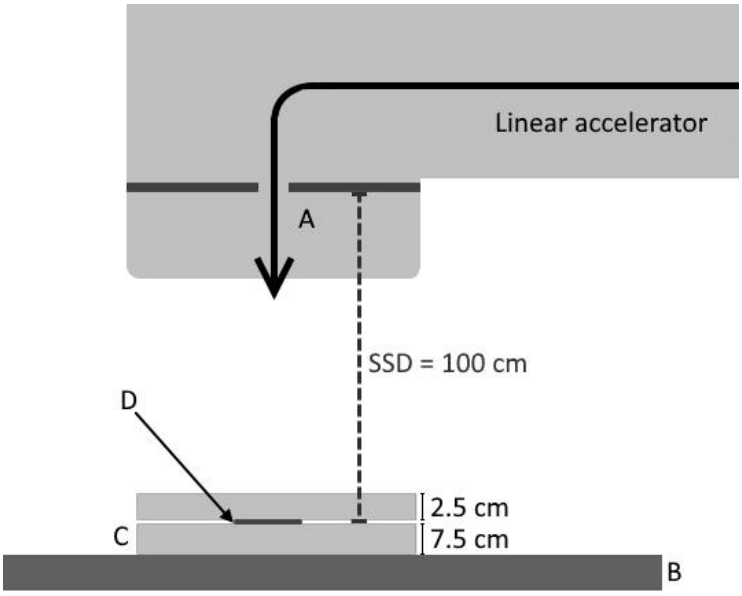

FIGURE 20. EXPERIMENTAL SETUP FOR ELECTRON CALIBRATION OF GAFCHROMIC EBT3 FILMS. THE FILMS WERE PLACED BETWEEN TO SLABS OF SOLID WATER, AND IRRADIATED WITH A CIRCULAR (5 CM IN DIAMETER) 12MEV ELECTRON BEAM IN SSD 100 CM. A: ELECTRON BEAM. B: TREATMENT BENCH. C: TWO SLABS OF SOLID WATER OF 2.5 CM AND 7.5 CM. D: GAFCHROMIC EBT3 FILM PLACED BETWEEN SLABS OF SOLID WATER.

Films were cut in squares with sides of 7.5 cm. Orientation of films where marked and accounted for at all times. This was important in order to ensure same orientation during both irradiation and scanning. In addition the films were handled carefully to avoid contamination by fingerprints, and kept out of light for most of the time.

Calibration was later done individually for the different ionizing radiations, 220 keV x-rays, ^{60}Co gamma rays and 16 MeV protons.

Protons

Proton calibration of the films was performed with a tungsten scattering filter and a monitor chamber (MC) in front of the film. The positioning of the equipment was identical to setup during some of the clonogenic cell survival experiments, with the film in the cell irradiation position. Films were placed in a holder with dimensions $60 \times 65\ mm$ and a circular frame $50\ mm$ in diameter, designed for these experiments. To fit in the holder, the films were cut in rectangles of $59 \times 64\ mm$. The positioning of the equipment can be seen in Figure 21. A total of 10 films where irradiated with individual doses. It was attempted to irradiate two

and two film with similar doses ranging from approximately 1-12 Gy. The dose delivered was calculated from the monitor chamber readings. Before film calibration, the dose at film irradiation position was measured with the dose calibrated ionization chamber, PTW Advanced Markus, and corresponded to monitor chamber reading. The doses delivered to the films with corresponding MC output can be found in Appendix A, Table 29.

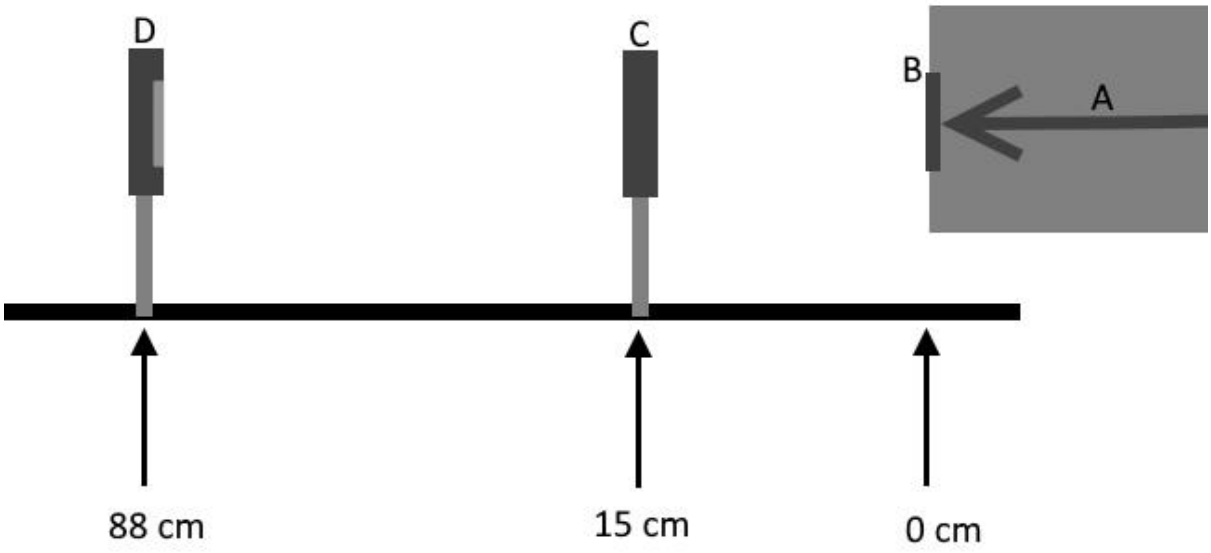

FIGURE 21. A: ILLUSTRATION OF SETUP DURING CALIBRATION OF GAFCHROMIC EBT3 FILM WITH 16 MEV PROTONS. CALIBRATION WAS DONE FOR ZERO DEPTH, IGNORING THE THICKNESS OF THE PLASTIC IN FRONT OF THE ACTIVE LAYER AND MONITOR CHAMBER. A: PROTON BEAM DIRECTION. B: BEAM EXIT WINDOW WITH 50 μm TUNGSTEN SCATTERING FILTER. C: PTW MONITOR CHAMBER TYPE 34014. D: HOLDER CONTAINING A GAFCHROMIC EBT3 DOSIMETRY FILM.

X-rays

The x-ray calibration was performed at the same x-ray tube and with similar setup as the clonogenic cell survival experiments with x-rays. An illustration of the setup can be seen in Figure 22. Filtration of the x-ray beam was done by a 1 mm Be inherent filtration, and secondary filtration with 0.5mm Cu. Gafchromic EBT3 dosimetry films where irradiated in a

steel chamber with two films at 4 different doses raging from 1-10 Gy. The doses and delivered time to each dose can be seen in Appendix A, Table 27.

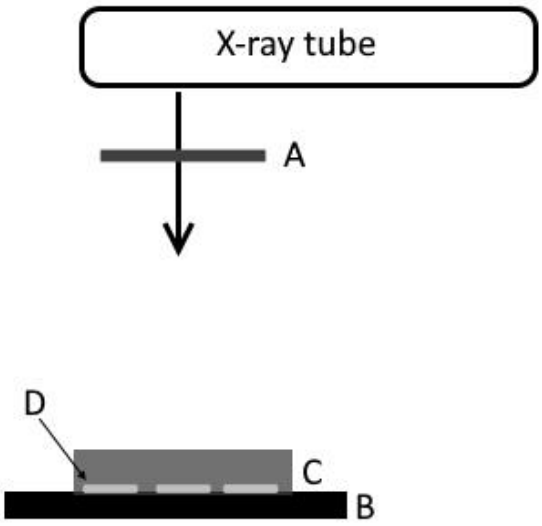

FIGURE 22. SETUP DURING CALIBRATION OF DOSIMETRY FILMS WITH 220 keV X-RAYS. A: FILTRATION OF THE X-RAY BEAM; 1 MM BE INHERENT FILTRATION, AND SECONDARY FILTRATION WITH 0.5MM CU. B: PLATE. C: STEEL CHAMBER. D: GAFCHROMIC EBT3 FILMS.

^{60}Co

The calibration to ^{60}Co was performed at the NRH. 4 films were irradiated at three different doses between 2-10 Gy. The doserate was $0{,}40602\ Gy/min$ at $SSD = 70\ cm$. Delivered doses and irradiation times are given in Table 28. The setup was similar to setup during clonogenic cell survival experiments with ^{60}Co, and can be seen in Figure 23. The films where placed on a lift in position $SSD = 70\ cm$. A styrofoam lid was placed over the films as this is the case during cell survival experiments. Irradiation was done at room temperature.

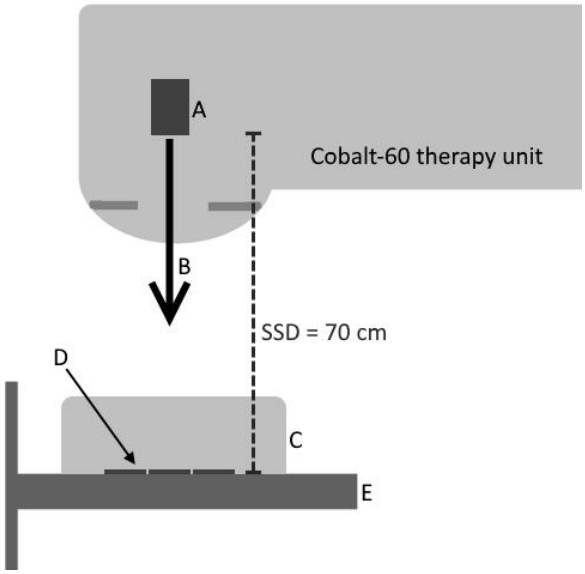

FIGURE 23. SETUP OF ^{60}CO CALIBRATION OF GAFCHROMIC EBT3 FILMS. A: CYLINDER CONTAINING THE RADIOACTIVE ^{60}CO SOURCE. B: COLLIMATED BEAM. C STYROFOAM LID SURROUNDING THE FILMS, AS PLACED DURING CELL IRRADIATION. D: GAFCHROMIC EBT3 FILMS. E: LIFT SET TO HAVE SURFACE 70 CM FROM THE SOURCE.

Proton Measurements

All positions and depths for irradiation of Gafchromic EBT3 dosimetry films with protons are listed in Table 30. In addition, film irradiation done to visualize beam centration and shape was performed every day before irradiation. These films were not further analysed. The number of films irradiated in each position and the dose delivered had great variation and is not listed in detail. Film irradiations were conducted to evaluate the beam positioning and homogeneity, as well as for dosimetric purposes.

Analysis

The scanned films were analysed using IDL 8.5. The optical density (OD) was calculated as an average optical density in a circular area with radius 1 cm. The centre of the averaged area was placed at the centre of the irradiated area. The best fit to the parameters a, b and c in Table 17 was found by using Least Squares Fitting (LSF) with the known dose and the corresponding measured OD. This was done for all three colour channels individually, and for the average over all three channels. The most accurate result was obtained using an average of all the three colour channels, red, green and blue.

3.2.3 Ionization chamber dosimetry

X-ray

Dosimetry was done at the x-ray machine used for x-ray cell survival experiments in order to decide the exact dose-rate. Setup was similar to Gafchromic EBT3 calibration, as seen in Figure 22. The only difference was that the dosimetry films were replaced with an ionization chamber, and the steel chamber was removed for some measurements. A cylindrical, kerma in air calibrated ionization chamber was used for dose measurements. The calibration coefficient was $N_{k,air}(mGy/nC) = 43{,}77 \pm 0{,}39$, for irradiation with ^{60}Co and the Kerma-rate was 11 mGy/s. Calibration was obtained in ambient conditions with temperature,T_0, 20^{o}C and pressure, p_0, 1013 hPa. Dose to water is given in equation 28 (Rosser, 1996).

$$D_w = M_u N_k k_u \left(\frac{\bar{\mu}_{en}}{\rho}\right)_{w,air} p_u \tag{28}$$

Where D_w is the dose to water in Gy, M_u is the chamber reading measurement in nC corrected to the ambient conditions for calibration(pressure and temperature), N_k is the calibration factor for standard ambient conditions, k_u is a factor that accounts for the change in spectral distribution of the x-rays when moving from air to water, $(\bar{\mu}_{en}/\rho)_{w,air}$ is the mass energy absorption coefficient ratio between water and air, averaged over the photon spectrum at 5 cm water depth, and p_u is the perturbation factor. The room temperature, T, was 23^{o}C and the pressure, p, was at 1029 hPa during dosimetry measurements. M_u was found by multiplying the direct measurement M with the correction factor k_{Tp}, found from equation 29.

$$M_u = M \cdot \frac{273{,}2 + T}{273{,}2 + T_0}\frac{p_0}{p} = M \cdot k_{Tp} \tag{29}$$

All factors included in equation 28 is listed in Table 4. Perturbation factor (Rosser, 1996) and mass energy absorption coefficient ratio (Attix, 1986) were found from literature.

TABLE 4. KNOWN FACTORS FOR DOSIMETRY AT THE X-RAY UNIT INCLUDED IN EQUATION 28.

$N_{k,air}$	k_u	$(\bar{\mu}_{en}/\rho)_{w,air}$	p_u	k_{Tp}
$43{,}77 \pm 0{,}39$	≈ 1.0	1.07	$1{,}023 \pm 0{,}001$	$0{,}9945$

Measurements where done both inside and without a steel chamber as the one used for x-ray cell survival experiments. The ionization chamber was irradiated at various positions in the field, with and without the build-up cap. Each irradiation was for 2 minutes, with 10 mA and 220 keV.

^{60}Co

Dosimetry was done at the ^{60}Co treatment unit in order to verify the dose rate from the source, estimated by exponential radioactive decay in time, from previous measurements. Temperature, T, was at 16^{o}C and pressure, p, at 1013 hPa. Setup was similar to the one for dosimetry film calibration as can be seen in Figure 23, except the films were replaced by an ionization chamber. Measurements were conducted at 5 positions in the radiation field, which are illustrated in Figure 24. The ionization chamber was dose to water calibrated for ^{60}Co with a calibration factor of $N_{D,W}(mGy/nC) = 47{,}69 \pm 0{,}48$. Thus the dose is given by equation 30.

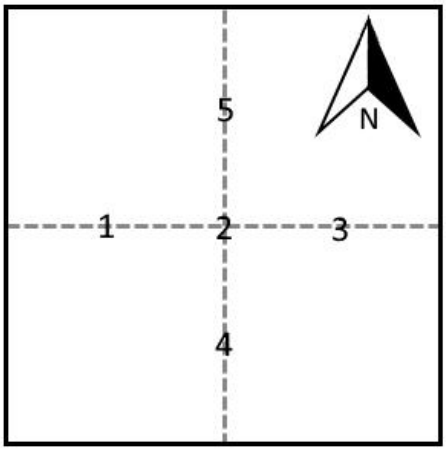

FIGURE 24. ILLUSTRATION OF IONIZATION CHAMBER MEASUREMENT POINTS IN THE ^{60}CO RADIATION FIELD. SEEN FROM ABOVE. NUMBERS INDICATE POSITIONING OF THE SENSITIVE AREA OF THE IONIZATION CHAMBER, AND THE ARROW INDICATES THE ORIENTATION.

$$D_W = N_{D,W} \cdot M \cdot k_{Tp} \tag{30}$$

where D_W is the dose to water in Gy, $N_{D,W}$ is the calibration coefficient in Gy/nC, M is the ionization chamber output, and k_{Tp} is the correction for pressure and temperature to ambient conditions. Known coefficients for dose calculation are given in Table 5.

TABLE 5. COEFFICIENTS NEEDED FOR ^{60}CO IRRADIATION DOSE CALCULATION WITH EQUATION 30.

$N_{D,W}(mGy/nC)$	k_{Tp}
$47{,}69 \pm 0{,}48$	$0{,}987$

Protons

Before each cell irradiation experiment, dosimetric measurements were conducted with an ionization chamber and a monitor chamber. The monitor chamber was included in order to ensure precise dose measurements. Sometimes dosimetry was done a day before each week of experiments in addition to these daily measurements. Measurements were performed at different depths and distances from the beam exit window. Different depths in the Bragg-Peak was achieved using layers of "solid water" (Nylon6), and of Parafilm. In some cases the cell dish bottom was used as an absorber as well. All combinations of depths, ionization chamber positions and monitor chamber positions for each setup and experiment can be seen in Appendix A, Table 31. Each depth component with corresponding thickness, density, stopping power and water equivalent thickness can be seen in Table 6.

TABLE 6. WATER EQUIVALENT THICKNESSES OF DEPTH COMPONENTS USED IN PROTON DOSIMETRY.

	Thickness (mm)	Density rel. to water	Stopping power rel. to water at ≈5 MeV	Water eq. effective thickness (mm)
Parafilm	0.130	0.90	1.09	0.128
Nylon6 (N6)	0.500	1.15	1.02	0.587
Film(EBT3)	0.280	1.33	0.93	0.347
Dish bottom	0.850	1.04	0.99	0.873
Half EBT3*	0.155	1.32	0.93	0.190
*** Half thickness of dosimetry film (EBT3) including the whole active layer.**				

3.3 Clonogenic Cell Survival Experiments

To obtain a measurement of surviving cells after *in vitro* irradiation, we used the Clonogenic assay. The aim was to seed a known amount of cells in dishes, irradiate them, and let the surviving cells form colonies large enough to count.

3.3.1 Equipment, Chemicals and Sterile techniques

Chemicals

For the T98G cells we used sterile filtered RPMI 1640 medium (Lonza, Belgium). To detach the cells they were trypsinized with EDTA trypsin (Lonza, Belgium). Upon fixation the cell colonies were rinsed with PBS Phosphate-buffered saline (Lonza, Belgium), fixated with technical ethanol (Antibac, Norway) and dyed with Methylene blue. 75% ethanol Antibac overflatedesinfeksjon (Antibac, Norway) was used for surface sterilization.

Equipment

For subculturing, 25 cm^2 (5 ml) sterile flasks (Thermo Fisher Scientific Nunc A/S, Denmark) were used, and for experiments these flasks as well as 8.8 cm^2 (3 ml) and 21.5 cm^2 (5 ml) sterile vent dishes (Thermo Fisher Scientific Nunc A/S, Denmark) were chosen. During proton cell irradiation, a thin paraffin film, Parafilm M Laboratory Film (Pechiney Plastic Packaging, Menasha, WI 54952), with thickness 13 mm was sterilized with surface disinfectant and used as a replacement for cell dish lids.

The cells where handled with sterilized and disposable plastic pipettes and tubes (Sarstedt, Germany). Pipettes from 5 mL – 30 mL where used with electrical handles (Pipetus-akku Hirschmann Laborgeräte, Germany), and 2mL pipettes where handled with rubber bubbles. 20-200 µL Pipet-Lite XLS Single Channel Manual Pipette (RAININ, USA) were used for transference of cell solution to Bürker chamber. The Bürker chamber (KOVA,USA) was used for cell counting during seeding.

Three different centrifuges were used; Beckman GS-15 Centrifuge (Beckman Coulter, USA) and Rotofix 32A (Hettich, Germany) at UiO, and Labofuge I Heraeus Christ (Heraeus, Germany) at the Norwegian Radium Hospital (NRH). The cells where centrifuged to pellets

with a Relative Centrifuge Force (RCF) of approximately 150 g. An optical microscope (Nikon TMS, Japan) with x10 magnification was used for monitoring cell growth and conditions, as well as Bürker chamber counting. The cells were kept in incubators between procedures, maintaining 37 ^{o}C, 80% humidity and 5% CO_2 for optimal cell conditions. Two Steri-Cult 200 CO_2 incubators (Forma Scientific, USA), and one Thermo Forma Series II, Water Jacketed CO_2 Incubator (Forma Scientific, USA) were used at UiO. At NRH a Thermo Forma Steri-Cycle CO_2 incubator (Forma Scientific, USA) was used.

Sterile techniques

For keeping a sterile environment, a Laminar flow cabinet (LAF-bench) was used when working with cells, and the bench surface was sterilized by 70% ethanol before and after use. Three different LAF-benches was used, two at UiO: Class 100 Laminar Air Flow cabinet (Gelaire, Australia) and VB 2040 Laminar Air Flow cabinet (Odd A. Simonsen, Norway), and a Class 100 Laminar Air Flow cabinet (Gelaire, Australia) at the NRH. All tubes and pipettes were sterile and disposable, and other equipment used was sterilized by 70% ethanol, autoclaved or dry sterilized by heat at UiO.

3.3.2 The Cell Line

Most normal cells will have a limited amount of cell divisions before they stop dividing. This is caused by the telomere shortening in in the DNA, making the cell stop dividing when the telomere is sufficiently short. What we often can see in cancer cells, is mutations immortalizing the cells and giving them infinite divisions, an ability that can also be manipulated in a laboratory. This will make subculturing possible, giving the opportunity of doing repeated experiments using the same type of cells.

The cell line used in this thesis was the T98G cell line. This is a human cell line originating from a glioblastome multiform brain tumour of a Caucasian male of age 61 (Stein, 1979). The cells used in this thesis were obtained from ATCC, and were subcultered in the Biophysics and Medical Physics Cell Laboratory at the department of physics at Oslo University.

3.3.3 Cell Cultivation

After a period of time, depending on the cell line and proliferation speed, the flask containing the cells will be filled with a layer of cells attached to the treated bottom. When the cells run out of space they stop dividing and are referred to as confluent. To keep them alive and healthy they need space to grow, enough nutrition and protection against infections. The added medium provides antibiotics and important cell growth factors. Twice a week, each Monday and Friday, a fraction of old cells were transferred to new flasks. The fractions of old cells varied from 1/3 to 1/13 as the speed of proliferation fluctuated over time after the cells were thawed. Change of medium was conducted three times a week, every Wednesday, and in combination with the subculturing every Monday and Friday. This was done by the laboratory engineer.

First, the old medium was removed, then the cells were rinsed twice by adding and removing 1.5ml trypsin. The flask with the cells was left in an incubator until the cells detached from the bottom, usually taking 2-5 minutes. When all the cells had detached, an amount of fresh medium was added and the solution was gently suspended. The amount of added medium should correspond to the fraction of cells being moved to a new flaks. 0.5 ml should be added to a new flask holding 4.5 ml fresh RPMI. When cells were needed in experiments, these were ordered from the cell laboratory, and flasks were subcultered 1-3 days before the day of the experiments.

3.3.4 Seeding

A 25 cm^2 flask with cells was first rinsed with 1.5 ml trypsin, then 3 ml trypsin was added and it was put in an incubator for 5 minutes. After the cells had detached, they were suspended to single cells by passing them through a 2 ml needle 3-6 times. 3 ml medium was added to neutralize the effect of the trypsin, and the cell solution was rotated in a centrifuge (Rotofix 32A) at approximately 144 G for 5 minutes to a pellet. The trypsin-medium solution was removed, and 2.5 ml fresh medium was added.

The solution was diluted 1:10, and a small sample of the solution was counted in a Bürker chamber. The solution was then diluted to different concentrations of cells, and pipetted to

dishes prepared with the proper amount of RPMI. A 25 cm^2 flask was added approximately 10 000 cells, for multiplicity evaluation.

3.3.5 Incubation and Fixation

After irradiation the cells were kept in an incubator, keeping the temperature at 37 °C, and the CO2 level at 5.0 %. The cells were left in the incubator to form colonies in a period of 10 days to three weeks, depending on given dose and proliferation speed of the cells. When the colonies were sufficiently large, about 50 cells per colony, they were fixated.

The medium on the dishes were removed, and the dishes were rinsed with approximately 1.5ml PBS. The PBS was removed and 1.5 ml of 75 % technical alcohol was added and left for 3-5 minutes. Then the alcohol was removed and colour was added and left for 3-5 minutes. The used colour was poured back, and the dishes were rinsed in a regular, cold water-bath. The rinse with water was repeated about 4 times for each dish before it was put to dry.

3.3.6 X-ray irradiation

The x-ray experiments were performed at the Roentgen laboratory, room VK08 in the chemistry building at UiO. Cells were seeded and prepared in dishes/flasks the afternoon previous to irradiation and left in an incubator over night. 3 mL (8.8 cm^2) dishes was used for the first experiment named “X-ray1”, and 5mL (25 cm^2) flask was used for the two latter: “X-ray2” and “X-ray3”. All cell containers where transported to an incubator closer to the irradiation room, and prepared in a LAF-bench located in a room with a temperature of 37 ^oC. At 37 ^oC the cells have the highest proliferation speed, while below this temperature the cells may be arrested in the cell cycle, which gives time for repair leading to a higher resistancy against radiation. As it was desired to have conditions similar to in vivo irradiation, it was vital to keep the temperature as close to 37 ^oC as possible to avoid unwanted effects.

Preparations included removing the medium from the containers. In the case of cell dishes, sterilized Parafilm was wrapped around the side of the dish to close the gap between the bottom and lid. In the case of flasks the cap was closed thightly after removal of the

medium. For proton experiments the medium had to be removed due to the dishes being situated vertically during irradiation. The medium would in any case have to be removed due to the low proton energy because the medium would have absorbed all the protons. It was therefor decided to remove the medium for the x-ray experiments as well, to try to keep conditions during irradaition at different modalities as similar as possible. By removing the medium the cells were exposed to a great difference in pH level, so it was attempted to keep the time without medium as short as possible. When the gap between the lid and bottom of the dishes, and the caps of the flaskes, were closed, the cells were kept sterile and protected from infections. In addition the cells were kept from drying out after the removal of the medium.

The cell dishes/flasks where then placed 5 at a time in a steel chamber pre-heated to 37 ^{o}C, and transported to the irradiation chamber. The chamber was placed on a heated plate in order to maintain a temperature of 37 ^{o}C, and irradiated for the determined period of time. After irradiation, fresh medium was added. The irradiation setup can be seen in Figure 25. Multiplicity flasks were fixated after irradiations had finished, in order to correct for all the cells that were not single cells, but douplets or triplets.

A total of six experiments were conducted, three experiments giving results. The doses, number of cells seeded and number of dishes/flasks determined for the three clonogenic x-ray experiments can be seen in Appendix A, Table 32. The irradiation time on the x-ray machine corresponding to each dose in are also shown in Appendix A, Table 33. The cells were then stored in an incubator for 10-14 days, forming colonies. When colonies were visible and of wanted size they were fixated, dried and counted.

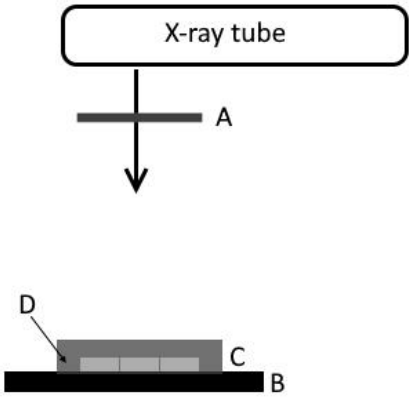

FIGURE 25. ILLUSTRATION OF CELL IRRADIATION WITH X-RAYS. CELL DISHES WERE IRRADIATED VERTICALLY FROM THE TOP WITH 220KEV X-RAYS, IN A STERILIZED STEEL CHAMBER. THE CHAMBER WAS PLACED ON A PLATE HEATED BY WATER TO KEEP THE TEMPERATURE AT 37°C. A: X-RAY FILTRATION. B: HEATED PLATE. C: STEEL CHAMBER. D: CELL DISHES.

3.3.7 ^{60}Co irradiation

^{60}Co- irradiations and seeding were performed at NRH. Cells where seeded in 5 mL dishes the afternoon previous to irradiation, and left in an incubator overnight. Preparations were performed in a sterile environment in a LAF-bench. The medium was removed, and the gap between lid and bottom of the dish was sealed with Parafilm. The dishes were placed on a heated board sterilized with 70 % ethanol and positioned in SSD = 65 cm with a lever. A Styrofoam lid was placed over the cell dishes to help maintain 37 ˚C. An illustration of the setup can be seen in Figure 26. The dishes were irradiated vertically from the top. Determined doses, number of cells and dishes are shown in Table 34. After irradiation fresh medium was added, and the dishes were placed in an incubator for 10-20 days until colonies had reached the proper size. They were then fixated, dyed and counted. Three identical experiments were performed.

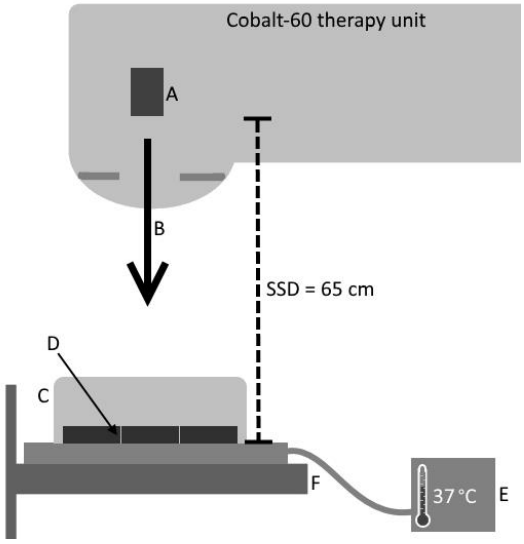

FIGURE 26. ILLUSTRATION OF CELL IRRADIATION WITH A ^{60}CO TREATMENT UNIT. CELLS WERE IRRADIATED VERTICALLY FROM THE TOP IN DISHES, 4 AT A TIME. THEY WERE PLACED ON A HEATED BOARD AND COVERED WITH A STYROFOAM LID IN ORDER TO MAINTAIN 37 °C. THE BOARD WAS POSITIONED IN SSD = 65 CM USING A LEVER. A: ^{60}CO SOURCE. B: COLLIMATED BEAM. C: STYROFOAM LID. D: CELL DISHES. E: HEATER CONNECTED TO A BOARD. F: POSITIONING LEVER.

3.3.8 Proton irradiation

The clonogenic cell survival experiments with 16-17 MeV proton irradiation were performed at OCL, at the University in Oslo. Cell seeding was done at two laboratories at the Biophysics and Medical Physics department at the university. There were a total of 4 weeks of experiments, with three experiments each week, except the last week were only one experiment was conducted. The same setup was used for all the experiment throughout a week. After results were obtained, the setup was reviewed and improved for the next week of experiments.

The aim was to irradiate the cells with both low LET and high LET values. In order to get a low LET, the cells were irradiated at small depths, before the Bragg-Peak. To get high LET values, solid water and Parafilm was added to reach depths as far back in the Bragg-Peak as possible. Position 1 is referred to as the depth before the Bragg-Peak, and position 2 as the depth in the Bragg-Peak. Setup included a positioning system, dosimetry equipment and a heated cell container. A steel rack with a rail and an attached measuring tape was used to position the equipment horizontally in the beam line. Holders were made to attach the monitor chamber and the ionization chamber to the rail. A heating container and blocks

made from polymethyl methacrylate (PMMA) that could fit inside it was produced as well. The blocks were for holding the dishes in place and keep an even temperature during irradiation.

Before irradiation experiments, pieces of Parafilm cut to cover the cell dish bottoms, and cell dish holders were sterilized with 70% ethanol. The reason for replacing the lid with Parafilm, was due to the thickness of it. If left on, irradiations in front of the Bragg-Peak would not be possible because the thickness of the lid would cause the cells to be far back or behind the Bragg-Peak. Pieces of Parafilm were soaked in ethanol for 20 minutes, and left to dry on a sterile surface in a LAF-bench for 24-48 hours so the ethanol could fully evaporate. This was to make sure the Parafilm would be sterile without traces of the ethanol that could be toxic for the cells. Image of Parafilm left to dry in the LAF-bench can be seen in Figure 27.

Cells where seeded the evening previous to irradiation, and left in an incubator overnight. They had to be given time to properly attach to the treated layer, but not too much time to start dividing so there would still be single cells left. It was important to do the seeding in the evening rather than the afternoon as the cell irradiations did not start until late morning/lunch time due to a more complicated setup procedure than on the x-ray tube and the ^{60}Co unit. The setup of the cyclotron could take 1-4 hours in the morning of irradiation, and would be done by an engineer at OCL. In addition, warmup and nulling of electrometers, and dosimetric measurements had to be done prior to cell irradiation. Transport of cell dishes between incubators over longer distances than a few feet was conducted in a sheet sterilized by autoclave. Both 8.8 cm^2 (3 mL) and 21.5 cm^2 (5 mL) dishes were used in the experiments.

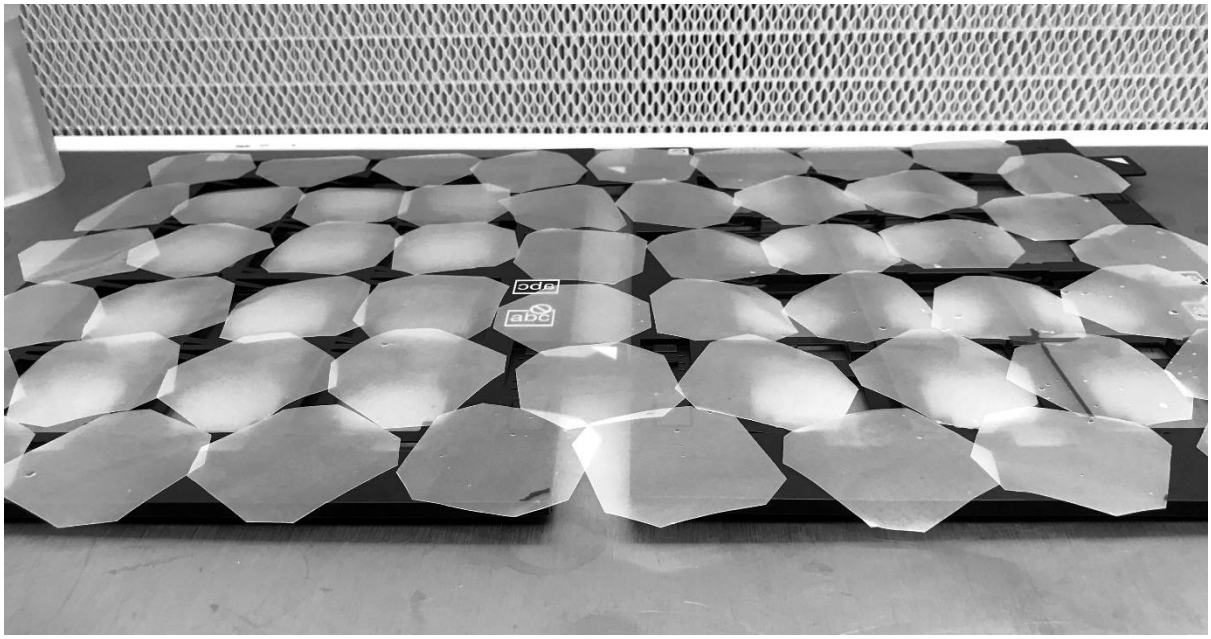

FIGURE 27. PARAFILM PIECES LEFT TO DRY IN A LAF-BENCH AFTER 20 MINUTES SOAKED IN 70% ETHANOL.

The day of each experiment, dosimetry measurements were conducted at OCL. Bragg-peak depth and shape were identified, and a calibration of monitor chamber readings to dose at relevant depths were performed. In the case of setup 1, the monitor chamber was not applied during cell irradiation. Instead a dose/time calibration was performed, and an irradiation time was determined. To change the position in the Bragg-peak, slaps of solid water of 0.5 mm and pieces of Parafilm were put in front the ionization chamber. Two positions in the Bragg-peak were chosen for irradiation, and the corresponding depth was achieved by using solid water and Parafilm in front of the cell dish during irradiation. There was always one Parafilm attached to the cell dish as a lid to protect the cells from the non-sterile surroundings, as the dish lid was too thick for the proton energy of 16 MeV.

After dosimetry and calibration, the connection between the monitor chamber output and the dose at a defined depth was found. This produced a calibration constant k dependent of depth as can be seen in in equation 31. By this equation the monitor chamber output was found to match each desired dose level. Each day new calibration constants were found.

$$D(x) = f_{MC}^{IC}(x) \cdot N_D \cdot O_{MC} = k(x) \cdot O_{MC} \tag{31}$$

Where $D(x)[Gy]$ is the delivered dose in a position x in the Bragg-Peak, f_{MC}^{IC} is the fraction between the ionization chamber (IC) output and the monitor chamber (MC) output at the same position x, $N_D[mGy/nC] = 1.411$ is the dose calibration constant for the ionization

chamber, and $O_{MC}[nC]$ is the MC output. k is the combined constant $f_{MC}^{IC} \cdot N_D$, and is unique for each experiment as the f_{MC}^{IC} also is. In the case of setup 1, an irradiation time was determined.

Then the heated cell container was positioned in such a way that the cell dish bottom position would correspond to the ionization chamber position during measurements. The height was adjusted with a laser to ensure alignment. Solid water and pieces of Parafilm to achieve two depths was prepared as well.

Dishes were taken to the LAF-bench and prepared at the cell laboratory for irradiation one or two at a time. The LAF-bench was situated in a room with a temperature of 37 ^{o}C. Medium was removed, the dish was covered with Parafilm and sealed with tape. Each dish was uniquely marked to be corresponded with a delivered dose and a position in the Bragg-Peak. In the case of setup 1, two dishes were stacked on top of each other. The top one would then be in position 1 in the BP, and the bottom one would be in position 2. The dishes were placed in a holder, and put in a sterilized Styrofoam box together with heated water elements to maintain a temperature 37 ^{o}C.

The dish was then transported by foot to the OCL situated a short distance from the cell laboratory. The holder with the cell dish was placed in the heated container attached to the rack. The determined dose was then attempted delivered, and the monitor chamber reading, and/or irradiation time was noted. When the monitor chamber was in use, a live video feed was sent to the cyclotron operating laboratory to be able to time the target dose delivery. For position 1 irradiations, nothing was placed in front of the cell dish. For position 2 the amount of solid water and Parafilm was put in front of the heated cell container was decided from dosimetry measurements.

After being put back in the Styrofoam box, the dish was transported back to the cell laboratory, Parafilm was removed, fresh medium was added and the lid was placed back. The irradiated cells where left in an incubator for 10-14 days until colonies had formed. When they had reached desired size they were fixated, dyed and counted.

Setup 1

The first week of clonogenic cell survival experiments at OCL with 17MeV protons in April 2016, three experiments were conducted. A 50 µm W scattering filter was attached on the beam exit window. A dose rate and position in the Bragg-Peak at position 1 and 2 was decided from dosimetric measurements. No solid water (Nylon6) or additional Parafilm other than the ones covering each dish was added. Two dishes were irradiated stacked upon each other simultaneously. In front of the dishes a styrofoam piece cut to fit in the container was placed in order to keep an even temperature during irradiation. The monitor chamber was removed during cell irradiations as dosimetric measurements showed that the dish in position 2 would end up behind the Bragg-Peak and have a dose rate of 0 if it was included. Setup 1 is illustrated in Figure 28

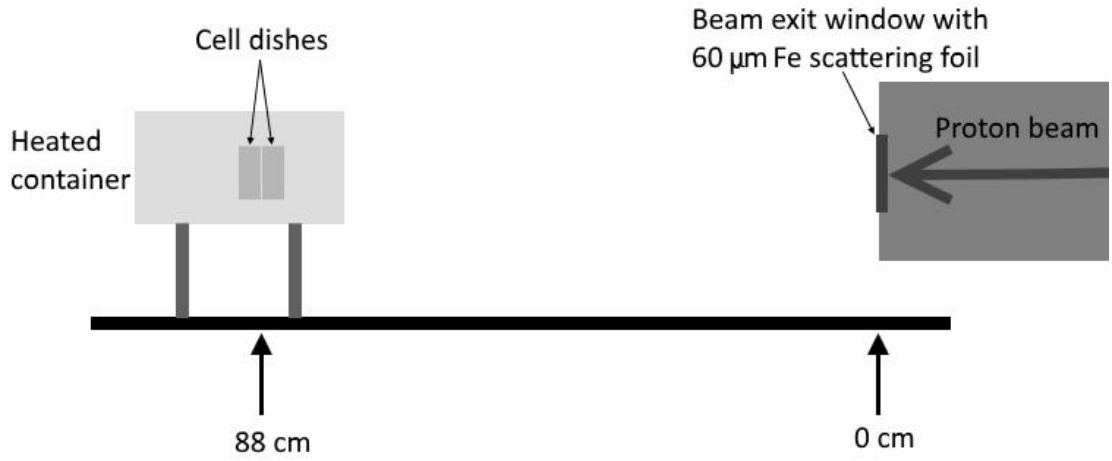

FIGURE 28. SCHEMATIC ILLUSTRATION OF SETUP 1 FOR CELL IRRADIATION AT OSLO CYCLOTRON LABORATORY (OCL). THE 16 MEV PROTON BEAM PASSED THROUGH THE BEAM EXIT WINDOW HORIZONTALLY, AND WAS SCATTERED PASSING THROUGH THE IRON SCATTERING FOIL. THE CELL DISHES WERE STACKED VERTICALLY SO THE RADIATION FIELD HIT PERPENDICULAR TO THE CELL DISHES. THE TWO LAYERS OF CELLS WERE IRRADIATED IN TWO DIFFERENT POSITIONS IN THE BP. THE CELLS WERE KEPT IN THE HEATED CONTAINER DURING IRRADIATION TO KEEP THE TEMPERATURE STABLE AT 37 ^{O}C.

The number of seeded cells and number of dishes for each position was the same for all three experiments. These can be seen in Table 35. For these experiments 3mL dishes were used. The dose rate in position 1 on the first day of experiments was 3.729 Gy/min, and was adjusted to this on the two following days. The dose rate at position 2 would vary slightly due to variations in proton energy each day. Irradiation time and approximate doses at the two positions is listed in Table 7. The three experiments using setup 1 has been named;

“proton_setup1_1”, “proton_setup1_2” and “proton_setup1_3” chronologically after date of irradiation.

TABLE 7. TARGET IRRADIATION DOSES AND IRRADIATION TIME AFTER DOSIMETRIC MEASUREMENTS FOR THE THREE EXPERIMENTS USING SETUP 1.

Positon	Approximate target dose (Gy)	Irradiation time
-	0	0 sec
1	2	32 sec
2	3	
1	5	1 min 20 sec
2	7.5	
1	10	2 min 40 sec
2	15	

Setup 2

Three clonogenic cell survival experiments with 17 MeV protons using setup 2 were conducted in June 2016. From the first week of experiments to the second, a few changes were made. Firstly, the scattering foil was changed from 60 µm Fe, to 50 µm W. This was to give better homogeneity in the beam, and to have a smaller energy loss through the foil. This would enable us to include the monitor chamber during irradiations for better dosimetry and more accurate dose delivery. This solved the problem with significant fluctuation in proton flux and consequently in the dose rate (Gy/time) that turned out to cause great problems in delivered dose accuracy in setup 1.

Secondly, it was decided to irradiate one dish at a time. A greater depth resolution in position 2 was desired, and as we also wanted to move position 2 further into the Bragg-Peak. This was made easier by eliminating the thickness of the cell dish bottom. Another problem was discovered; in each irradiated dish from setup 1, a thin donut in the edges had gotten less dose. The dishes had been irradiated in the middle of a container, therefore the low dose region in the edges was assumed to be caused by side-scatter collimation from the holder and heated container. A solution to this problem was to move the cell dish to the front of the container, to minimize this effect. The new setup, named setup 2 is illustrated in Figure 29.

The depth for position 2 was decided from dosimetry in preparation of the clonogenic cell survival experiments. We added 0.5 mm solid water (Nylon6) and a Parafilm in addition to

the Parafilm attached on the cell dish. For position 1, nothing was added. Target doses, number of dishes, and cells seeded in all three experiments using setup 2 is given in Table 36. 5 mL dishes were used for statistical purposes.

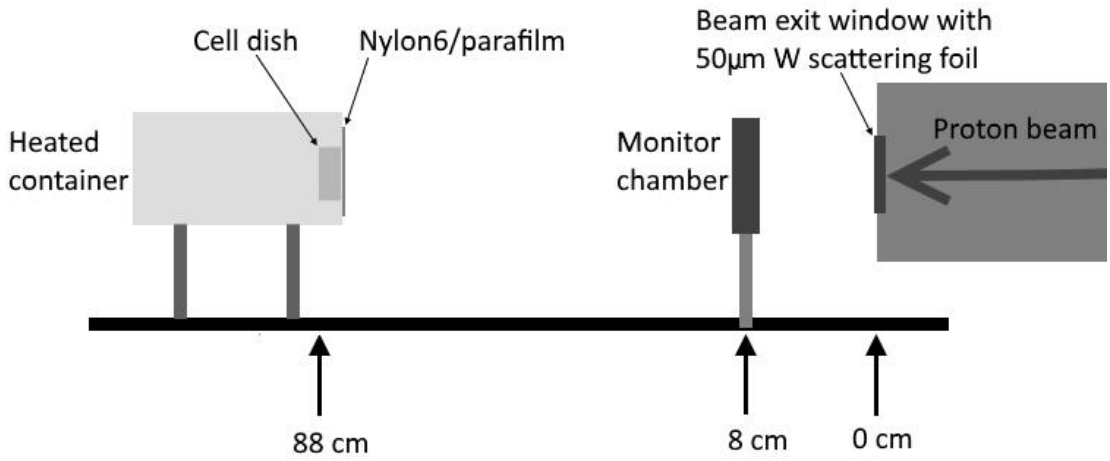

FIGURE 29. SCHEMATIC ILLUSTRATION OF SETUP 2 FOR CELL IRRADIATION AT OCL. THE HORIZONTAL 16 MEV PROTON BEAM WAS SCATTERED THROUGH A TUNGSTEN SCATTERING FOIL. THE BEAM THEN PASSED THROUGH A MONITOR CHAMBER THAT WAS CALIBRATED TO DOSE IN POSITION 2 ON THE DAY OF IRRADIATION. FOR IRRADIATION IN POSITION 1 IN THE BP, NOTHING WAS ADDED IN FRONT OF THE HEATED CONTAINER. FOR POSITION 2, 0.5MM OF SOLID WATER AND ONE PARAFILM WAS ADDED. DETERMINED DOSE WAS ATTEMPTED DELIVERED BY WATCHING A LIVE FEED OF THE MONITOR CHAMBER OUTPUT ON THE ELECTROMETER.

In order to use the monitor chamber (MC) as a measure for dose, a calibration from the dosimetry session previous to each of the three cell survival experiments was used. The calibration factor k for position 1 was assumed to be constant from day to day, as slight variations in energy would cause no significant variation in the IC output per MC output dose-rate in this depth. This was the case for position 1 that was in front of the Bragg-Peak. In the Brag-Peak however, slight energy variations from day to day would cause variations in the calibration constant that needed to be taken into account. Daily measurements to find the relationship between MC output and dose (calibration constant$k$) in position 2 was therefore needed each day. The same MC output was used for both positions. The desired MC output (O_{MC}), for each dose was found by the constant k for position 2, and equation 31.

The experiments using setup 2 was named “proton_setup2_1”, “proton_setup2_2” and “proton_setup2_3”. The individual values of $1/k$ in position 2 for each experiment in setup 2 are listed in Table 8. These were used to prescribe a monitor chamber output to doses in

position 2. Both positions were delivered the same monitor chamber output, not dose. The k -values, and corresponding doses in position 1 were calculated after the experiments were finished. The $1/k$ values as well as estimated dose rates (Gy/min) in position 1 for all three experiments can be seen in Table 9.

TABLE 8. $1/k$ AND ESTIMATED DOSE RATES IN POSITION 2 FOR ALL EXPERIMENTS USING SETUP 2.

	proton_setup2_1	**proton_setup2_2**	**proton_setup2_3**
$\boldsymbol{1/k}$ $[\boldsymbol{nC/Gy}]$	421	537	448.5
Approximate dose rate $[\boldsymbol{Gy/min}]$	7±1	5.1±0.8	4.2±0.7

TABLE 9. ESTIMATED $1/k$, AND DOSE RATES IN POSITION 1 FOR ALL EXPERIMENTS USING SETUP 2.

	proton_setup2_1	**proton_setup2_2**	**proton_setup2_3**
$\boldsymbol{1/k}$ $[\boldsymbol{nC/Gy}]$	830	830	830
Approximate dose rate $[\boldsymbol{Gy/min}]$	3.5±0.6	3.3±0.5	2.3±0.4

Setup 3

Three cell survival experiments with 16MeV protons were performed in January 2017. This time further changes were made. It was decided to optimize position 2 by moving the irradiation distance from the beam exit window. As dose homogeneity was good, the irradiation position was moved closer to the beam exit window. The monitor chamber was moved slightly further away from the beam exit window. In order to deliver the same doses at both positions, an individual k was found for *each position, each day*. Then individual MC outputs were delivered to the two positions to obtain the decided dose levels. In this way the two positions would get the same dose instead of the same MC output. An additional dose point at 14 Gy was added in these experiments in order to investigate high dose effects noticed in the previous experiments. Target doses, number of cells seeded, and number of dishes for all three experiments with setup 3 is listed in Appendix A,

Table 37.

The experiments using setup 3 were named; “proton_setup3_1”, “proton_setup3_2” and “proton_setup3_3”. The new setup can be seen in Figure 30. Position 1 was defined as the

place in the BP when only 1 Parafilm (the one attached to the cell dish) was in front of the irradiation spot. Position 2 was defined as the place in the BP where 0.5mm solid water and three Parafilm (two additional to the one attached to the cell dish) were in front of the irradiation spot. $1/k$ values for the two positions are given in Table 10. The corresponding approximate dose rates (Gy/min) is listed in Table 11.

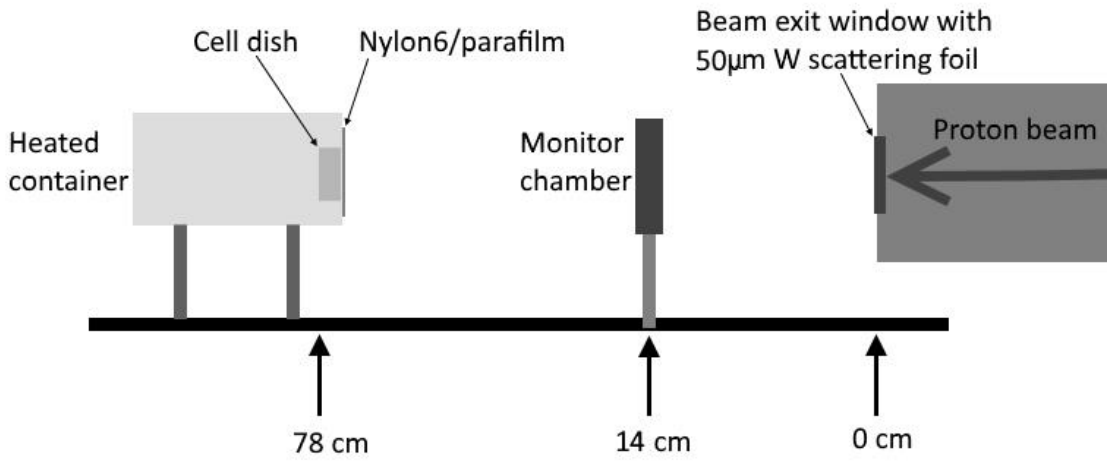

FIGURE 30. SCHEMATIC ILLUSTRATION OF SETUP 3 FOR CELL IRRADIATION AT OCL. THE HORIZONTAL 16 MEV PROTON BEAM WAS SCATTERED THROUGH A TUNGSTEN SCATTERING FOIL. THE BEAM THEN PASSED THROUGH A MONITOR CHAMBER THAT WAS CALIBRATED TO DOSE IN BOTH POSITIONS ON THE DAY OF IRRADIATION. FOR IRRADIATION IN POSITION 1 IN THE BP, NOTHING WAS ADDED IN FRONT OF THE HEATED CONTAINER. FOR POSITION 2, 0.5 MM OF SOLID WATER AND TWO PARAFILM WAS ADDED IN ADDITION TO THE PARAFILM COVERING THE CELL DISH. DESIRED DOSE WAS ATTEMPTED DELIVERED BY WATCHING A LIVE FEED OF THE MONITOR CHAMBER OUTPUT ON THE ELECTROMETER. THE EXACT READINGS WERE REGISTERED FOR EACH IRRADIATION.

TABLE 10. $1/k$ IN POSITION 1 AND POSITION 2 FOR ALL EXPERIMENTS USING SETUP 3.

Experiment	$1/k$ $[nC/Gy]$	
	Position 1	Position 2
proton_setup3_1	667	370
proton_setup3_2	672	552
proton_setup3_3	673*	2283

*Calculated from previous experiments by extrapolation of the dose rate increase between two surrounding positions.

TABLE 11. APPROXIMATE DOSE RATES (GY/MIN) IN POSITION 1 AND POSITION 2 FOR ALL EXPERIMENTS USING SETUP 3.

Experiment	**Approximate dose rates** $[Gy/min]$	
	Position 1	Position 2
proton_setup3_1	2.6	4.7

proton_setup3_2	5.5	7.4
proton_setup3_3	6.1	1.8

Setup 4

One final experiment with 16 MeV protons was conducted in May 2017 with setup 4. This time only one position was investigated, position 2. This was due to a lack of results from the part of the experiments in the Bragg-Peak. For the point in front of the Bragg-Peak enough results had been obtained from the previous experiments. Setup 4 was almost identical to setup 3, except for a few small changes. Due to a slightly lower proton energy, the depth for position 2 had to be reduced. The new depth for position 2 was 0.5 mm solid water, and two Parafilm, where one of the Parafilms were covering the dish. The irradiation distance from the beam exit window was increased slightly in order to pinpoint wanted point in the Bragg-Peak. Setup 4 is illustrated in Figure 31.

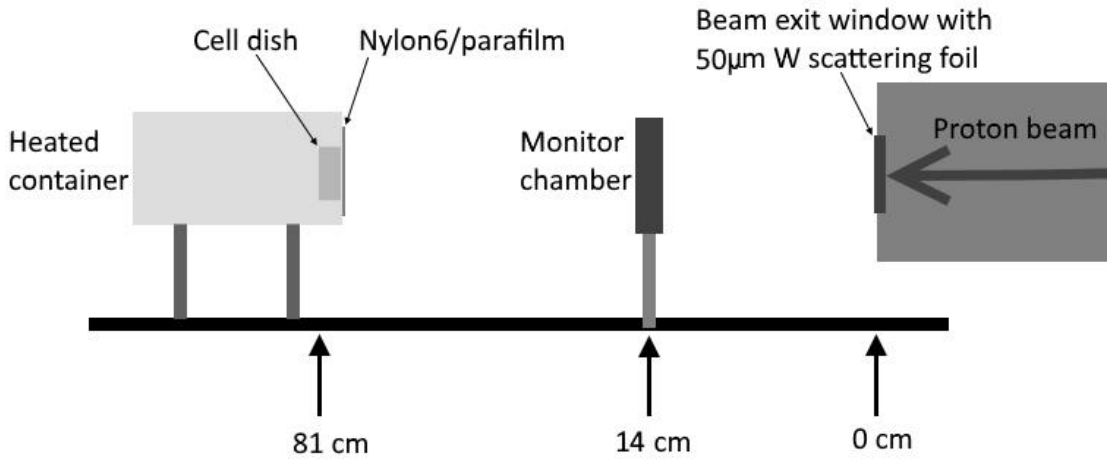

FIGURE 31. SCHEMATIC ILLUSTRATION OF SETUP 4 FOR CELL IRRADIATION AT OCL. THE HORIZONTAL 16 MEV PROTON BEAM WAS SCATTERED THROUGH A TUNGSTEN SCATTERING FOIL. THE BEAM THEN PASSED THROUGH A MONITOR CHAMBER THAT WAS CALIBRATED TO DOSE IN BOTH POSITIONS ON THE DAY OF IRRADIATION. FOR IRRADIATION IN POSITION 2, 0.5 MM OF SOLID WATER AND ONE PARAFILM WAS ADDED IN ADDITION TO THE ONE COVERING THE CELL DISH. DESIRED DOSE WAS ATTEMPTED DELIVERED BY WATCHING A LIVE FEED OF THE MONITOR CHAMBER OUTPUT ON THE ELECTROMETER.

Due to problems with fungi infections on 5 mL dishes, 3 mL dishes with a smaller gap between dish and lid was chosen in order to minimize the risk of infection. Target doses, number of seeded cells and the number of dishes is listed in Table 38. $1/k$ values used for

target monitor chamber output for different doses, as well as approximate dose-rates can be seen in Table 12.

TABLE 12. $1/k$ VALUES AND APPROXIMATE DOSE RATES IN BOTH POSITIONS FOR THE EXPERIMENT WITH SETUP 4.

Experiment	$1/k$ $[nC/Gy]$		**Approximate dose rate Gy/min**	
	Position 1	Position 2	Position 1	Position 2
proton_setup4_1	1011±2	454±2	7.9	3.5

3.4 Water Equivalent Thickness

For calculating thicknesses of components in the setups, water equivalent thickness (WET) (Zhang and Newhauser, 2009) with the thin target approach was used, see equation 32.

$$\mathrm{WET} = t_w = t_m \frac{\rho_m}{\rho_w} \frac{S_m(E_i)}{S_w(E_i)}, \tag{32}$$

where t_w and t_m are the thicknesses of water and the material, respectively. ρ_w and ρ_m are the mass densities of water and the material, respectively, and S_w and S_m are the values for mass stopping power for water and the material at initial energy E_i entering the material.

4 Results

The results from dosimetry and cell survival experiments will be presented related to the setup used, and the day of each setup. A short recap describing the setups can be seen in Table 13. Remember that the cell survival experiments are named by the setup used in addition to a number indicating the order in which experiments were performed.

TABLE 13. SHORT SUMMARY OF THE DIFFERENCES BETWEEN SETUPS AT THE CYCLOTRON FOR PROTON IRRADIATION.

	Scattering filter	**Monitor Chamber position (cm)**	**Irradiation position (cm)**	**Cell irradiation depth of position 2 (mm)**
Setup 1	60 µm Fe	Not included	88	1.1
Setup 2	50 µm W	8	88	0.8
Setup 3	50 µm W	14	78	1.0
Setup 4	50 µm W	14	81	0.8

4.1 Ionization Chamber Measurements

Series of Ionization Chamber (IC) and Monitor Chamber (MC) measurements were acquired the 4 weeks of experiments. The MC was calibrated to delivered dose at the position of the cells, making it possible to calculate the *dose* received by each dish as long as the MC was in the beam line during irradiations. In addition to this, IC measurements were done at different depths in order to find the Bragg-Peak and make a *depth-dose curve* each day of experiments. These were used as a way to estimate the *initial energy* of the protons from tables with stopping powers and CSDA ranges, knowing all materials in the beam line. They were also used for estimation of the *LET* at cell irradiation depths (done by comparison with Monte Carlo simulations). In the depth-dose plots below, the depths are the absorber depth, neglecting the depth of scattering filter, Monitor Chamber and air. In the estimation of proton range and initial energies these components were included.

4.1.1 Depth-dose Bragg-Peak plots

Ionization chamber measurements were performed in different distances (from beam exit window) and depths as described in section 3.2.3 . For each setup the measured dose-rates

were plotted as a function of absorber depth for the distances were cell irradiations were performed. All dose-rate plots were normalized to its maximum value that was estimated from the assumption that at distance 88 cm from beam exit window, with no absorber (zero depth) the dose-rate was at 25 % of maximum. This assumption was made from Monte Carlo simulations performed by collaborators as described in section 4.1.2. The theoretical depth dose-rate curves were estimated from the published shapes by Dahle et al (Dahle et al., 2017), from the same Monte Carlo simulations. These curves were only used for visualization; the experimental points were for used for all calculations.

Setup 1

Setup 1.1

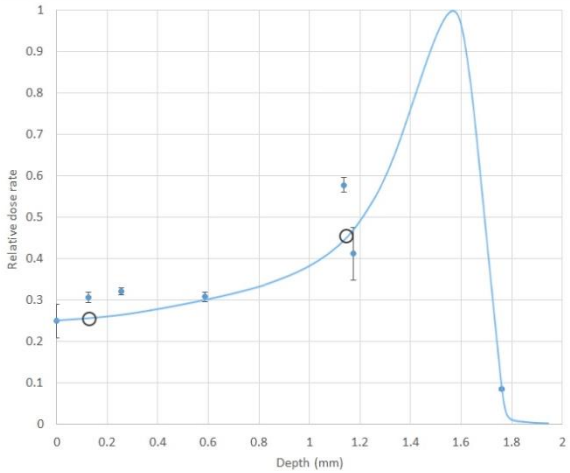

Setup 1.2

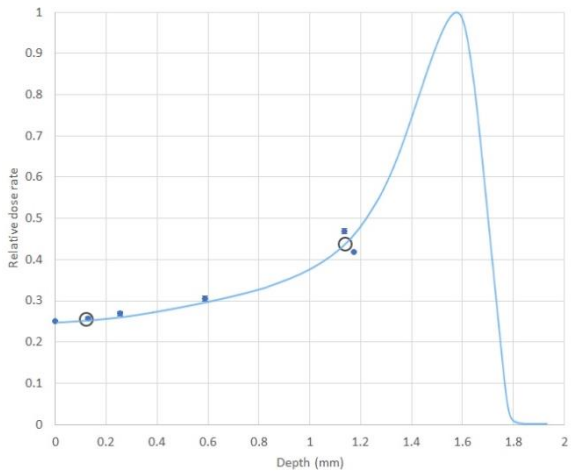

FIGURE 32. BRAGG-PEAK SHAPE ESTIMATED FROM IONIZATION CHAMBER MEASUREMENTS OF DOSE RATES (GY/MIN) CREATED FROM MEASUREMENTS ON SETUP 1. POSITIONS 1 AND 2 FOR CELL IRRADIATION ARE MARKED WITH GREY CIRCLES IN THE PLOT. IC POSITION WAS AT 88 CM, AND AN $60\ \mu m$ IRON SCATTERING FILTER WAS USED.

As described in chapter 3.3.8, the ion source did not provide a stable proton flux and dose-rate to ensure a precise dose delivery. Up to 30 % variation in dose rate (Gy/min) at one point was observed using setup 1, indicating that the experiment would leave big uncertainties and that a different way of measuring dose rate was necessary. The poor accuracy made it impossible to be sure what dose was received by cells irradiated at position 1 and 2. An attempt to estimate the Bragg-peak shape by measured dose-rate point was done, and is shown in Figure 32.

Setup 2

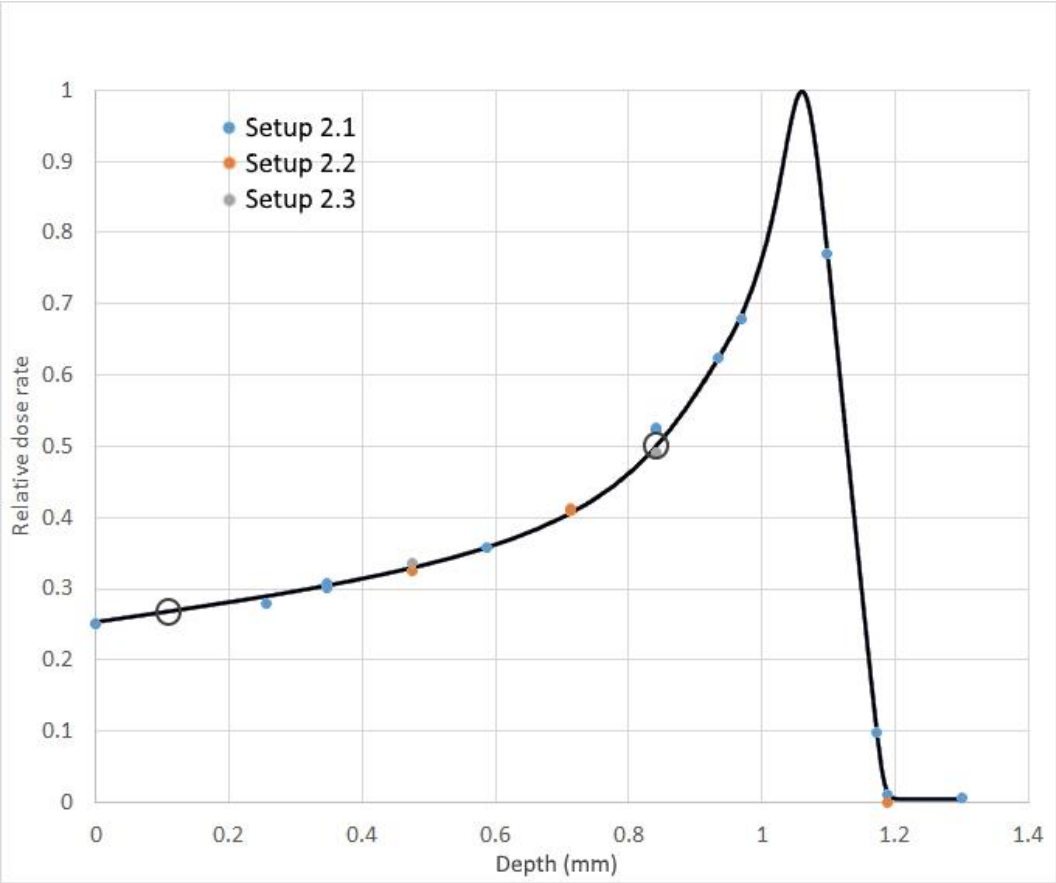

FIGURE 33. BRAGG-PEAK SHAPE ESTIMATED FROM IONIZATION CHAMBER AND MONITOR CHAMBER MEASUREMENTS OF THE DOSE RATE (GY/MC) NORMALIZED TO MAXIMUM VALUE ON SETUP 2. POSITIONS 1 AND 2 FOR CELL IRRADIATION ARE MARKED WITH GREY CIRCLES IN THE PLOT. IC WAS IN POSITION 88 CM WITH MONITOR CHAMBER IN BEAM LINE, AND A $50\ \mu m$ TUNGSTEN SCATTERING FILTER.

In setup 2 the scattering foil was changed from 60 µm Fe to 50 µm W, reducing the range of the protons by 0.1 mm. This was estimated by using the thin-target approach for water equivalent thickness (WET), with stopping power values of 15 MeV (M.J. Berger, 2017). The values used for calculation of scattering filter WET can be seen in Table 14. Dosimetry was optimized by including a monitor chamber in the beam line in order to correct for varying proton flux to ensure the wanted doses. However, the monitor chamber reduced the range further by 0.2 mm. Concurrently, there was a reduction in energy as can be seen in Table 15, resulting in the Bragg-Peak plot shown in Figure 33. Ratios in dose-rates between two absorber depths corresponded well for each day of irradiation, indicating constant proton energy and range.

TABLE 14. SCATTERING FILTERS WET

Scattering filter	Thickness (mm)	ρ_m/ρ_w	S_m/S_w $(15\ MeV)$	**WET (mm)**
Iron	0.060	7.874	0.6409	**0.302**
Tungsten	0.050	19.25	0.4219	**0.406**

Setup 3

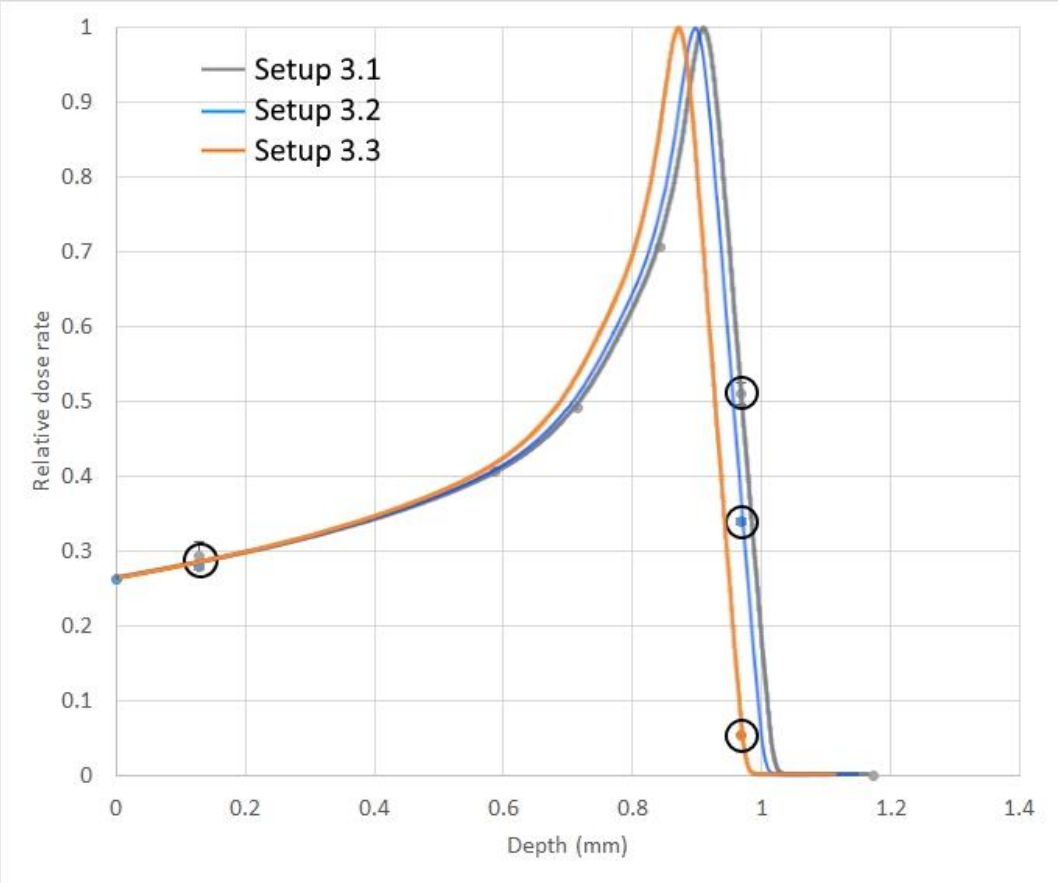

FIGURE 34. BRAGG-PEAK SHAPE ESTIMATED FROM IONIZATION CHAMBER AND MONITOR CHAMBER MEASUREMENTS OF THE DOSE RATE (GY/MC) NORMALIZED TO MAXIMUM VALUE ON SETUP 3. POSITIONS 1 AND 2 FOR CELL IRRADIATION ARE MARKED WITH GREY CIRCLES IN THE PLOT. IC WAS IN POSITION 78 CM WITH MONITOR CHAMBER IN BEAM LINE, AND A $50\ \mu m$ TUNGSTEN SCATTERING FILTER.

In setup 3 the distance between beam exit window and irradiation was reduced by 10 cm. Despite this, the lower initial proton beam energy reduced the proton range from setup 2, as can be seen in Figure 34. As can be seen from the plot, by changing the distance in air, we managed to strike the edge of the Bragg-Peak, in order to achieve a high LET. Very small changes in energy resulted in large dose rate changes from day to day in position 2. It was also clear that small positional uncertainties would cause large dosimetric uncertainties.

Setup 4

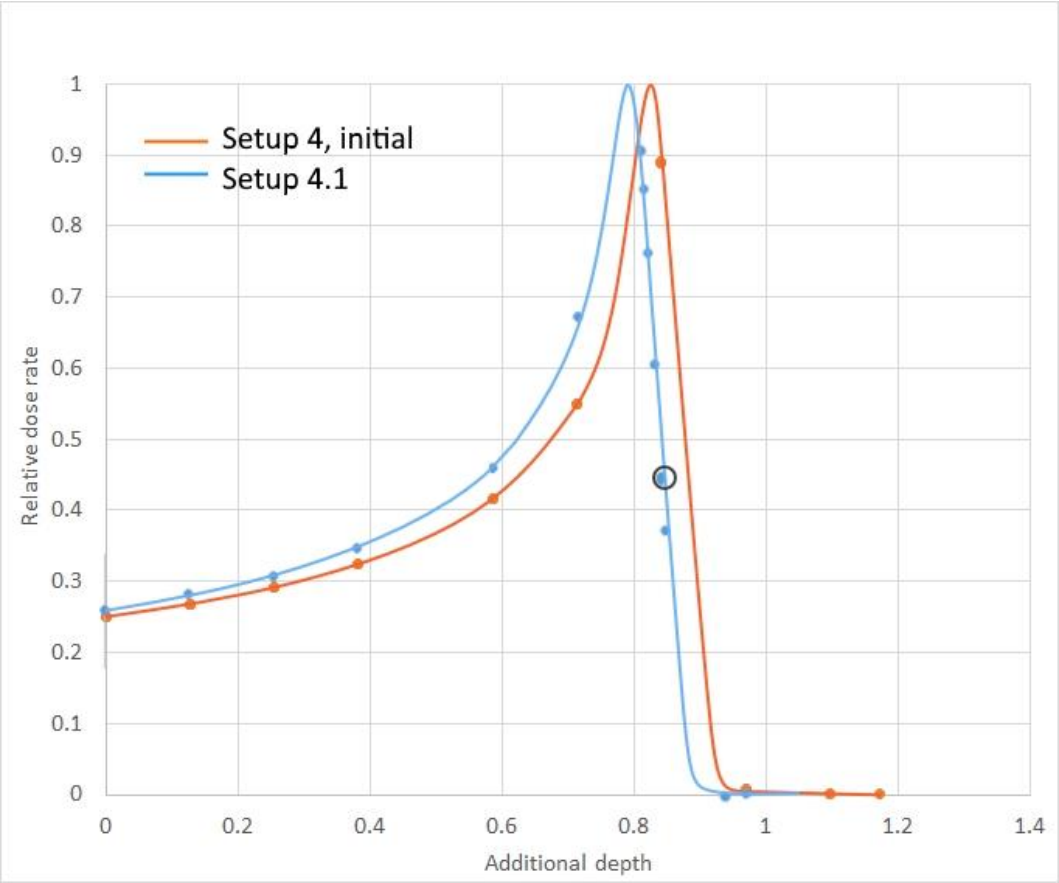

FIGURE 35. BRAGG-PEAK SHAPE ESTIMATED FROM IONIZATION CHAMBER AND MONITOR CHAMBER MEASUREMENTS OF THE DOSE RATE (GY/MC) NORMALIZED TO MAXIMUM VALUE ON SETUP 4. POSITION 2 FOR CELL IRRADIATION IS MARKED WITH A GREY CIRCLE IN THE PLOT. FOR INITIAL MEASUREMENTS ON SETUP 4, THE IC WAS IN POSITION 78 CM, WHILE FOR THE DAY OF CELL SURVIVAL (SETUP 4.1) EXPERIMENTS IT WAS IN POSITION 81. IN BOTH CASES THE MONITOR CHAMBER WAS IN THE BEAM LINE, AND A $50\ \mu m$ TUNGSTEN SCATTERING FILTER WAS USED.

In setup 4 we did new positional changes on the day of cell survival experiments in order to obtain a dose rate in position 2 as close to position 1 as possible. In Figure 35, the Bragg-Peak is plotted against initial measurements a day prior to cell irradiation, and measurements obtained on the same day of the cell survival experiment. One can see that the energy changed from the initial measurements to the day of cell survival experiments (4.1), showing the necessity of using the distance form beam exit window as an additional parameter to obtain similar dose-rates at both irradiation depths.

4.1.2 Initial proton energy

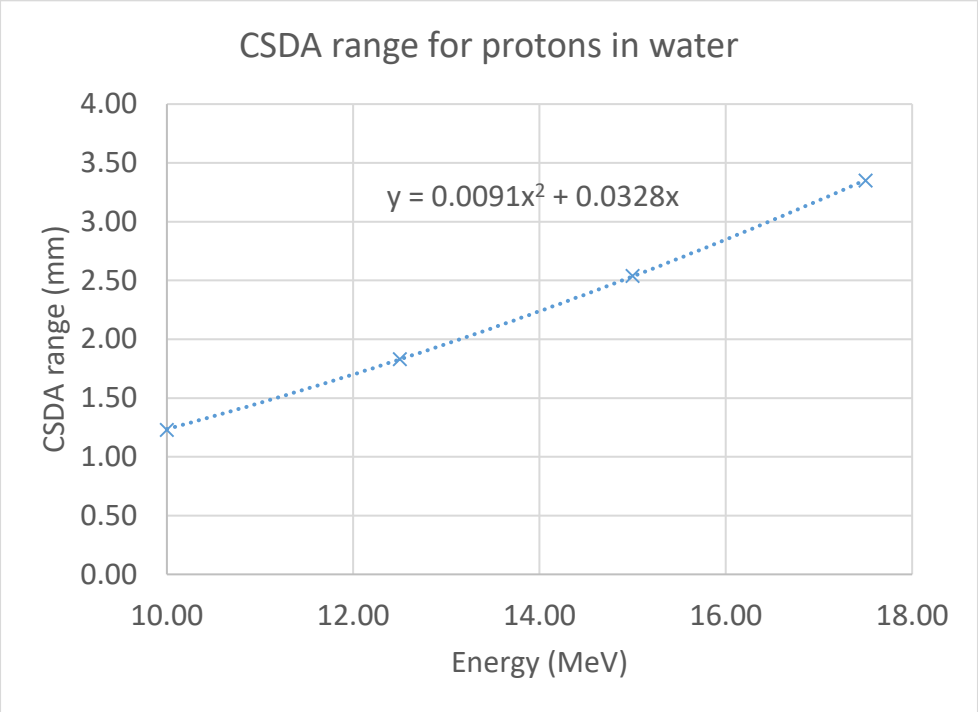

FIGURE 36. 2ND DEGREE POLYNOMIAL FIT TO CSDA RANGES FOR FROM PSTAR TABLES (M.J. BERGER, 2017) IN WATER FOR 10-17.5 MEV PROTONS. FOUND IN THE EXPECTED ENERGY RANGE 10-17 MEV.

A collaboration with the Department of Physics and Technology at the University of Bergen with the representatives Kristian Ytre-Hauge and Tordis Dahle, resulted in Monte Carlo simulations based on our setup at Oslo Cyclotron Laboratory (OCL). The aim of the collaboration was to obtain precise estimates of the LET-values and -spectra in our low-energy proton beam. This was necessary in order to connect our experimentally measured RBE values to the increasing LET values. It was also a way of comparing the LET distribution in the low-energy beam at OCL to clinically available proton energies. The simulations were preformed shortly after experiments using setup 2 (described in section 3.3.8) was conducted, and we provided ionization chamber measurements as well as beam homogeneity measurements from EBT3 Gafchromic dosimetry films in the form of relative dose distribution profiles. Monte Carlo simulations of setup 2, with dose profiles and ionization chamber measurements from setup 2.1 concluded with a proton energy of 15.5 MeV (Dahle et al., 2017). By using CSDA range (approximation to average pathlength) for protons we were able to estimate the proton energy for each day. This was done by observing that the total range (in water equivalent depth) for setup 2 calculated from

measurements, corresponded well with the theoretical tabulated value for CSDA range of 15.5 MeV protons in water. The CSDA range was found from the point at 55 % of maximum dose rate at the distal edge of the Bragg-Peak, from the depth-dose curves measured for each setup and day (see below). As the depth-dose plots only contained absorber depth, the water equivalent thickness (WET) of the scattering filter, air and the monitor chamber was added in order to find the total CSDA range. The measured range from Bragg-peak plots and the estimated CSDA range with corresponding energies can be seen in Table 15. In setup 1 the dosimetry was too imprecise for a day-to-day energy estimation, in addition to only one measurement point in total at the edge of the Bragg-Peak. For setup 2, the energy remained stable within the range of ± 0.1 MeV for all days.

TABLE 15. ESTIMATED INITIAL ENERGY OF PROTONS FROM ESTIMATION OF CSDA RANGE.

SETUP		Measured range* (mm)	Estimated total CSDA range (mm)	Estimated Energy (MeV)
Setup 1		1.65	2.88	16.2
Setup 2	**1**	1.15	2.69	15.5
	2	1.15	2.69	15.5
	3	1.15	2.69	15.5
Setup 3	**1**	0.96	2.39	14.6
	2	0.95	2.38	14.5
	3	0.92	2.35	14.4
Setup 4		0.90	2.36	14.5

* Found from Bragg-Peak plots with dose-rate against absorber depth in section 4.1.1.

4.1.3 Estimation of linear energy transfers (LET)

The LET values were estimated from a Monte Carlo simulation of setup 2 (Dahle et al., 2017). The curves used for estimation can be seen in Figure 37. Measurements, both IC measurements and dose profiles from Gafchromic EBT3 dosimetry films, acquired from setup 2 were used to estimate the initial energy, energy distribution and the LET curve as a function of water equivalent depth. The position in the Bragg-Peak was used to find the corresponding LET value from this curve, see Figure 37B. The estimated LET values are listed

in Table 16.

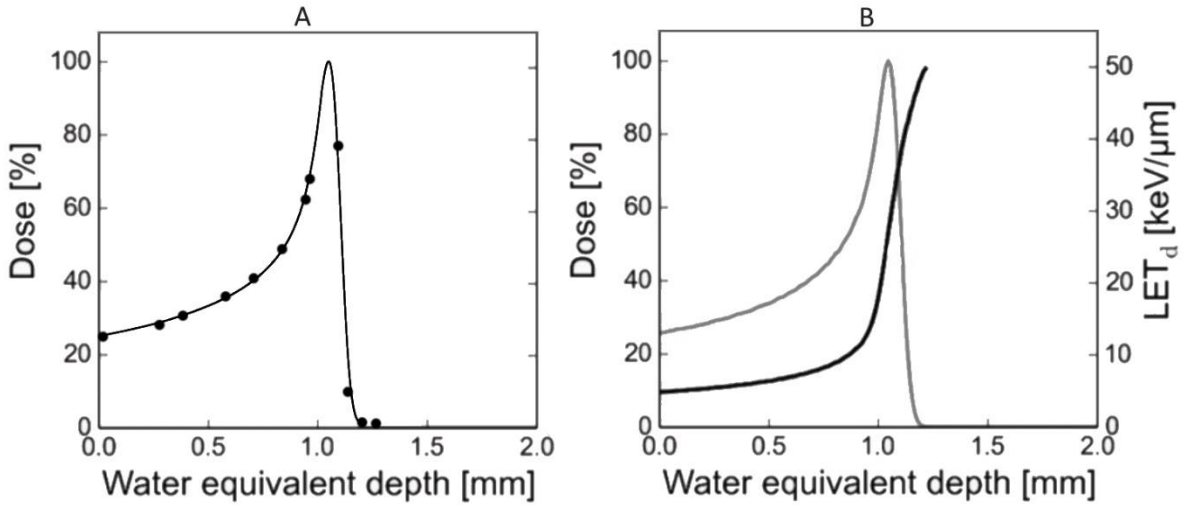

FIGURE 37. DEPTH DOSE CURVES FROM MONTE CARLO SIMULATIONS ON SETUP 2.1 WITH INITIAL ENERGY OF 15.5 MEV. (MODIFIED FROM FIGURE 1 AND FIGURE 3 IN (DAHLE ET AL., 2017)) THE RELATIVE DOSE NORMALIZED TO MAXIMUM IS PLOTTED AGAINST THE WATER EQUIVALENT DEPTH. A: THE SIMULATED DEPTH DOSE CURVE WITH ENERGY ADJUSTED TO FIT THE MEASURED DOSE RATES AT DIFFERENT DEPTHS, PLOTTED TOGETHER WITH THE MEASURED POINTS. B: THE SIMULATED DEPTH DOSE CURVE WITH ENERGY ADJUSTED TO FIT THE MEASURED DOSE RATES AT DIFFERENT DEPTHS, PLOTTED TOGETHER WITH THE CORRESPONDING LET CURVE.

As the dose-rates have relatively large uncertainties, it would not make a lot of sense to distinguish between the LET values in the range 38-44. It would be sufficient to treat them as an average value of 41. With an estimated standard deviation of ± 3 for each of the values, this resulted in a relative standard deviation of the average LET value of 16 %.

TABLE 16. ESTIMATED LET VALUES FOR EACH EXPERIMENT.

	LET (keV/µm)	
	Position 2	Position 1
Setup 1	10	5
Setup 2	10	
Setup 3.1	38	
Setup 3.2	42	
Setup 3.3	44	
Setup 4.1	39	-

4.2 Gafchromic EBT3 Measurements

4.2.1 Calibrations

The Gafchromic EBT3 dosimetry films were calibrated to four different radiation modalities. Originally, it was thought that the electron calibration could be used to estimate the homogeneity in the proton beam and as a tool for calculating dose received in the cell dishes at position 1 and 2. Due to the significant thickness of the films and its impact on dose estimates, the films where rejected for absolute dosimetry in the cell dishes. In addition, it was clear from film analysis that the calibration for electrons could not be applied to proton measurements. We therefore did a proton calibration to be used to estimate beam homogeneity. After discovering the necessity to calibrate the films separately for protons and electrons, it was of interest to investigate the calibration curve differences for the two other radiation qualities used in the thesis as well: x-rays and ^{60}Co. The calibrations resulted in calibration curves following equation 33 (the inverse of equation 27):

$$net\ OD = -\log\left(\frac{a + bD}{c + D}\right) \tag{33}$$

where a, b, c were the calibration curve parameters. The calibration parameters for the four different modalities are listed in Table 17. The plotted curves can be seen in Figure 38. It can be seen that the curves of x-ray and ^{60}Co are more or less the same. The dose response seems to be greatest for protons and electrons, while the response from x-ray and ^{60}Co are slightly lower and overlapping.

TABLE 17. EBT3 FILM CALIBRATION CONSTANTS FOR THE DIFFERENT RADIATION MODALITIES.

	a	b	c
Electrons	10.5 ± 0.6	0.44 ± 0.02	10.5 ± 0.7
X-rays	8.5 ± 1.2	0.46 ± 0.05	8.5 ± 1.3
^{60}Co	9.0 ± 1.8	0.46 ± 0.05	9.1 ± 1.9
Protons	10.2 ± 0.5	0.46 ± 0.01	10.2 ± 0.6

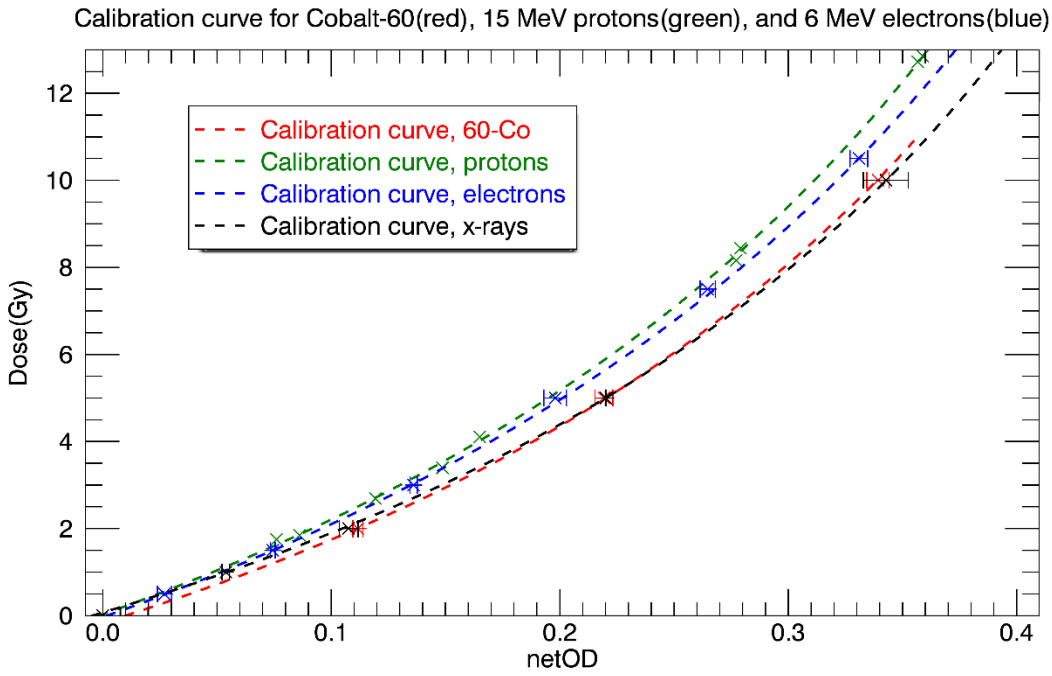

FIGURE 38. CALIBRATION CURVES FOR EBT3 GAFCHROMIC FILMS. THE CALIBRATION WAS DONE INDIVIDUALLY FOR THE FOUR DIFFERENT RADIATION MODALITIES; ^{60}CO, 1 6MEV PROTONS, 6 MEV ELECTRONS AND 220 KEV X-RAYS. THE NET OPTICAL DENSITY (NET OD) CORRESPONDS TO A KNOWN DOSE, RESULTING IN A CALIBRATION CURVE THAT CAN BE APPLIED IN ORDER TO FIND THE DOSE FROM THE NET OD.

4.2.2 Proton Irradiations

All irradiated films were analysed, and an average dose with a standard deviation was calculated inside a circle with a radius similar to petri dish area used in cells survival experiments in the same setup. The circular films in the petri dishes were small so the largest radius possible to be used for analysis was 1.5 cm. In some cases the films suffered from unevenness in the edges, and the radius used was 1.4 cm. For the square films a radius of 2.5 cm was used for experiments using 25 cm^2 dishes. The results of the film analyses are sorted for the four setups and represented in the Appendix B, in Table 39, Table 40, Table 41, and Table 42. Measured dose with standard deviation (σ), positioning and placement of the film, radiation time, water equivalent depth of the active layer in the film, and the dose rate is listed. For setup 4, the films were only used to evaluate the homogeneity, as it was unclear as to how we could use the films for dosimetric purposes.

Homogeneity in the Proton Beam

As a measure of homogeneity, the relative standard deviation (σ) was used. Examples of the dose distributions for two different depths in setup 2 are shown in Figure 39. The relative standard deviations in a radius 2.5 cm was found to be 8 % for position 1, and slightly worse for position 2 at 10 %. Examples of histograms of the dose-distribution in the same depths are plotted in Figure 40.

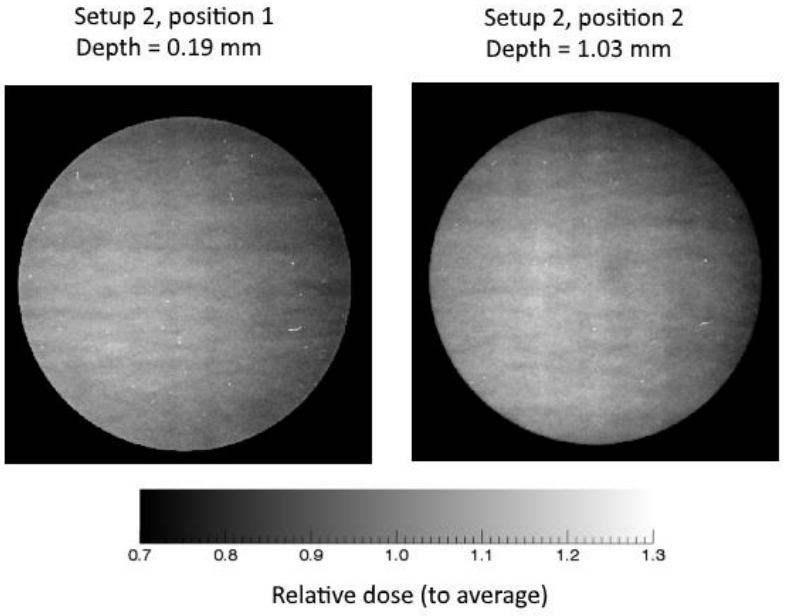

FIGURE 39. DOSE DISTRIBUTION FOR FILMS IRRADIATED IN TWO DIFFERENT DEPTHS IN FRONT OF THE BRAGG-PEAK. BOTH FILMS WERE NORMALIZED TO ITS AVERAGE DOSE. STANDARD DEVIATIONS FOR POSITION 1 AND POSITION 2 IN A RADIUS 2.5 CM WAS FOUND TO BE 8 % AND 10 %, RESPECTIVELY.

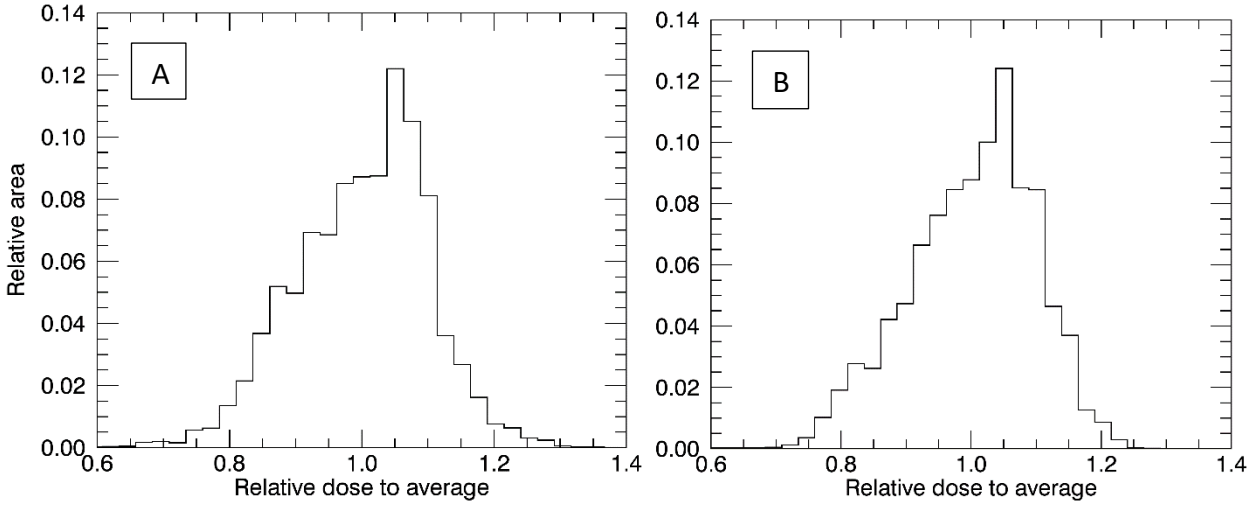

FIGURE 40. DOSE DISTRIBUTION HISTOGRAMS OF EBT3 DOSIMETRY FILMS IRRADIATED IN DEPTHS OF 0.19 MM (A) CORRESPONDING TO POSITION 1 IN SETUP 2, AND 1.03 MM (B) CORRESPONDING TO POSITION 2 IN SETUP 2. THE HISTOGRAMS ARE PLOTTED AS AN AVERAGE OF ALL FILMS IRRADIATED IN THE SAME DEPTH IN SETUP 2.

The homogeneity was estimated for each setup as an average of all relative standard deviations measured using the setup, as they were fairly consistent during each week. Calculated homogeneity can be seen in Table 18. A smaller relative standard deviation indicate better homogeneity. The homogeneity of setup 1 was not optimal, which led to the change of scattering filter from 60 µm iron to 50 µm tungsten (higher Z-material) to achieve more scattering of the protons. In addition, the proton beam shape and centration became better as the engineers preparing the cyclotron for irradiation got more experienced, giving better homogeneity as well.

TABLE 18. BEAM HOMOGENEITY ESTIMATED FROM DOSIMETRY FILMS FOR EACH IRRADIATION SETUP.

Dose homogeneity over cell dish area		
Setup	**Relative standard deviation (%)**	**Cell dish area (cm^2)**
1	19.0	8.8
2	12.6	25
3	10.3	25
4	4.9	8.8

4.2.3 Transforming IC measured dose-rates to averages

The ionization chamber (IC) used in the proton experiments had a radius of 2.5 mm, so the measured dose rate by the IC chamber would not correspond to an average dose over the irradiated cell dish. By analysing the dosimetry films irradiated each day of experiments, a ratio was found between the average dose inside a radius of 2.5 mm, and an average dose across the cell dish. This resulted in a number of dose-rate correction factors to be multiplied with the measured dose-rate from the IC, to ensure correct dose calculation in each dish. All corrections were found from films irradiated at a depth corresponding to position 1. The correction factors are listed in Table 19. For setup 3, film irradiation was done at only one occasion, and a single correction factor was therefore used for all the experiments. The correction factors tend to be similar for each day of experiments, so this is a reasonable approximation.

TABLE 19. DOSE-RATE CORRECTION FACTORS THAT TRANSFORMS A MEASURED DOSE WITH THE IONIZATION CHAMBER TO AN AVERAGE DOSE-RATE ACROSS THE CELL DISH.

Dose rate corrections factors	
Setup 1.1	0.89
Setup 1.2	0.91
Setup 1.3	0.82
Setup 2.1	0.93
Setup 2.2	0.91
Setup 2.3	0.90
Setup 3	0.91
Setup 4	0.97

4.2.4 Observation of anomalies

Quite few film irradiations were performed at the distal edge of the Bragg-Peak (BP). For these, a structure pattern in the dose distribution was observed. Even if the homogenity seemed to be quite good, there appeared to be areas receiving significantly lower doses. The same problem did not appear on the film irraidated in front of the BP. Irraidated films in front of the BP and in the distal egde og the BP can be seen in Figure 41. The films received an average dose of 1.6 and 1.5 Gy respectively.

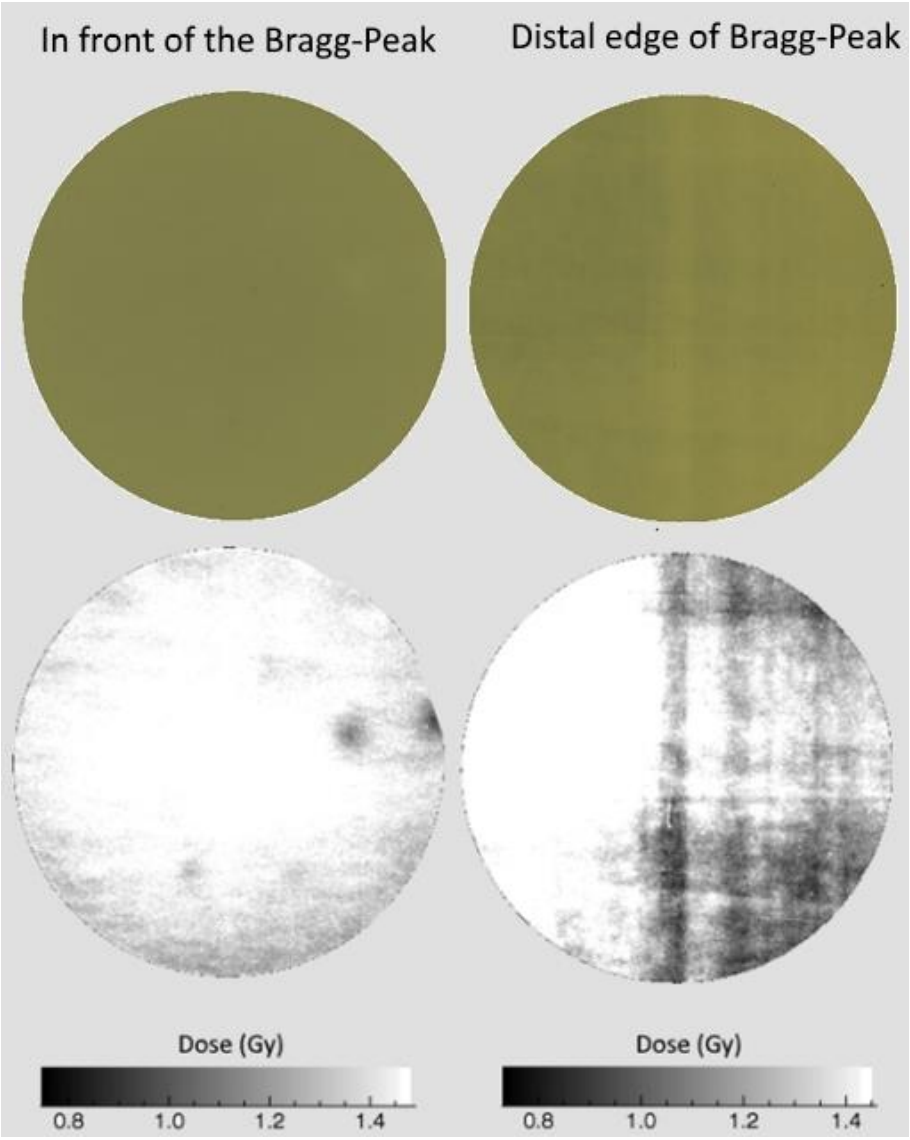

FIGURE 41. IRRADIATED EBT3 FILMS IN FRONT OF THE BRAGG-PEAK (DEPTH OF 0,19 MM) AND IN THE DISTAL EDGE OF THE BRAGG-PEAK (DEPTH OF 1,03 MM) USING SETUP 3.1. THE TOP ONES SHOW HOW THE FILMS LOOK TO THE NAKED EYE, AND THE BOTTOM ONES SHOWS THE DOSE RANGE IN A GREY SCALE BETWEEN 50 % AND 100 % OF AVERAGE DOSE. A STRUCTURE PATTERN IN THE DOSE DISTRIBUTION CAN BE OBSERVED IN THE DISTAL EDGE OF THE BP.

To further investigate this issue, a binary plot of the dose in the range between 50 % of average and average was made. This can be seen in the bottom of Figure 41. In the distal edge of the BP there appeared to be substantial areas receiving less than 50 % of average dose. In front of the BP the same thing could be observed, but in smaller and fewer areas. It was not clear if this was due to the setup or the film structure itself. In further discussion these areas receiving 50 % of average dose or less will be referred to as “cold areas”.

4.3 Cell Survival Experiments

Results from cell survival experiments with x-rays, ^{60}Co and different LET-protons was found. The x-ray survival curves were chosen as the reference in RBE calculations, as the toxicity of elevated pH in ^{60}Co deemed them useless. The results of these experiments are presented in Appendix B, Figure 62. Proton and x-ray survival curves are presented below.

4.3.1 X-rays

Three cell survival experiments were conducted with 220 keV x-rays. Only two of these were included in a fitting to the LQ-model for survival, as one had been exposed to an elevated pH value for longer periods of time than the other ones. Comparing the results to available data for x-ray survival of the T98G cell line (Nina F. Edin, Personal communication) at the institute, supported this assumption. The LQ-fit was therefore fitted to the two experiments together with the three experiments used in the comparison conducted previously by Nina F. Edin.

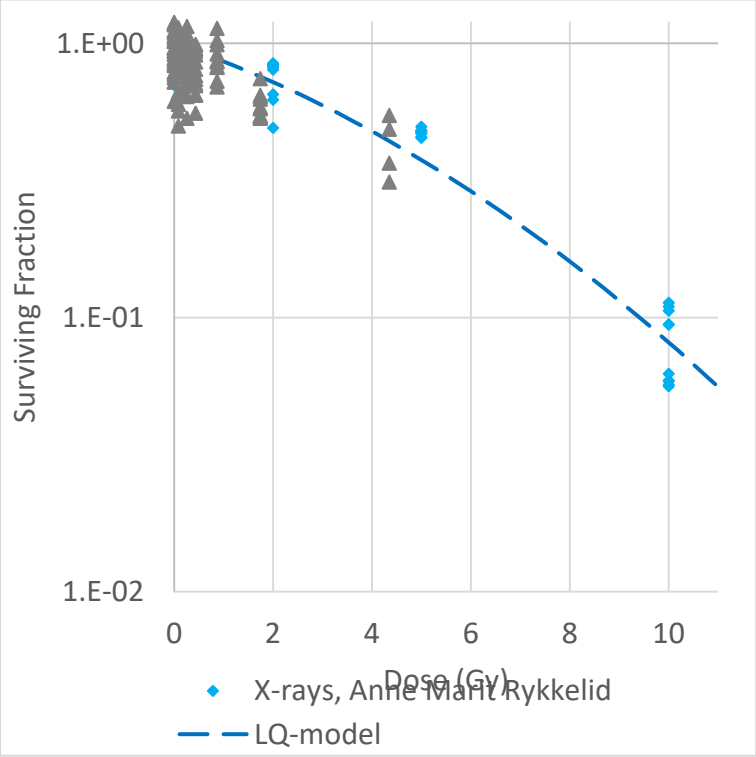

FIGURE 42. SURVIVING FRACTION OF CELLS (T98G) IRRADIATED WITH 220 KEV X-RAYS AS A FUNCTION OF DOSE. EXPERIMENTAL DATA PRODUCED FOR THIS THESIS, PLOTTED TOGETHER WITH PREVIOUS EXPERIMENTS BY NINA F. EDIN. THE RESULTING LQ-MODEL IS PRESENTED AS WELL.

TABLE 20. LQ-MODEL PARAMETERS FOR CELL SURVIVAL EXPERIMENTS WITH X-RAYS

LQ-parameters	
β	0.011 ± 0.002
α	0.14 ± 0.02

4.3.2 Protons

The experimental data from all proton experiments were split into two groups. One group including all cells irradiated with protons with LET values from 5-10 keV/µm, and one group with LET values between 38-44 keV/µm. They will be referred to as Group 1 (low LET) and Group 2 (high LET) respectively. No significant difference between cells irradiated with an LET of 5 and 10 were found, as the 95 % confidence intervals of their fitted LQ –models overlapped, so these were gathered in a single group. No marked difference between the experiments with varying LET values were detected in group 2 either.

In both groups a "tail" was found when moving towards high doses in the cell survival plot. Together with the film anomalies, the "cold areas", this lead us to the theory that there was an issue with the setup, causing some areas with lower doses and thus unexpectedly high cell survival. We will refer to this as *background colonies*. On basis on this, we derived corrections for the background colonies, and fitted the corrected data to the linear quadratic model (LQ-model). Note that all corrections were applied to doses larger than 0, as it would not make sense to correct the un-irradiated controls for background colonies.

The possibility that no correction was needed at all was always present, as there were few dose point available above 10 Gy in group 1, and a LQ-model fit to the uncorrected experimental survival was also applied.

Front of the Bragg-Peak

The resulting surviving fractions for separate dishes in group 1 were calculated, but due to large variations in dose-rates (Gy/min) in setup 1, these were excluded from further analysis. All measured surviving fractions are plotted as single dishes in Figure 43.

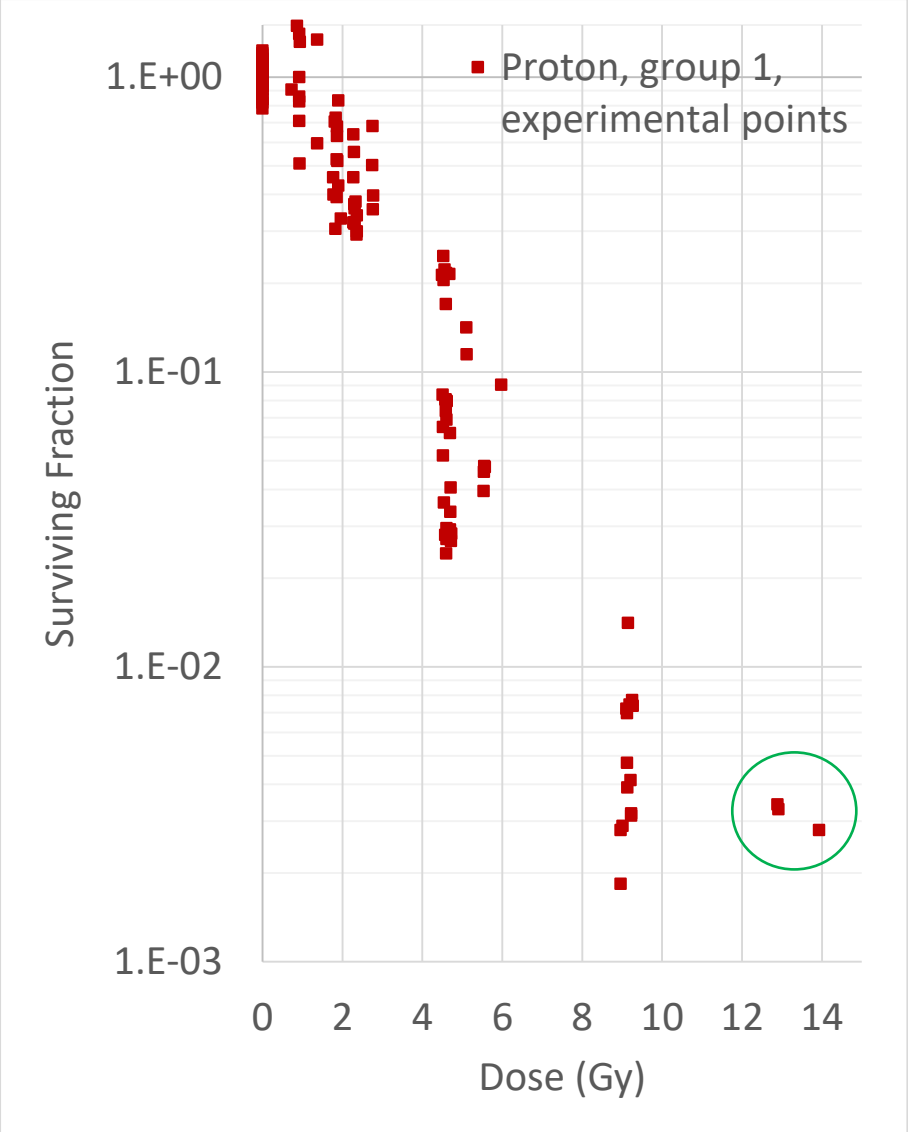

FIGURE 43. SURVIVING FRACTIONS OF SINGLE DISHES IN GROUP 1 (LET FROM 5-10 $\mathbf{keV/\mu m}$) PLOTTED AGAINST DELIVERED DOSE. POINTS WITH A HIGHER SURVIVAL THAN EXPECTED IS MARKED WITH A GREEN CIRCLE.

Analysis - Front of Bragg-Peak

For group 1 (G1), the collection of all cell survival experiments in front of the Bragg-Peak, the survival was modelled in two ways. The models were developed under the assumption that the survival of *irradiated cells* were to follow a pure LQ-model.

The first way to do this was by doing a regular LQ-model fit on the data from 0-10 Gy, excluding the "tail" (marked with a green circle in Figure 43) for doses exceeding 10 Gy. We named this model F_1^{G1}, and the corresponding LQ-parameters are listed in Table 21. As this

model did not make a good fit for survival data with doses exceeding 10 Gy, a correction to our experimental data by withdrawing a constant fraction was attempted. This was done under the assumption that a constant fraction had remained un-irradiated. An additive constant taking the background colonies into account, a_0, was found by manual iteration and by observing when the LQ-model plus the constant overlapped the experimental survival at doses around 13 Gy. The constant was subtracted from the experimental data, and a new LQ fit was performed. The experimental survival corrected for background colonies, F_2^{G1}, can be seen in equation 34, and the parameters for correction and for the resulting LQ-model is listed in Table 21.

$$F_2^{G1} = F_{experimental} - a_0 \tag{34}$$

Where F_2^{G1} is the corrected data to be fitted to the LQ-model, $F_{exsperimental}$ is the experimentally measured survival and a_0 is the correction constant.

A correction on the form; $(F_{experimental} - a_0)e^{a_1 D}$, was attempted similarly to that described for group 2 below, but this resulted in $a_1 = 0$, and was discarded.

TABLE 21. PARAMETERS FOR CORRECTION AND RESULTING MODEL FOR CELL SURVIVAL IN GROUP 1. GREEN INDICATES THE PREFERABLE MODEL.

	Correction parameters		LQ-model parameters				
	$\boldsymbol{a_0}$	$\boldsymbol{a_0}$ **s.e.**	**α**	**α s.e.**	**β**	**β s.e.**	**Adjusted** $\boldsymbol{R^2}$
$\mathbf{F_1^{G1}}$	0	0	0.44	0.03	0.015	0.005	0.94
$\mathbf{F_2^{G1}}$	0.0027	5.E-5	0.50	0.04	0.014	0.004	0.93

As the 95 % confidence interval completely overlapped for both α and β in the two models, the model which best predicted our experimental data ($\mathbf{F_2^{G1}}$) was chosen for further RBE analysis. We will refer to the corrected experimental data from group 1 (G1) as, $F_2^{G1} = \boldsymbol{F^{G1}}$, and the corresponding LQ- model as $\boldsymbol{F_{LQ}^{G1}}$. The group 1 data is plotted with the corresponding LQ-model in Figure 44.

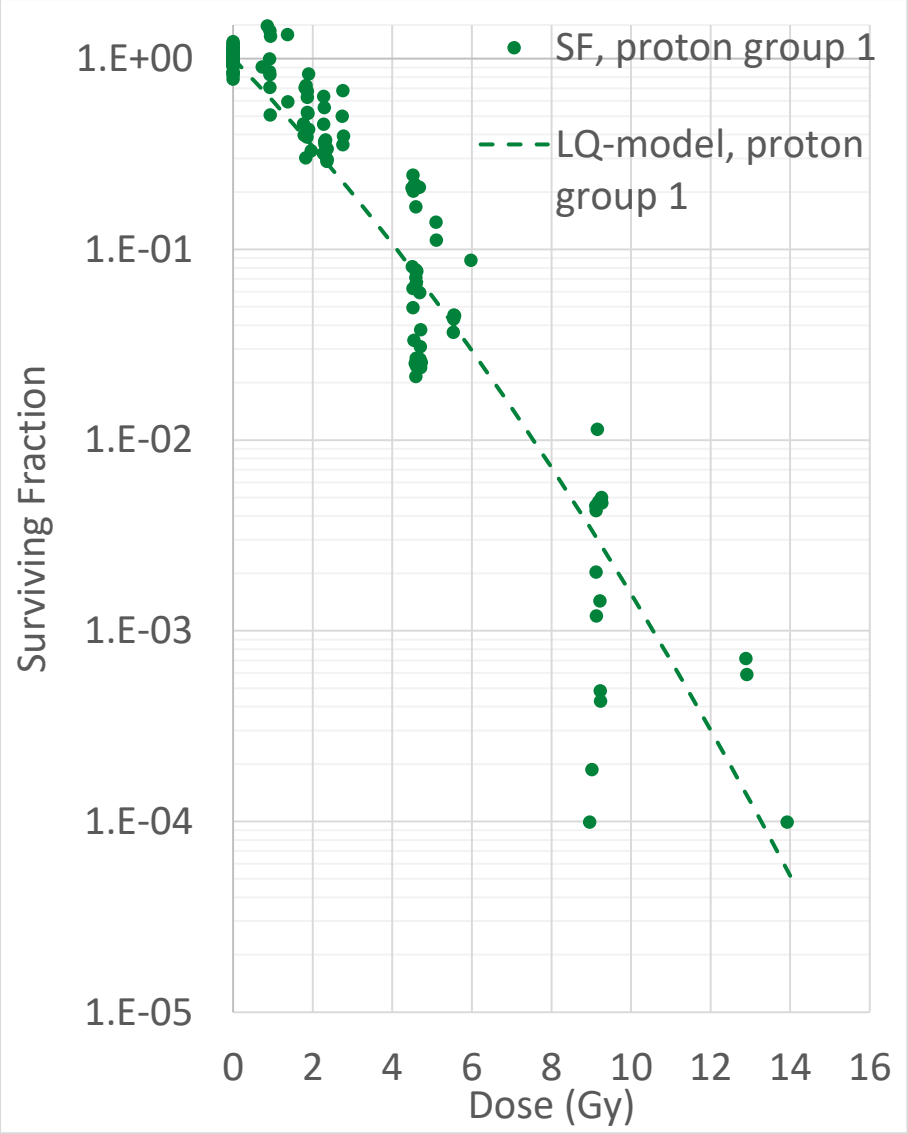

FIGURE 44. SURVIVING FRACTION OF GROUP 1. CORRECTED FOR BACKGROUND COLONIES WITH A CONSTANT VALUE, AND PLOTTED AGAINST DOSE TOGETHER WITH THE FITTED LQ-MODEL.

Distal edge of the Bragg-Peak

In group 2 there was a very distinct tendency towards a constant surviving fraction when the dose increased. This can be seen in Figure 45. Group 2 was treated independently of group 1 because of the large differences in absorbers and position in the Bragg-Peak during the irradiations. If background colonies were present in both cases, the fraction of them would follow parameters (both constants and dose dependent ones) differently. We found two models for correction of our experimental data, both leading to the same model of survival. In the first one we derived two correction terms to correct for the background colonies, and found a model for survival of the irradiated population. Other types of

corrections were also tested, which will be discussed further in the discussion part of this thesis. In the second model a dose-distribution correction was found as a function of the α-value, derived as a sum of fractions receiving different doses measured in the distal edge BP by an EBT3 film. This will be explained in further detail below.

Analysis – Distal edge of the Bragg-Peak

Background colony correction

For group 2 (G2), the first term was found from the surviving fraction the data points from irradiated cells converged towards at doses exceeding 8 Gy. There was no surviving fraction dependency of dose in this dose range, so the constant b_0 was subtracted from the experimental data as can be seen in equation 35.

$$F^{G2}_{correction1} = F_{exsperimental} - b_0 \quad (35)$$

Where $F^{G2}_{correction1}$ is the experimental data after correction 1, $F_{exsperimental}$ is the measured survival, and b_0 is the constant correction term.

Corrected data was split into two parts, below and above 6 Gy. All points below 6 Gy was fitted to the LQ model with a β=0 as the β tended to be negative. We then assumed the data to follow the LQ-model with the obtained α value. The deviation from the model on all the $F^{G2}_{correction1}$data was analysed, which led to an exponential correction term including a dose dependent term, as can be seen in equation 36.

$$F^{G2}_{correction2} = F^{G2}_{correction1} e^{b_1 D} \quad (36)$$

The measured experimental survival is plotted together with survival after application of correction term 1 alone and after application of both correction term 1 and 2 in Figure 45. The $F^{G2}_{correction2}$ including both correction terms will be referred to as F^{G2}_1. A fit to the LQ-model was then done on the corrected data F^{G2}_1 with β=0, which will be referred to as F^{G2}_{LQ}. The corrected experimental survival is plotted together with the corresponding LQ-model in Figure 46. Both correction parameters and LQ-parameters are listed in Table 22.

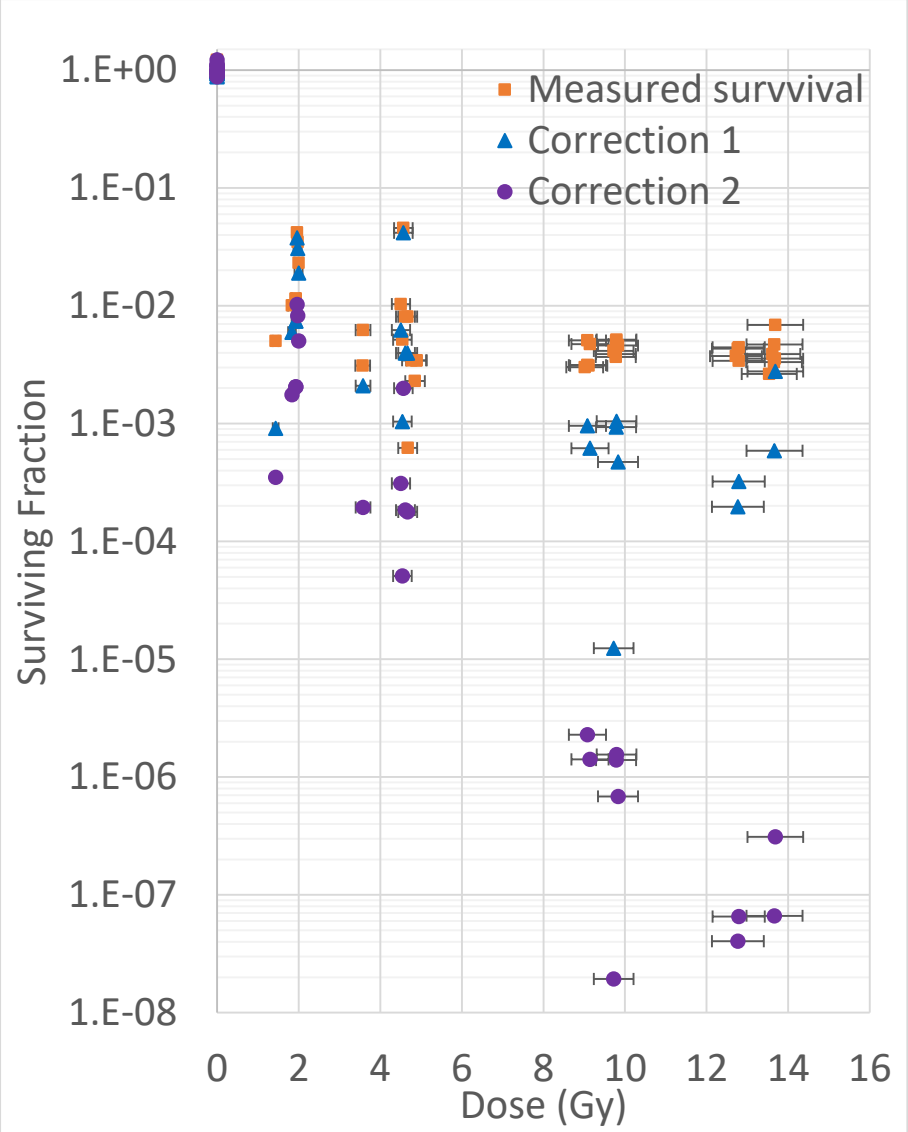

FIGURE 45. SURVIVAL OF GROUP 2 AFTER PROTON IRRADIATION (LET= 38-44 $\mathbf{keV/\mu m}$).THE MEASURED SURVIVAL (ORANGE) IS PLOTTED TOGETHER WITH TWO ITERATIONS OF CORRECTIONS FOR BACKGROUND COLONIES. IN CORRECTION 1 (BLUE) A CONSTANT VALUE (VALUE OF CONVERGENCE AT DOSES EXCEEDING 8 GY) IS WITHDRAWN FROM THE EXPERIMENTAL DATA. IN CORRECTION 2 AN EXPONENTIAL TERM LINEARLY DEPENDENT ON DOSE WAS ADDED TO CORRECTION 1.

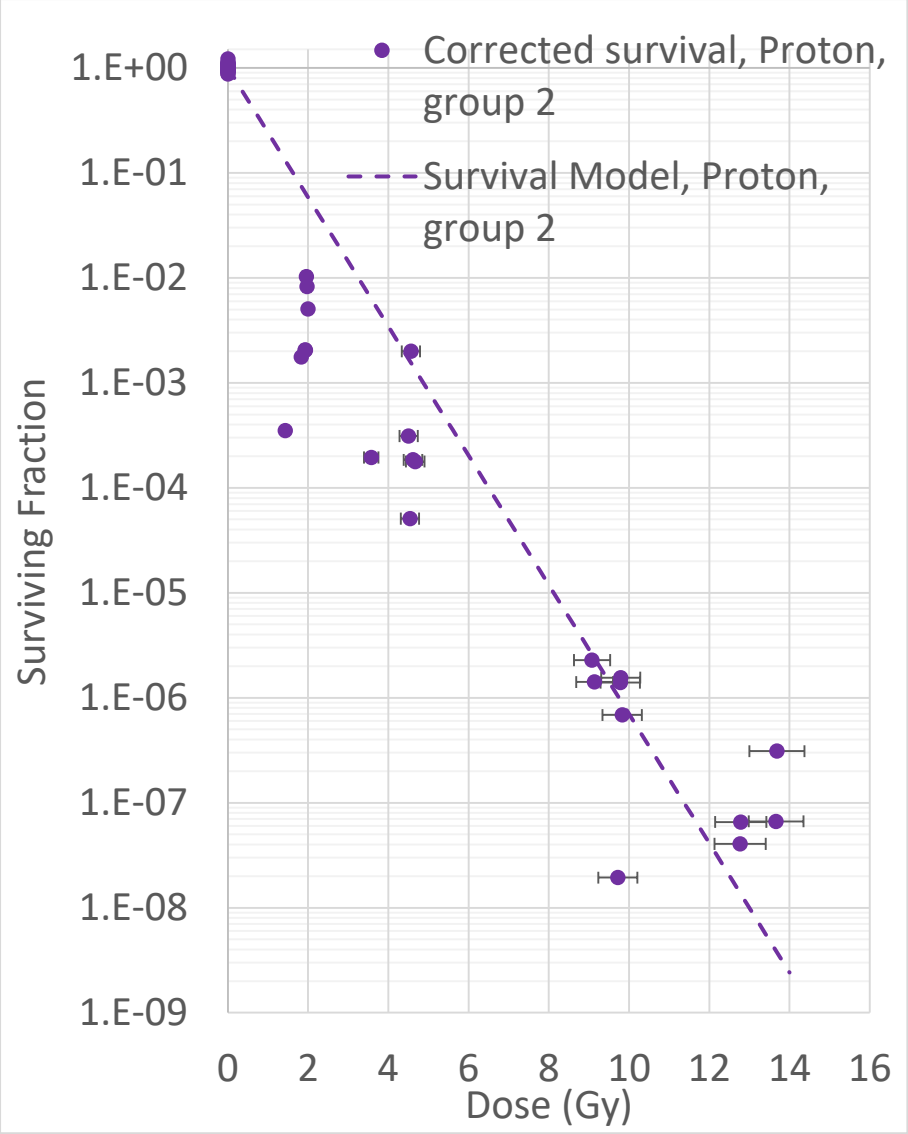

FIGURE 46. EXPERIMENTAL SURVIVAL OF GROUP 2 CORRECTED AS F_1^{G2} PLOTTED TOGETHER WITH THE CORRESPONDING LQ-MODEL.

TABLE 22. CORRECTION PARAMETERS AND FITTED LQ-MODEL PARAMETERS FOR PROTON GROUP 2.

	Correction parameters				LQ-model parameters		
	b_0	b_0 s.d.	b_1	b_1 s.d.	α	α s.d.	Adjusted R^2
F_1^{G2}	0.0041	0.0009	-0.66	0.05	1.42	0.05	0.92

Dose-distribution correction

From the film analysis described in section 4.2.4, a method to correct for the error that arise in the survival plot using an average dose in the place of a dose-distribution was developed. The analysed film were divided into dose levels with a resolution of 0.1 of mean dose, and

the fraction of the total cell dish area receiving each dose was analysed. The surviving fraction was found as a sum of all surviving fractions with the different doses, weighted with fractions of the cell dish area, as can be seen in equation 37:

$$SF(\alpha) = \sum_i w_i e^{-\alpha \cdot d_i} \tag{37}$$

where SF is the survival curve when dose distribution is taken into account, w_i is the fraction of the cell dish area receiving dose d_i, and α is the LQ-parameter. So if 20 % of the cell dish area received a dose that was in the range 0.8-0.9 of mean, it was added to the sum as $0.2e^{-\alpha \cdot 0.85D}$, where the D is the mean dose. Different α's were used for calculating the correction, both the one found from initial slope from 0-5 Gy listed in Table 22, and one based on the initial slope from 0-3 Gy.

The correction was found from the deviation between the standard LQ model and equation 6, with both models having a single α term as shown in equation 38:

$$\ln(e^{-\alpha \cdot D}) - \ln\left(\sum_i w_i e^{-\alpha \cdot d_i}\right) \tag{38}$$

When incorporating doses from the EBT3 films into d_i, it was found empirically that the difference increased as a second order polynomial on the form $f_1 D + f_2 D^2$. A correction term to $F_{experimental}$ was thus identified as $e^{f_1 D + f_2 D^2}$, resulting in the correction model F_2^{G2} as can be seen in equation 39:

$$F_2^{G2} = F_{experimental} e^{f_1 D + f_2 D^2} \tag{39}$$

Depending on the α value, the correction for the heterogeneous dose distribution changed. The change in the shape of the survival curve as a consequence of a heterogeneous dose-distribution for α = 1.42 can be seen Figure 47.

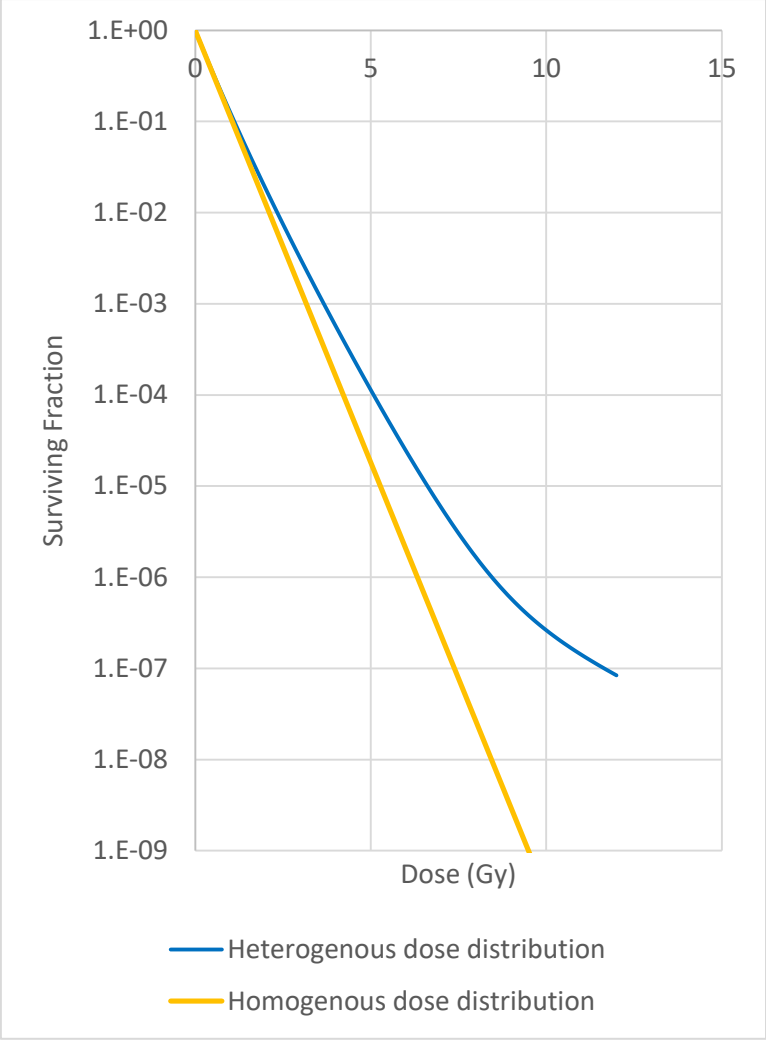

FIGURE 47. THE LQ-MODEL WITH AN ALPHA = 1.42, WITH HOMOGENOUS DOSE DISTRIBUTION (YELLOW), AND HETEROGENEOUS DOSE-DISTRIBUTION (BLUE).

Dose-distribution correction including background colonies

The reproduced model for our experimental data found from equation 39, did not fit our data nicely until an un-irradiated population with a fraction of 0.0041 was added to the sum. Then we obtained a very good fit to our experimental data as can be seen in Figure 48. Thus, it was concluded that the LQ model with corrections based on heterogeneous dose distribution and background colonies was the best for group 2.

The corrections to the experimental data gave good results, but somewhat independently of choice of α, making it difficult to extract more information from the corrections. Examples of correction factors for two different alpha values can be seen in Table 23, both including an un-irradiated population from the model and not. The corrected cell survival together

with the corresponding model can be seen in Figure 49. Notice the similarity with the corrections made in Figure 46, where the main difference to the correction is a term quadratic with dose. An alternative would be to do a regular LQ-fit to the uncorrected data, and only treat the resulting α-value as the survival with homogenous dose-distribution. This resulted in the parameters $\alpha = 1.46 \pm 0.07$ and $\beta = 0.082 \pm 0.006$. This would however result the corrected data to have a curvature in the opposite direction due to a lack of correction linear with dose.

TABLE 23. EXAMPLES OF CORRECTION FACTORS FOUND IN ORDER TO ACCOUNT FOR HETEROGENEOUS DOSE-DISTRIBUTION, WITH TWO DIFFERENT ALPHA VALUES. GREEN INDICATES THE PREFERRED MODEL.

	Including un-irradiated population		**Excluding un-irradiated population**	
α	**f1**	**f2**	**f1**	**f2**
1.42	-0.137 ± 0.024	-0.0685 ± 0.002	-0.060 ± 0.002	-0.0228 ± 0.0002
2.18	-0.76± 0.05	-0.080 ± 0.004	0.00±0.01	-0.0682 ± 0.0007

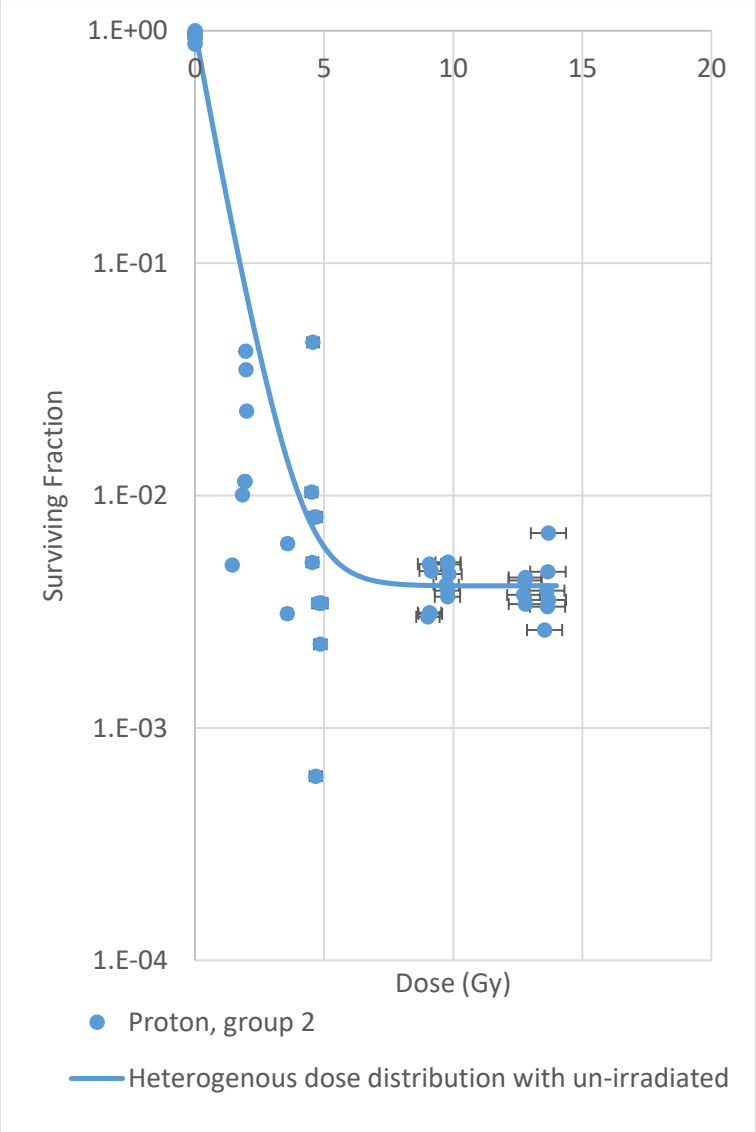

FIGURE 48. MODEL WITH HETEROGENEOUS DOSE DISTRIBUTION, INCLUDING A FRACTION OF UN-IRRADIATED CELLS. PLOTTED TOGETHER WITH EXPERIMENTAL MEASUREMENTS OF SURVIVING FRACTIONS FOR PROTONS, GROUP 2.

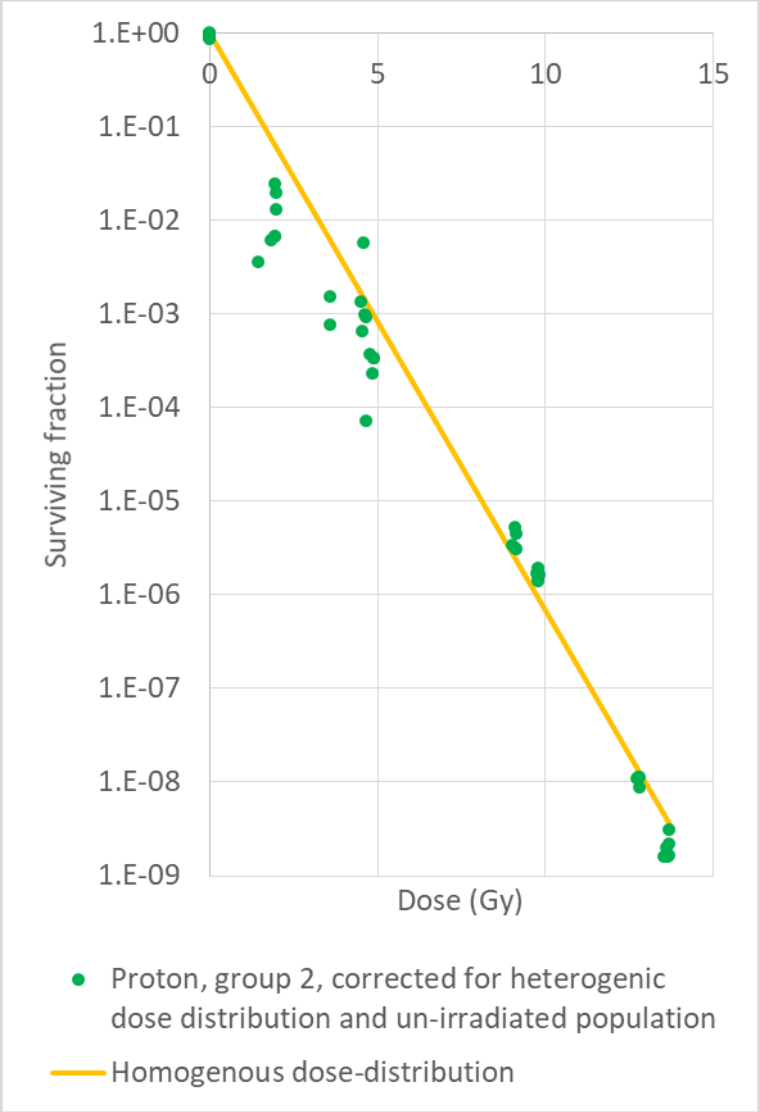

FIGURE 49. PROTON, GROUP 2 CORRECTED FOR HETEROGENEOUS DOSE-DISTRIBUTION AND AN UN-IRRADIATED POPULATION (BACKGROUND COLONIES) WITH THE MODEL F_2^{G2}, AND $\alpha = 1.42$. PLOTTED TOGETHER WITH THE LQ-MODEL.

4.3.3 RBE values

The RBE values were calculated from the fitted models to protons and x-rays. The RBE was found as $RBE(SF) = \frac{D_{x-rays}(SF)}{D_{protons}(SF)}$. The fitted LQ-models for 220 keV x-rays together with the corrected models for group 1 and 2 irradiated with protons with different LET can be seen in Figure 50. Assuming a relative survival of 10 %, RBE was found to be up to 5.8 for cells irradiated in the distal edge of the Bragg-Peak (proton, group 2), and 2.3 in front of the Bragg-Peak (proton group 1). The RBE values with estimated errors for 10% and 37% survival level can be seen in Table 24. RBE as a function of the surviving fraction can be seen in

Figure 51. We can observe that the RBE for proton group 1 is almost constant at approximately 2, while the RBE for proton group 2 varies a great deal from 4 to almost 10.

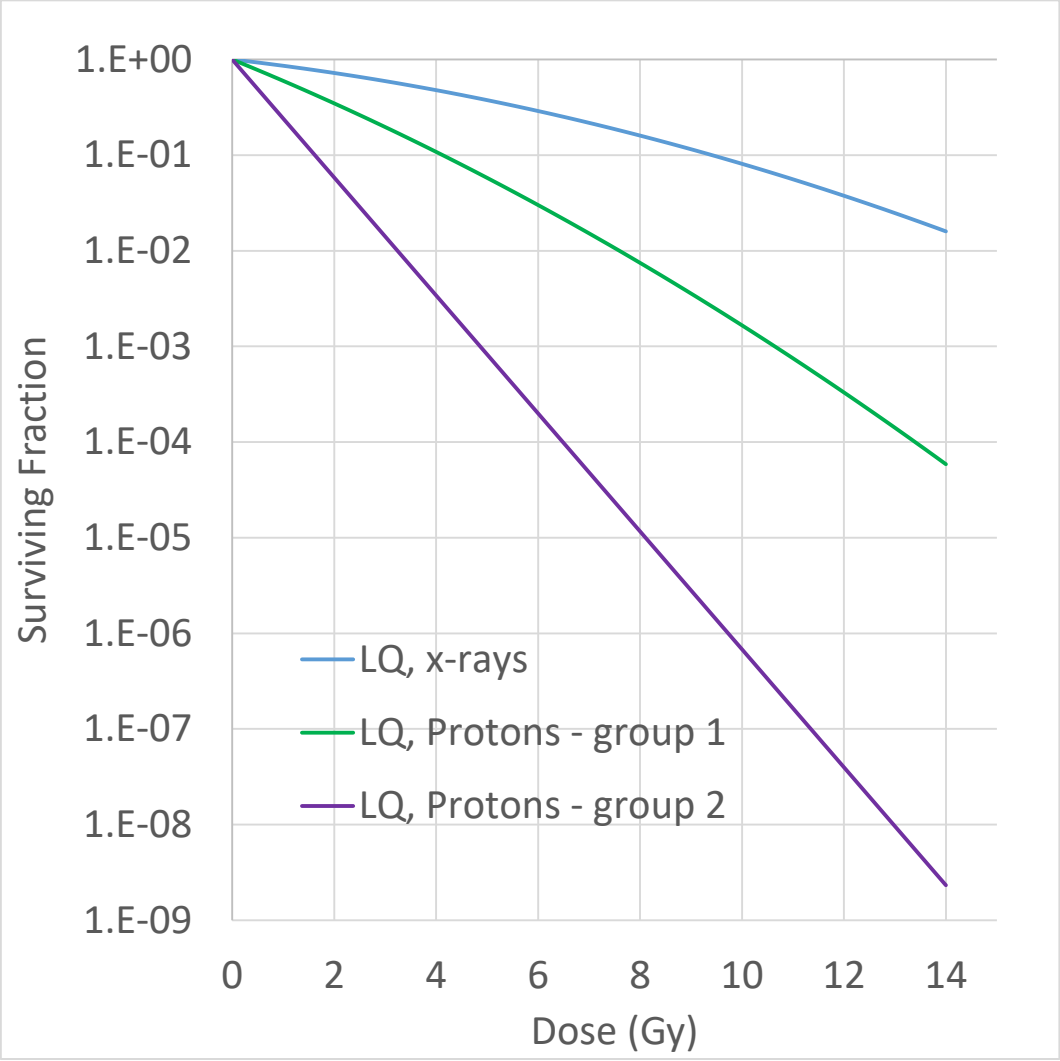

FIGURE 50. LINEAR QUADRATIC FIT TO SURVIVING FRACTIONS FOR 220KEV X-RAYS (BLUE), AND PROTON GROUP 1 (GREEN) AND 2 (PURPLE). PROTON GROUP 1 WITH AN AVERAGE LET OF 7.5, AND PROTON GROUP 2 WITH AN AVERAGE LET OF 41.

TABLE 24. CALCULATED RBE VALUES AT TWO DIFFERENT SURVIVING FRACTIONS FOR PROTONS IRRADIATED IN FRONT OF (GROUP 1) AND IN THE DISTAL EDGE OF (GROUP 2) THE BRAGG-PEAK. 220 KEV X-RAYS WERE USED AS REFERENCE.

Cell dish position	LET	RBE(F = 0.37)	RBE(F = 0.1)
In front of Bragg-Peak (group 1)	7.5	2.7 ± 0.1	2.3 ± 0.3
In distal edge of the Bragg-Peak (group 2)	41	7.3 ± 0.2	5.8 ± 0.3

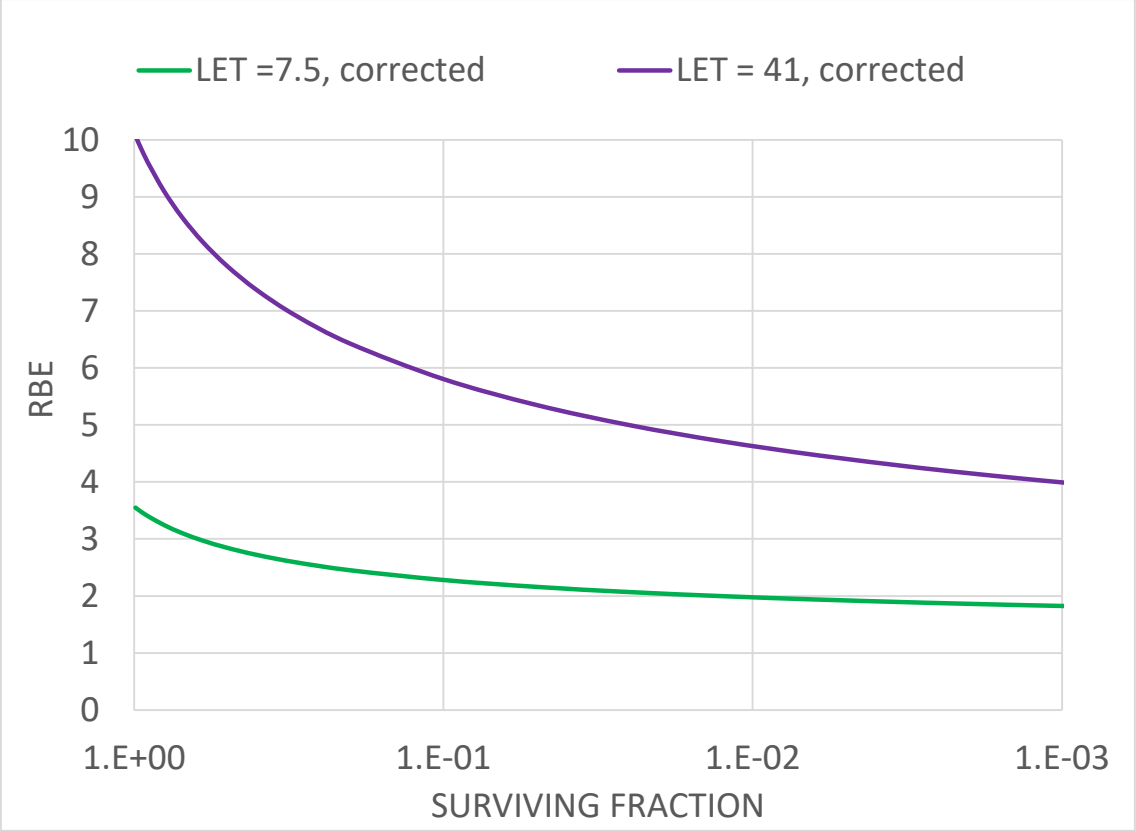

FIGURE 51. RBE FOR CELLS IRRADIATED WITH PROTONS WITH DIFFERENT LET VALUES IS PLOTTED AS A FUNCTION OF THE SURVIVING FRACTION. 220 KEV X-RAYS WHERE USED FOR REFERENCE IN RBE CALCULATION.

5 Discussion

5.1 Errors, Uncertainties and Setup issues

In experiments with living cells, there are always substantial uncertainties included. The effect of accumulated uncertainties both from dosimetry and cell survival modelling left us with relatively large uncertainties of the RBE values calculated. The distal edge of the Bragg Peak proved to be a difficult area to work with, as very small positional errors and absorber thickness errors resulted in large variations in the dose-rate, affecting the LET estimation as well. All errors and uncertainties and their effect on the final results will be discussed in this chapter.

Dosimetric uncertainties

The dosimetric challenges in this thesis have had a great impact on the RBE uncertainties. Since the setup was developed as we went forward with experiments, there were no clear protocol for what type of dosimetric measurements that was needed. This made the dosimetric data somewhat inconsistent, where important measurements were sometimes omitted. While the dosimetric data have been improved, some assumptions we did early on still resulted in some missing data.

The first week of experiments using setup 1, we assumed the proton beam intensity to be constant and stable over time, but this was soon proven wrong. From then on the Monitor Chamber became a permanent addition to the setup. From the beginning, we assumed that the energy delivered by the cyclotron was accurate with an uncertainty of approximately 0.1 MeV and that it was the same each day of irradiation. Thus we assumed the dose-rate to have a constant ratio between two measurement positions in the Bragg-Peak as long as the depths were the same between experiments. This lead to insufficient dosimetry at the chosen irradiation depths, especially in setup 2. The few measurements obtained from setup 2 however, indicated that the proton energy in this case was very similar each day.

Dosimetry with EBT3 films also had a few challenges. Initially we assumed the dose response of the films irradiated with protons to be similar those of electrons, consequently using the electron calibration for dose calculations in the proton beam. After further investigation this proved wrong, and a proton calibration was performed. The second problem was that initially we failed to include the thickness of the film itself in the depth calculation. This was

corrected in retrospect, but even after the inclusion of the films thickness, we were still not able to obtain the same depth for the active layer in the film as for the irradiated cells. This was due to a poor resolution of absorber thickness, as half of the water equivalent thickness (WET) of the film was greater than that of one Parafilm.

The apparent problems with the film dosimetry resulted in less use of the films in setup 3 and 4. This proved to cause new problems. The beam hitting the cell dish had a dose distribution, and the IC measured the dose in the centre of the setup, in only a radius of 2.5 mm. The films were therefore necessary to obtain an average dose delivered to the cells, and not just an average dose very close to the proton beam centre. In setup 3 the IC to average correction was only measured on day one of experiments, as the beam centration, shape and homogeneity varied day-to-day, this resulted in additional uncertainties in the dose to cell dish calculations.

In general, a recurring problem was the lack of film irradiations in the distal end of the BP. The analysis of the films irradiated in the far back of the BP indicated that the homogeneity got worse further back in the distal edge. There especially appeared to be areas with up to 50 % less dose than the average. This resulted in an even bigger uncertainty in the actual dose delivered in the distal end of the BP. We were unable to make a good estimate of this error. Even with films irradiated in the back of the BP, it would be very difficult to aim for the active layer depth to be identical to the cell irradiation depth.

Even with consistent and thorough dosimetry, some uncertainties would have been unavoidable with the current setup. Included here are the dose-rate variation in the calibration from monitor chamber to dose, and the positional uncertainties in the BP. The uncertainties in the electrometers were so small compared to dose-rate uncertainties and Monitor Chamber uncertainties, that they could be neglected. The most significant one was the positional errors that had great impact on dosimetry in the distal edge of the Bragg-Peak. By placing the cell dish ± 1 mm off the point of ionization chamber measurements in air, the resulting dose-rate changed by up to 6 %. This resulted in very large dose-rate uncertainties in the distal edge of the BP.

One should also include that small changes in absorber thickness would have the same effect. If the absorber thickness of the Parafilm wrapped around each dish was inconsistent, this would add to the dose-rate uncertainties. Consequently, it was difficult to decide the

LET value. The LET value at a certain point in the Bragg-Peak is a distribution that increases in width with depth (Dahle et al., 2017), and by adding the uncertainty in position in the Bragg-Peak one must assume that the uncertainty in LET increases as well. As there was a positional and Parafilm thickness uncertainty for each dish, this lead to a LET variation within each experiment. This is the reason why the 4 experiments performed in the back of the Bragg-Peak with estimated different average LET was treated as one group, with an average LET of 41. To reduce uncertainties in the LET, irradiation in the same position in the BP in each experiment would be beneficial. A way to do this could be to aim for the same dose-rate (Gy/µC) for irradiations in the front and the distal edge of the BP. To achieve this the distance from the beam exit window could be used as an extra variable, adapting the setup to the energy of each day to obtain as similar conditions as possible.

Energy and LET spectrum

Even though we had problems with precise estimation of the LET values, collaborators in Bergen have provided us with a lot of useful information about the energy and LET spectrum from Monte Carlo simulations. The simulations were done on setup 2, so an optimal energy for new experiments would be around 15.5 MeV for comparison.

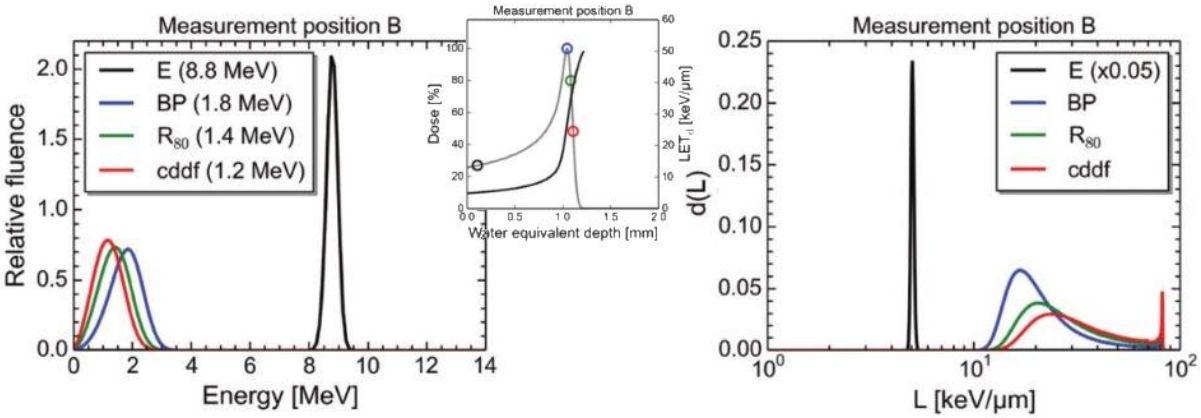

FIGURE 52. EDITED FROM FIGURE 3 AND 4 IN (DAHLE ET AL., 2017). SETUP 2.1 IS NAMED MEASUREMENT POSITION B IN THIS FIGURE. ENERGY SPECTRA (LEFT) AND DOSE WEIGHTED LET SPECTRA (RIGHT) AT FOUR POSITIONS ON THE DEPTH DOSE PROFILE AT MEASUREMENT POSITION B; THE ENTRANCE (E), THE BRAGG PEAK (BP), THE PROTON BEAM RANGE (R80) AND THE CENTRE OF THE DISTAL DOSE FALL-OFF (CDDF). THE LET SPECTRUM AT THE ENTRANCE WAS SCALED TO MAKE ALL THE SPECTRA VISIBLE WITHIN THE SAME VERTICAL AXIS. THE MEAN ENERGIES OF THE SPECTRA, AS WELL AS THE SCALING OF THE ENTRANCE LET SPECTRA, ARE GIVEN IN PARENTHESIS IN THE LEGENDS.

From Figure 52 one can see how the energy spectrum broadens the further into the Bragg-Peak you get. We also have information about the mean energy at the different positions,

which can be used to estimate the energy at different positions in the setup. We can also see how the LET spectrum broadens after the peak in the depth dose plot, and how LET values up to 100 keV/µm already is present half way down the distal edge of the BP. This can be an effect introducing saturation in DNA-damages that will be further discussed below.

Cell survival uncertainties

During cell seeding, a Bürker chamber was used for counting the cells and through further dilution the correct number of cells was obtained. There will be variations and possible errors in the cell counting but most of this was corrected for by using a control group diluted from the same solution. The time from seeding to irradiation was about 15 hours, leaving some cells to finish one or more cell cycles. There will not just be single-cells anymore, and a multiplicity control was fixated after finish of irradiation to correct for this.

Under normal circumstances in clonogenic cell survival experiments, the cells are irradiated in the medium, in an air-tight environment that maintains the CO_2 concentration. As the cyclotron at OCL had a horizontal beam exit, the cell dishes had to be placed vertically during irradiation. To avoid spilling, and to avoid further positional uncertainties, the medium had to be removed prior to irradiation. When the medium is removed, the pH will change and the cells will experience distress. As this is an unfavourable environment for proliferation, it is a risk that the cells will induce cell cycle arrest, resulting in better resistance against DNA-damage, and a higher rate of repair. An even greater risk with the increase in pH is that it will result in killing the cells over time.

This was the reason for our choice of performing clonogenic cell survival experiments without medium for 220 keV x-rays and ^{60}Co in order to obtain the same environment as the cells irradiated with protons. The problem with this was the low dose-rate available for these modalities, resulting in irradiation times exceeding 20 minutes for high doses. Including time for preparations, this lead to a time without medium present of up to 30 minutes during irradiation with ^{60}Co. In comparison, all proton experiments were conducted with a time without medium of a maximum of 15 minutes. The x-rays had a slightly better timing with a maximum time without medium of about 25 minutes. The x-ray survival curves without medium were compared to available data at the institute, where the irradiation was done with the medium present (personal communication, Nina F. Edin), and no significant

differences was found. For the ^{60}Co experiments, very low cell survival was found at 10 Gy, indicating that the irradiation time without the medium resulted in additional killing of the cells. The data from x-ray irradiations without medium present were therefore chosen to be used as the reference in RBE calculations, and the ^{60}Co results were discarded for this purpose.

Due to Fungi-infections, we lost quite a big part of some experiments. This resulted in few data points for some doses of each experiment. The experiments were treated as single points and not mean values, as each dish got a different dose because the dose was determined manually and the precision depended on the human reaction time when the right MC reading was reached. However, the dose for each dish was registered.

Fungi infection became a problem after the change from 8.8 cm2 dishes in setup 1, to 25cm^2 dishes in setup 2. In setup 2, it started with a few dishes, but in setup 3, we lost about half of the irradiated dishes. Statistically, this obviously caused some problems, but in addition to that, concerns of whether we could trust the remaining dishes arouse. Only dishes without visible fungi were included in the results, but the question still remains if the fungi could affect the survival of the cells before it became evident. The same problem was the case for some x-ray experiments, were a total of 5 whole experiments were lost. In the last x-ray experiments, only a very few dishes were lost, resulting in enough data to produce a LQ-model fit. That the results did not differ significantly from previous experiments, was an indication that the results from cell dishes with no visible fungi could be trusted. The problem with fungi-infection was attempted solved by sterilizing the incubator, and improving the sterile techniques with more frequent cleaning of LAF-bench surfaces and equipment in contact with the cell dishes.

5.2 Necessary dosimetry and sterile techniques

After the development of a method for proton irradiation of cells *in vitro*, a lot of information on how to best ensure good dosimetry and obtaining reproducible results have been acquired. This has been collected in the following list with necessary dosimetry requirements and ways to improve the sterile techniques.

Dosimetry

1. Beam centration should be assed by gafchromic dosimetry films at the beam exit window.
2. In order to find the Bragg-Peak, do measuremetns at different depths, and remember to repeat each depth 3 times (at least). This will be useful for energy estimates and in comparing the experiments.
3. Do repeated (3-5) measurements at chosen cell irradiation depths, with 1 mm steps from the positions, up to 3 mm (this can be done after irradiation if time is scarce).
4. Chose depth for distal edge BP irradiation so that the dose rate is approximatly the same as in front of the BP.
5. Do 2 or 3 film irradiations at each position with no absober in front, in this way the active layer is placed approximately at cell irradiation depth at the back of the BP. Remember to bring two or more unirradiated films that can be used as a reference (0Gy).
6. Calculate dose per monitor chamber unit (Gy/uC) in each position to deliver the same dose in both positions.
7. Make sure you have everything you need to write all dosimetry down systematically. (I would recommend to bring a computer, as long as you have a backup as well)

Cell irradiation process and sterile techniques.

1. Make sure everything is sterile, clean all surfaces and all equipment in contact with cells with ethanol in advance, and repeat if possible between irradiations.
2. Wear sterile gloves and coat.
3. Transportation of cell dishes must happen wrapped in a sterile blanket.
4. Mark the dishes thorouhly, to aviod mixups. Each dish gets a different dose.
5. Remove medium with a sterile pipette, and change the pipette *often.*
6. The sterilized Parafilm used for “lids” during irradiation should not be streched. That would cause greater uncertainties in the positioning in the Bragg-Peak and dose homogeneity.
7. Position the cell dish in the holder with the top perfectly aligned with the top of the holder. This is to minimize positional varaiations between the dishes.

8. Transportation is done in styrofoam boxes that have been sterilized properly with ethanol in advance. Make sure to sterilize the heated elements as well and should be done as quickly as possible to reduce pH changes.
9. Place holder at the same position in the heater every time to avoid large positional errors.

5.3 Background Colony Correction

As described previously in section 4.3.2, a “tail” was observed at high doses in the surviving fractions of cells irradiated with protons. This could for example be due to a sub-population of the cells not receiving the full dose. These cells were denoted background colonies. Because of this, models for correction were made. We will split this part of the discussion into two parts. One under the assumption that the “cold areas” observed on the dosimetry films were due to the film structure itself and that the experimental result could be trusted. The other under the assumption that some cells got a significantly lower dose, or that some cells migrated from the un-irradiated area created by an inevitable drop of medium gathering at the bottom of the vertical dish (the cells here would be behind the BP) to create background colonies.

5.3.1 Assumption 1: No corrections are needed

If we make the assumption that no corrections are needed, we also have to assume that the dose variation we see in the films are either a product their own structure together with a positioning very far in the distal edge of the BP, or that these are irrelevant for the convergence to a constant surviving fraction at high doses. However, analysis of the surviving fraction as a function of average dose in comparison to a dose distribution obtained from films in the distal BP edge indicate that a correction for dose distribution still is necessary (see section 4.2.4). This dose-distribution observed in the films were most likely due to the variation in range of the protons. As they have been scattered differently, some will reach the active layer, and some will not, causing larger gradients in dose compared to the front of the BP. No film irradiations in the distal edge of the BP were done systematically each day of irradiation. From the films that were analysed, we saw that a different

transformation factor from ionization chamber dose to average dose should be performed for the distal end of the Bragg-Peak. As all dose transformations from ionization chamber measurements to an average dose were done from films irradiated in front of the BP, we may have overestimated the average doses for all dishes in proton group 2. Thus, even under the assumption that all cells were irradiated, a dose correction is still needed, but it should be noted that a systematic correction of the dose will *not* change the *shape* of the survival curve we observe.

Saturation due to extreme LET

As a correction to the dose would not explain the "tail" in the proton group 2 survival data, we looked at the possibility of a saturation effects of high LET values. For proton irradiations with LET values exceeding 25 keV/µm, little research has been done internationally. Previously, a saturation effect of RBE was observed as LET increased beyond 100 keV/µm (Hall and Giaccia, 2012). Looking at Figure 52, one can observe a small peak of such extreme

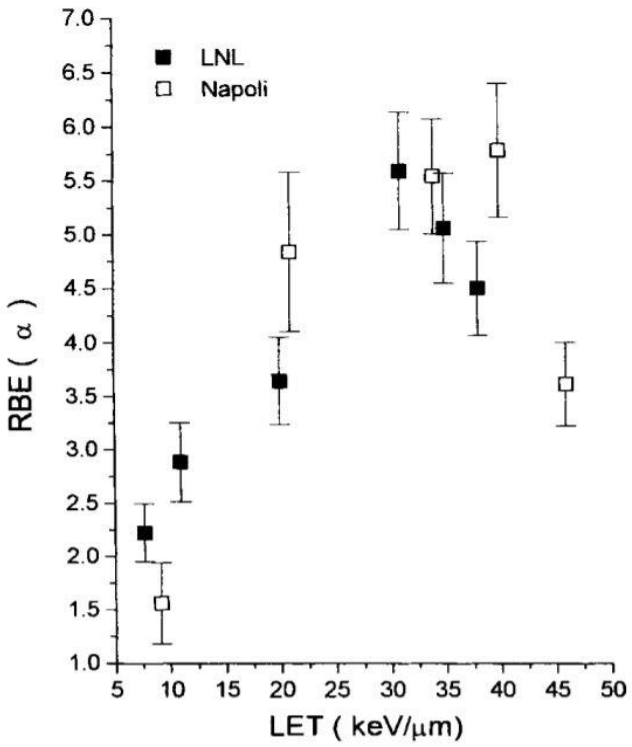

FIGURE 53. RBE(α) FOUND BY α RATIOS BETWEEN 200KVP X-RAYS AND THE BEST FITTED α FOR EXPERIMENTS WITH DIFFERENT LET VALUES. THE LET VALUES WERE EVALUATED FROM ICRU TABLES FOR MS20 TISSUE (1993). RESULTS FROM TWO DIFFERENT FACILITIES PLOTTED TOGETHER. LNL: CLONOGENIC CELL SURVIVAL EXPERIMENTS WITH 7 MV PROTONS ACCELERATED BY VAN DE GRAFF (LNL, LNFN, PADOVA). NAPOLI: CLONOGENIC CELL SURVIVAL EXPERIMENTS WITH 3 MV PROTONS ACCELERATED BY TANDEM ACCELERATOR (NAPOLI UNIVERSITY). FIGURE BY BELLI ET AL. (BELLI ET AL., 2000)

LET values of up to 100 keV/µm in the LET spectrum in the distal edge of the BP, that could induce saturation effects. Experiments conducted with 7 MeV and 3 MeV protons (Belli et al., 2000) indicated a reduction in the RBE already as the average LET exceeded about 35 keV/µm, as can bee seen in Figure 53. With the assumption that the RBE suddely recduces when reaching large LET values due to damage saturation, it is clear that this would be visable at high doses before it is observable for the lower doses. This would explain the steep sloap of the SF at low doses, before in flattens in a "tail".

One can mention the possibility that the type of cells used was escpecially resistant towards radiation, or that some clones of the cells were resistant, and that this is the reason for the "tail" we observe. If the cells are resistant to high LET radiation, they should also be resistant towards gamma radiation such as x-ray and ^{60}Co. This has not been observed (personal communication, Nina F. Edin).

Repair mechanisms

The shape of our survival curve has some resemblance to that of T98G cells treated with an Ataxia telangiectasia mutated kinase (ATM) inhibitor before radiation (Burdak-Rothkamm et al., 2008). The survival curves produced from T98G cells, which were exposed to different treatments prior to irradiation with x-rays from that study can be seen in Figure 54. The ATM molecule is related to sensing double strand breaks and signaling resulting in cell cycle arrest and DNA repair. By inhibiting this kinase, the cells become more sensitive to radiation as the repair mechanism is not induced as much. One can relate this to our situation by the assumption that when irradiated with high LET irradiation, the cells experience so many double-strand-breaks (DSBs), that only a very small amount are repairable. So in both cases the cells accumulate DSBs without the possibility to repair them. As seen by Figure 54, the most significant difference from repair-competent cells will occur at low doses, as these damages usually are repairable. With ATM inhibitor that prevents repair, or in our case with very high LET radiation resulting in damages so severe that they are not repairable, the difference will be highest for the lower doses. When reaching higher doses , the effect will be smaller, as the damages already are severe, thus reaching some sort of saturation effect where increased doses do not increase the level of biological damage resulting increased surviving fraction per dose. The ATM inhibited T98G cells were only irradiated with up to 5

Gy and a full saturation was not observed. However, there is a change in shape of the survival curve indicating a reduced response per dose as the dose increases.

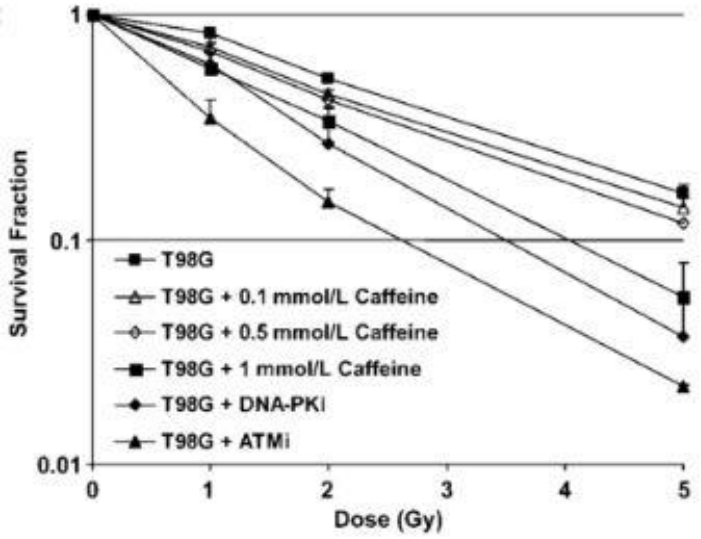

FIGURE 54. FIGURE FROM (BURDAK-ROTHKAMM ET AL., 2008) TO SHOW THE SHAPE OF THE SURVIVAL CURVE FOR T98G CELLS TREATED WITH ATMI TO PREVENT DBS REPAIR (BLACK FILLED TRIANGLE) COMPARED TO UNTREATED ONES (SMALL FILLED SQUARE), BEFORE IRRADIATION WITH X-RAYS. RESULTS FROM CLONOGENIC SURVIVAL EXPERIMENTS WITH DIRECTLY IRRADIATED CELLS (1, 2, AND 5 GY).

5.3.2 Assumption 2: Correction for background colonies are needed

If there is a need to correct for background colonies, it is a question of how to perform the optimal correction. This will of course be closely linked to the understanding of the problem, and why this artefact appears.

From investigation of one of the irradiated films positioned in the distal edge of the Bragg-Peak (BP), see section 4.2.4, areas with significantly lower doses were discovered. The hypothesis that arose from this observation was that a fraction of the cells had not been irradiated due to depth variations across the cell dish, causing zero-dose areas. This could be due to absorber structure of either Parafilm or the solid water, but we could not exclude the scattering filter or the monitor chamber either. Most likely it was a combination, and at the edge of the BP where the protons have been scattered maximally, the smallest variation may have affected the dose-distribution as some of the protons were stopped before reaching the cell dish (or the irradiated film in that case).

The only problem was that this seemed to occur for both groups (in front and in the distal end of the BP), though the problem was most prominent in the distal edge. This led us to believe that a constant fraction of cells survived, and at low survival this was made most visible. Another hypothesis was that the protons were scattered systematically, leaving very small areas un-irradiated, although not visible on the films maybe due to limitations in the resolution. As both groups converged to approximately the same value, we initially decided on a correction by withdrawing this constant term from all experimental data in both groups. The correction by withdrawing a constant did not change the behaviour of the curve of group 2. Some points were lost (due to surviving fraction (SF) less than zero after correction), but the "tail" was still present. Changing the term from a constant to a linear dependency of seeding density was discussed, but in some experiments the seeding density was the same for 10 and 14 Gy, and this did not seem to affect the survival curves any differently. The same was attempted for dose, which improved some of the points in group 2, but there seemed to be no general dependency for the whole group, only for separate experiments. This could not be possible, as different absorbers was used in distal edge irradiation in setup 3 (3 experiments) and 4 (1 experiment). The problem was that there were not enough data points in each experiment to make individual fits, which also was the reason for the data to be collected in groups.

By the assumption that the correction had some dependency on the absorber and absorber depth, group 1 and 2 would needed different corrections as group 1 had only 1 Parafilm as absorber during irradiation, and did not experience the same dose inhomogeneity as group 2.

Group 1

Based upon the assumption that the thin absorber caused less area with "cold areas", and that dose homogeneity seemed better for group 1, the correction needed was assumed to be smaller. As the SF was generally higher for group 1 the correction also had a smaller impact on the resulting LQ-model. One attempt was to apply no correction, and simply perform a LQ-fit on the data from 0-9 Gy. The assumption was that the correction would have small impact on the high survival levels only. An attempt on a correction to obtain a

good fit for the high doses as well was made by using the resulting LQ parameters from this fit, and adding a constant until the measured survival at high dose points seemed to overlap with the model. A new LQ fit was made on the corrected data, which gave a good fit. A term dependent of dose and on seeding density was attempted, but no significant difference in the resulting LQ-model was observed, and the correction with only one parameter was chosen.

Group 2

Origin of potential un-irradiated population

For a part of the cell population to be un-irradiated, it must either have been shielded by the absorber completely although this have not been observed in the irradiated films, or some cells have not been hit by the irradiation due to systematic scattering on a level smaller than the EBT3 film resolution. Another possibility is that the background colonies have originated from the un-irradiated area of the cell dish at the bottom of the vertical dish, where the cells were shielded by a remaining drop of medium during irradiation. These areas were not included in the counting of colonies, but one can imagine that after irradiation when fresh medium was added (see section 3.3.8), some of the healthy cells detached and was mixed in the medium. From there they could have attached uniformly across the cell dish, as is what we observe. If this is the case however, we would expect to see a large dependency on seeding density. The more cells in the un-irradiated area, the more cells would have detached when flushed with fresh medium. This was not the case.

Dose distribution impact

Even though a linear dose dependent correction term was not the way the go, it still seemed like there should be made a correction with dose dependency. An average dose found from IC measurements and the dose distribution in films irradiated in front of the BP had been used in the survival plot. Remembering the large dose variations in the film irradiated in the distal edge of the BP, the idea was to investigate how the surviving fraction would change if the dose was treated as a distribution. By more precise analysis of the film irradiated in the distal BP edge, normalized dose levels (to average dose) were investigated

in 10% steps (more detailed explanation in section 4.3.2). The relative area of each dose range was found. Then the expected SF (for the distal edge) was found as a sum of surviving fractions with the different dose levels, weighted with the % area covered by this dose. The expected SF was found from the LQ-model with an alpha value found from regression in the dose range 0-5 Gy after correction with a constant. What was discovered was that the curve would be expected to have a convex curvature (negative β value following the LQ-model) with the measured dose-distribution. Previously this had been discarded to be true as one would expect it to be concave or straight following the regular LQ-model, but after dose distribution analysis it was clear that such a curvature would be the result of dose-distribution inhomogeneity.

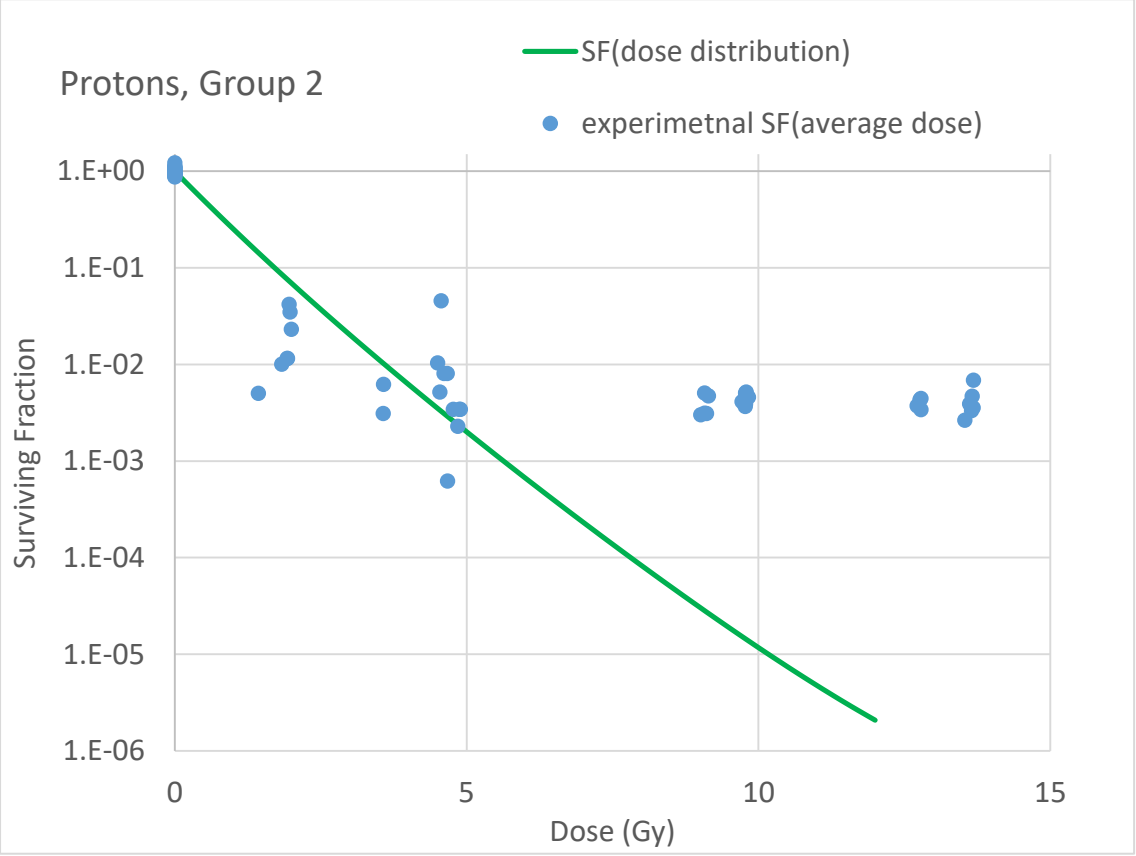

FIGURE 55. THE EXPECTED SURVIVAL FROM OBSERVED DOSE-DISTRIBUTION (GREEN) WITH $\alpha = 1.42$ PLOTTED TOGETHER WITH THE OBSERVED EXPERIMENTAL DATA (BLUE).

However, the observed dose-distribution did not account for the "tail" in the survival curve (Figure 55). By adding a small fraction of un-irradiated cells to the sum however, the model seemed fit for our experimental data, as can be seen in results, Figure 48.

The problem assuming an un-irradiated population arose when the constant correction was subtracted from the experimental data, and compared with the model without the un-irradiated population. It may be possible to picture that some of the irradiated cells have been even further back in the BP than the irradiated film. Then the dose distribution would have been even more extreme, resulting in larger fractions with low doses, and resulting in a more curved survival curve. It may be possible that the cell dishes have significant areas covered with doses down to zero dose, which could also explain that there appears to be an un-irradiated population. Based on this, a model with a small fraction of un-irradiated cells and an extra correction of dose distribution was made. The problem was that a large range of initial alpha values gave good fits and corrected data. Values from 1.42 to 2.18 were found to all be satisfactory, leaving the question: which alpha value is a good choice? As the corrections have the least impact on small doses, the best alternatives would be to use the alpha value found for either 0-3 Gy, or 0-5 Gy. Depending on whether we want to include a correction for an un-irradiated population or not, the alphas should be found from experimental data with a withdrawn constant or from the uncorrected experimental measurements.

Dose distribution origin

Additional experiments with EBT3 films were performed at the very end of the project, in an attempt to identify the source of the dose-distribution observed in the film irradiated at the distal edge of the Bragg-Peak (as explained in section 4.2.4). By varying the distance in air, as well as absorber type and depth, we were able exclude some possible sources. The Monitor Chamber was removed, and EBT3 film irradiations were done with both Parafilm and solid water as absorbers. This resulted in no significant change in dose-distribution, as can be seen in Figure 56.

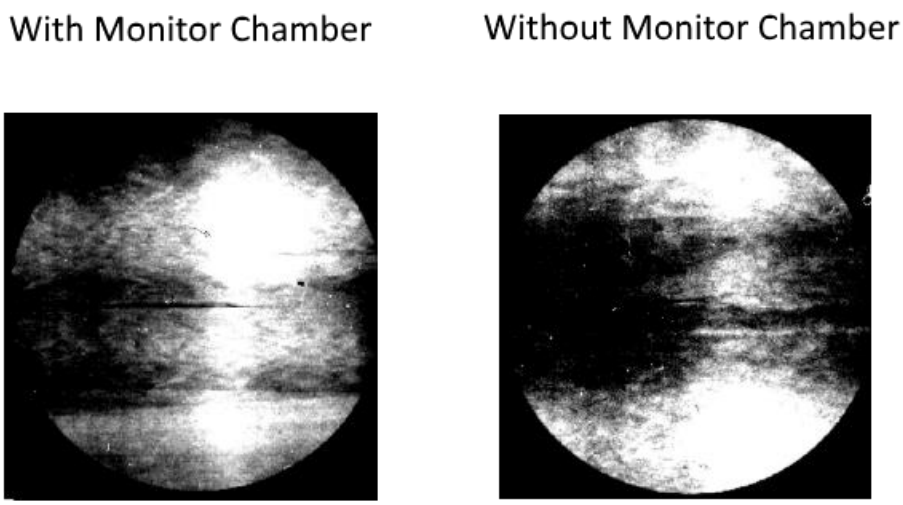

FIGURE 56. DOSE DISTRIBUTION IN THE DISTAL EDGE OF THE BRAGG-PEAK. IRRADIATION AT APPROXIMATELY SAME WATER EQUIVALENT DEPTH, WITH AND WITHOUT THE MONITOR CHAMBER (MC) IN THE BEAM LINE. TO ACHIEVE THE SAME DEPTH WITHOUT THE MC, THE DISTANCE FROM THE BEAM EXIT WINDOW WAS INCREASED, AND AN ADDITIONAL PARAFILM WAS ADDED. BINARY PLOT OF DOSES FROM 0.7-0.9 OF AVERAGE DOSE. LEFT: MC IN BEAMLINE. RIGHT: INCREASED DISTANCE WITH NO MC IN THE BEAM LINE.

Then the solid water was removed, and replaced by Parafilm. Unfortunately the estimated amount of Parafilm to bring the active layer of the film to the distal edge of the BP turned out not to be enough. However, one could still see that the Parafilm seemed to have a negative effect on the dose-distribution even before the BP. To confirm our suspicions that the Parafilm caused the structure pattern in the dose distribution, irradiations were performed at such distance that one layer of solid water was enough to bring the active layer of the film to the distal edge of the BP. This resulted in a much better dose-distribution as can be seen in Figure 57. One should mention that the increase in distance from the beam exit window may have affected the homogeneity, however a much larger increase in distance was made from the left to the right film in Figure 56, without any visible improvement in homogeneity.

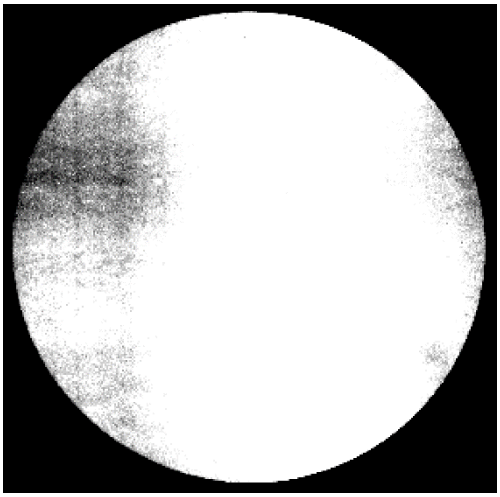

FIGURE 57. DOSE DISTRIBUTION IN THE DISTAL EDGE OF THE BRAGG-PEAK. EBT3 FILM IRRADIATED WITH ONLY SOLID WATER AS AN ABSORBER. BINARY PLOT OF DOSES FROM 0.7-0.9 OF AVERAGE DOSE.

For confirmation that the Parafilm was in fact the main cause for the variation in dose across the irradiated films, the direction of the Parafilm was varied, to see if the "cold areas", or stripes, could be observed to change their direction. As can be seen in Figure 58, this was in fact the case. As the Parafilm was turned, the stripes did the same. From this we could conclude that the structure of the Parafilms caused a greater variation in dose than the solid water, especially in the distal edge of the BP where the variation in proton range due to scattering amplified the dose variation. By using the Parafilm as a replacement for the cell dish lid, we introduced an artefact in the dose distribution. This effect is not observed in great extent in front of the BP, but is significant in the distal edge.

The elasticity of the Parafilm seemed to result in a structure like an accordion, with some areas of greater thickness, and some thinner areas. At the distal edge of the BP the protons are reaching the end of their track, and with just a small additional thickness in the Parafilm, this would lead to areas were the protons simply would not be able to reach. The same Parafilm was used throughout the experiments conducted in this thesis, strengthening the

hypothesis that this resulted in a constant fraction of cells surviving, as they were shielded by the thickest parts of the Parafilm, receiving zero (or very low) dose.

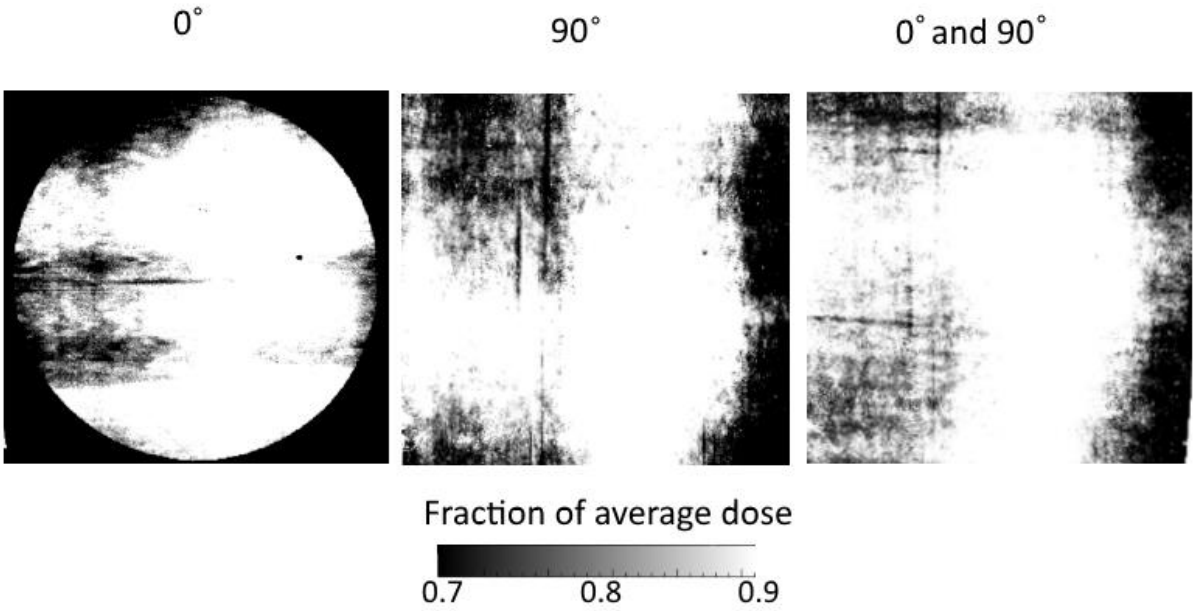

FIGURE 58. DOSE DISTRIBUTION IN THE DISTAL EDGE OF THE BRAGG-PEAK. BINARY PLOT OF DOSES FROM 0.7-0.9 OF AVERAGE DOSE. EBT3 FILMS WERE IRRADIATED WITH SOLID WATER AND TWO PARAFILM AS ABSORBERS. THE DIRECTION OF THE PARAFILM WAS KEPT THE SAME, CHANGED 90 DEGREES, AND CHANGED TO 90 DEGREES HALF WAY IN THE IRRADIATION. THE BLACK STRIPES CAN BE SEEN TO CHANGE THEIR DIRECTION AS THE ANGLE OF THE PARAFILM IS CHANGED.

Other observations of the "tail"

It was discovered that the same issue with a "tail" in the surviving fraction for high doses was discovered in an experiment performed by M. Belli (Belli et al., 2000). The behaviour was only observed in one of the cell lines; SQ20B, described as the most resistant cell line they had available. The curvature into a "tail" was visible already from 5 Gy as can be seen in Figure 59, which was the same case for our data. The SQ20B cells were explained to have a tendency of "clumping" in the growth phase before seeding. The only possible explanation discussed was that some cells had received an attenuated dose, and that the cells in question were cells that had clumped together. A model for the experimental surviving fraction ($SF_{experimental}$) was presented, with a model ($SF_{analysed}$) that was further analysed with the LQ-model. The suggested models can be seen in equations 40 and 41.

$$SF_{experimental} = f + (1 - f)e^{-\alpha D} \quad (40)$$

$$SF_{analysed} = e^{-\alpha D} \quad (41)$$

Where $SF_{experimental}$ was the measured cell survival, $SF_{analysed}$ was the model used for further analysis, and f and α were free parameters.

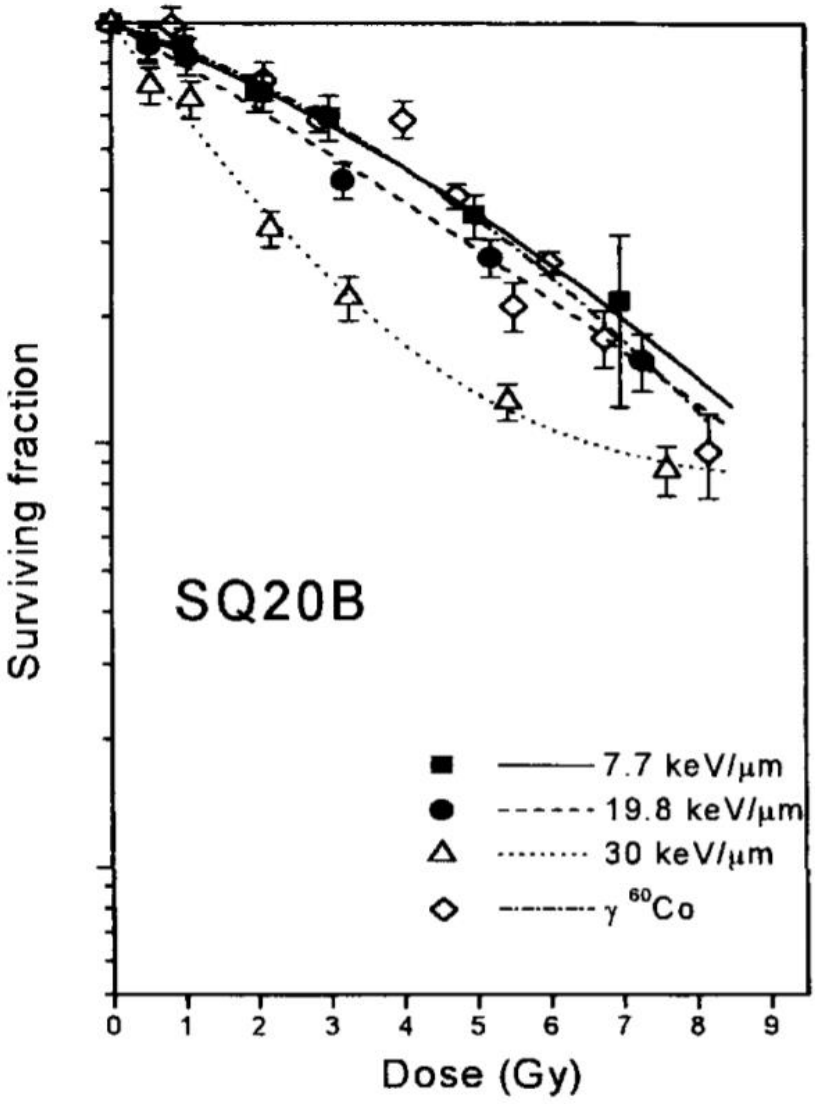

FIGURE 59. SURVIVING FRACTIONS OF SQ20B CELLS, IRRADIATED WITH 7 MV PROTONS WITH DIFFERENT LET VALUES, COMPARED TO IRRADIATION WITH GAMMA RAYS FROM ^{60}CO (BELLI ET AL., 2000). FOR THE LET=30 EXPERIMENT, A "TAIL" CAN BE OBSERVED.

As a multiplicity correction was always included in our experiments, this explanation did not seem to correlate well with our case. It also seems unlikely that clumping should only occur in the cells exposed to the highest LET as is the case in Figure 59. A fit to the suggested

model in equation 40 was attempted with our data, but with convergence problems. The best fit was obtained with an f identical to the correction constant b_0 used previously as described in section 4.3.2, and an alpha in the range 1.6-2.6. This was quite a large range of possible values, making the model difficult to handle. By correction of the experimental data, however, we were not able to reproduce the assumed slope from the model. So the problem was not in the issue of having a model to fit our data, the problem was finding the necessary correction on the experimental data to reproduce the modelled slope. The explanation of the origin of the "tail" is somewhat close to some of the scenarios we have discussed, where some cells receive less or no dose, but the reason why does not seem to correspond well with Belli's hypothesis. The corrections found in Belli et al. was not found to correspond well with our data, possibly due to us having a greater un-irradiated population, or simply that the model does not describe the general situation.

Correction impact on RBE

The different models for cell survival also results in different RBE values as a function of survival. Whether or not a correction is made to the cell survival data changes the RBE. Looking at the *uncorrected data* from protons group 2 (using a model for survival including dose-distribution and an un-irradiated population) in Figure 63, RBE values up to 13 can be found at high survival levels. At lower survival levels the RBE maintains over 6 before it is quickly reduced to zero due to the "tail" in the uncorrected model. Looking at the survival level of 0.1, the RBE value for the uncorrected model was measured to be 8.3, compared to the corrected model were it was 5.8.

The reason that the corrected model results in RBE values so much lower than the uncorrected model is due to the choice of α. In the corrected model we may have overestimated the survival for the doses under 5 Gy, which may indicate that an α = 1.42 is too low. This is dependent on the way one choose to find the α value for the LQ-model, e.g. if it is found from the initial slope in the dose range 0-3 Gy or 0-5 Gy and with or without a correction for the possibly un-irradiated population before estimation. The dose-distribution correction including an un-irradiated population left a large range of values possible, so this is the choice with the greatest impact on the calculated RBE values. It may seem that an estimation of alpha after the withdrawal of the un-irradiated population is the most correct,

as the hypothesis of the Parafilm shielding some of the cells is the most likely. We therefore chose to find the α from the initial incline from 0-6 Gy after the constant correction term. This was mainly a choice made for statistical reasons, as we would be left with few observation points if we were to use a smaller dose range.

Cell survival experiments conducted with the human lung cancer cell line H460 by Guan et al.(Guan et al., 2015) resulted in RBE (SF=0.1) values above 3 at LET values at 19 keV/µm. Similarly, Chaudhary et al. (Chaudhary et al., 2014) found RBE (SF=0.1) values up to 3 for the normal fibroblast cells (AG01522) with an LET value of 30 keV/µm. Keeping in mind that we achieved an LET with an average of 41, in addition to a more narrow energy spectra due to the low initial energy, RBE values of approximately 6 are not unlikely. Neither is the one for the uncorrected model with a value over 8. One should also keep in mind that the RBE values are highly dependent of the type of cell, which limits the information from these types of comparisons.

5.3.3 Summary of background colony corrections

From the analysis of the films irradiated in the distal edge of the Bragg-Peak it is clear that some of the curvature in proton group 2 is due to the dose distribution. If the “real” dose distribution experienced by the cells is more extreme resulting in parts of the cell population to be in fact un-irradiated, this would explain the curvature observed. This is supported by the last minute film irradiations in the distal edge of the Bragg-Peak, which concluded with the Parafilm as the reason for the large variation in dose. It is probable that the accordion-like structure of the Parafilm causes some areas of the cell dish to be shielded from the radiation, as just a tiny additional thickness in some areas is enough to position the cells behind the Bragg-Peak. This would, as discussed previously, result in a constant fraction of un-irradiated cells and would only have a significant effect in the distal edge of the Bragg-Peak were the protons will either reach the cells or not.

In the more unlikely event that the *measured* dose distribution is what the cells experience and that all cells are in fact irradiated, one can assume that exceeding a threshold dose at such extreme LET values, a saturation of damage occurs where only previously lethally struck cells get hit repeatedly.

It is clear is that independently of this, the film irradiations indicate that a homogeneity evaluation has to be done in front and in the distal edge of the BP, separately. This is required in order to transform the dose measured by the ionization chamber to an average across the cell dish as explained in section 4.2.3. By transforming the IC read-out to averages for group 1 and group 2 separately, the dose calculation will be improved. Additionally a dose distribution correction is required in the distal edge of the BP, and it seems necessary to include an un-irradiated fraction of cells in this correction.

5.4 RBE in Proton Therapy

There is great uncertainty in how the RBE impacts clinical proton therapy. As multiple fields are combined in order to cover the tumour volume the BP becomes a spread out Bragg-Peak (SOBP) and the increased LET values are distributed differently depending on the field placements and volume shape. In addition to this, the RBE varies as a function of the dose delivered in each fraction, and it is highly dependent of the cell type. A study on the RBE for proton beam therapy performed by Paganetti et al. (Paganetti, 2014) highlights the problem with a general RBE-LET relationship for all types of cells and tissue. In the article they have gathered available results from clonogenic cell survival experiments with protons of variable LET values, and evaluated the applied average RBE of 1.1.

An example of the variation in RBE they discovered can be seen in Figure 60. As can be seen, the RBE values vary from almost 0 and up to 3 for LET values below 15 keV/µm. Even though it is apparent that there sometimes is a significant increase in RBE, especially for low doses, their statistical analysis finds no larger average RBE values than 1.15. They seemed to find no abundant evidence that the average RBE of 1.1 was unreasonable, yet they conclude with the statement that there is a significant increase in RBE at the distal edge of the SOBP (RBE of 1.7 at the distal edge fall-off). It may seem like the general idea of the average RBE of 1.1 is a good idea, however when it comes to the distal edge and the distal edge fall-off, there is in fact, even for high energies used clinically, a significant increase in RBE that needs to be taken into account in proton therapy. This might be the source for confusion in the discussion of RBE.

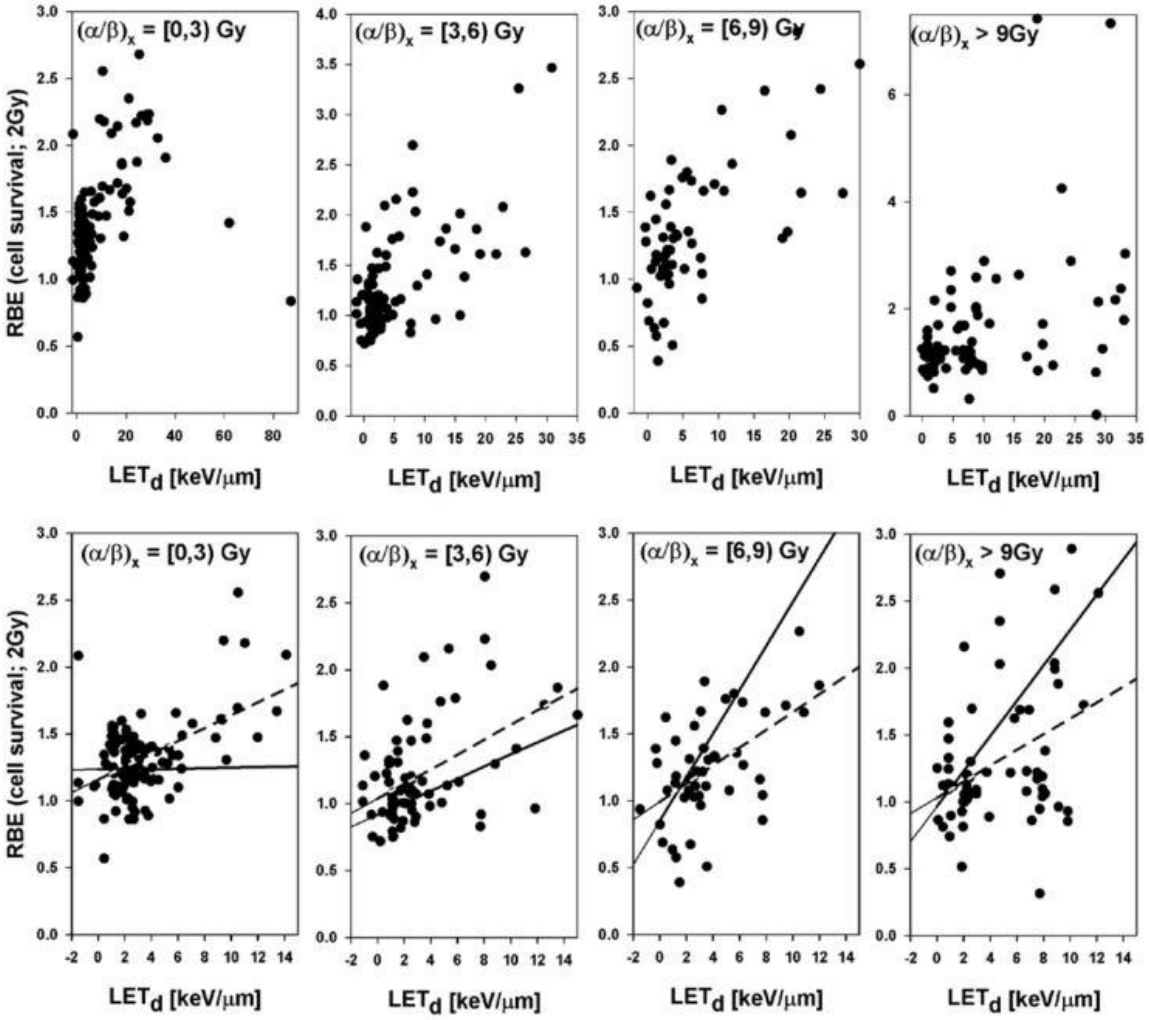

FIGURE 60. RBE FOR CELL SURVIVAL AS A FUNCTION OF LET_D AT A PROTON DOSE OF 2 GY . DIVIDED INTO GROUPS DEPENDENT ON X-RAY SENSITIVITY, BY THE MEASURE $(\alpha/\beta)_{x-rays}$. UPPER ROW SHOWS ALL DATA, LOWER ROW INCLUDES ONLY DATA WITH $LET_D \leq 15\ keV/\mu m$. THE LINES ARE FITS THROUGH THE DATA INCLUDED IN EACH PLOT. SOLID LINES ARE FITS CONSIDERING PUBLISHED UNCERTAINTIES, THE DASHED LINES ARE FITS EXCLUDING THE INDIVIDUAL UNCERTAINTIES. FIGURE FROM (PAGANETTI, 2014).

5.5 Impact on clinical proton therapy

Clinically an average RBE of 1.1 is used for proton treatment planning. With RBE values from 4-10 in the distal edge of the Bragg-Peak, today's method for treatment planning with protons may cause problems. In our case however, we have worked with low energy protons (14.5-16 MeV) while clinically, energies above 100 MeV are applied. This will affect both the energy spectrum and the LET spectrum at the distal edge of the Bragg-Peak, as can be seen in Figure 61. When the protons travel a longer distance, straggling and scattering

will cause a larger energy distribution as the depth increases. Thus the LET distribution will broaden as the protons stop at a bigger variation in depth. The possible maximal average LET will also decrease, but the distribution will still reach high LET in some areas. If these areas cover organs at risk (OAR), the increased RBE may cause more (or more severe) side effects. The end of the track is commonly placed at the edge of the tumour volume. One of the advantages with proton therapy is that there is no irradiation behind the Bragg peak and it therefore is possible to irradiate close to organs at risk. However, because of the high RBE small deviations in placement or organ motion may have more severe consequences compared to x-rays. Measurements in front of the Bragg-Peak that were performed in this thesis, with an average LET of 7.5 keV/µm, still had a significantly higher RBE than 1.1, namely 2.3. The cell dishes used for analysis contained cells that had been irradiated with average LETs of both 5 and 10, and one can imagine that this can illustrate a scenario with a higher initial energy and a broader energy spectra. This indicates that the average RBE of 1.1 is insufficient, as higher RBE levels are reached for LET values as low as 10 keV/µm, which are regularly obtained in clinical proton beams.

While this necessitates very precise dose delivery near OAR, the increased RBE values provide an efficient way to target the resistant areas of a tumour. By aiming the end of the proton track in regions with e.g. hypoxia one might achieve a larger tumour control. The RBE values however vary with the type of the cell, as well as depth and radiation quality. Therefore there are challenges on how to draw benefits from the increased RBE. In any case, the large variations in RBEs indicate that care must be taken when conducting radiotherapy with protons, as some cell types may have large biological effects of LETs present in the treatment beam. And even though the response of the cells varies, it would be a step forward to make a standardization for proton therapy where the end of the beam is placed inside the tumour volume as far as this is possible.

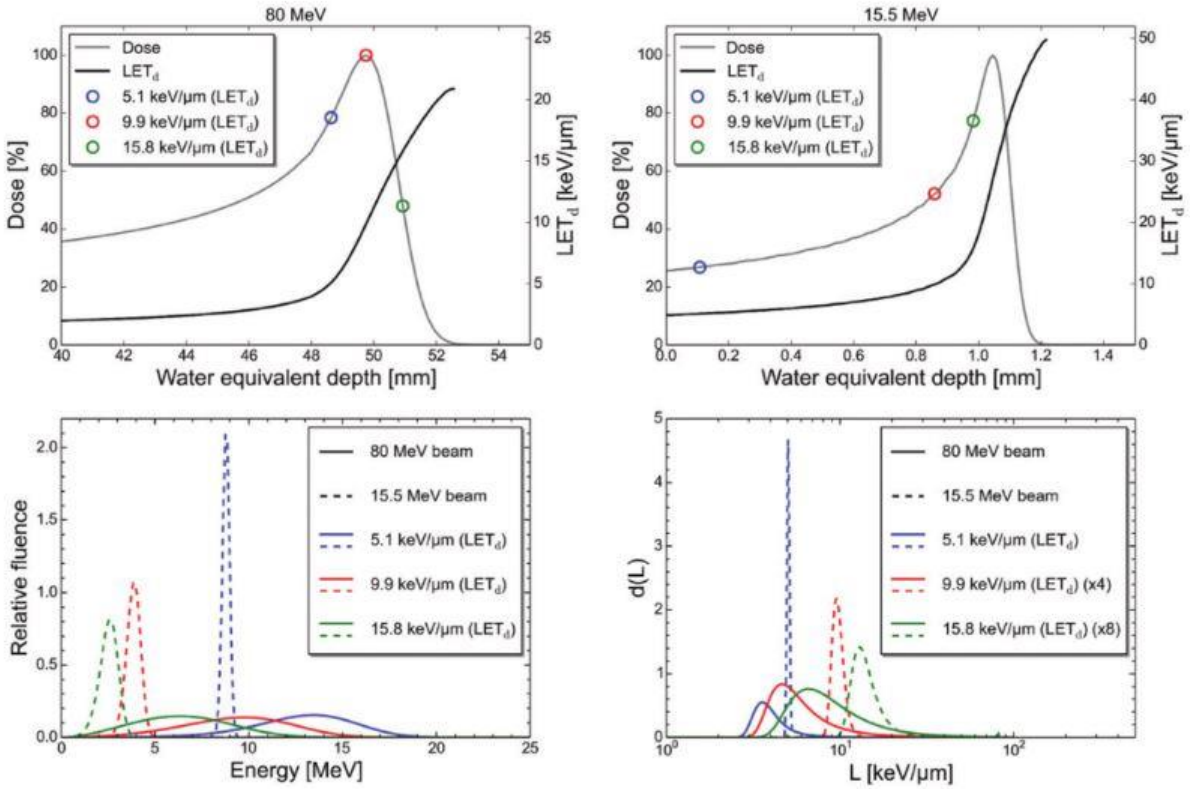

FIGURE 61. THE DIFFERENCE IN ENERGY AND LET SPECTRUM FOR 15.5 MEV AND 80 MEV PROTONS, AT DIFFERENT POSITIONS IN THE BRAGG-PEAK. FIGURE 5 FROM (DAHLE ET AL., 2017):"DOSE AND LETD VALUES AS A FUNCTION OF WATER EQUIVALENT DEPTH FOR THE 80MEV AND 15.5 MEV PROTON BEAMS, WITH CIRCLES MARKING LOCATION OF THREE SPECIFIC LETD VALUES AT THE DEPTH DOSE PROFILES (UPPER PANELS). ENERGY SPECTRA (LOWER PANELS, LEFT) AND DOSE WEIGHTED LET SPECTRA (LOWER PANELS, RIGHT) CORRESPONDING TO THE THREE MARKED LETD VALUES, FOR BOTH THE 80MEV AND 15.5 MEV PROTON BEAM. SCALING OF SOME OF THE LET SPECTRA IS SHOWN IN PARENTHESIS IN THE LEGEND."

5.6 Recommendations for future work

For future work it would be interesting to look closer at the repair mechanisms in the cells after high LET radiation in combination with more clonogenic cell survival experiments. This can be done by monolayer irradiation followed by counting of DBS (marking of phosphorylated H2AX and flow cytometer count), in combination with clonogenic survival experiments. Flow cytometry gives the option to gate out un-irradiated cells, thus avoiding the problem of background colonies.

Using nylon and Parafilm to obtain different positions in depth had some limitations because of the low energy and therefore short distance before the Bragg peak was reached. To achieve more similar conditions on a day to day basis it would also be possible to use the

distance in air to adjust to the same positions in the BP at each experiment required because the initial energy varies from day-to-day. In addition to this it is recommended to find a replacement for Parafilm as an absorber for cell irradiations in the distal edge of the Bragg-Peak. As the structure of the Parafilm only causes significant disruption in the dose-distribution in the distal edge of the BP, it can still be used in front of the BP. A possibility would be too use the cell dish lid during irradiations in the distal edge of the BP.

It would be interesting to do cell survival experiments at more positions in the Bragg-Peak as well, as experiments by Belli et al. (Belli et al., 2000) showed the "tail" present only for LET values at 30keV/µm. It would be a good way to find more information about how the "tail" occurs, if it is a LET effect, or if it is a setup issue with un-irradiated cells as suspected. Another way to investigate this would be to repeat the experiment for different cell lines. A test for checking if un-irradiated cells loosen during addition of medium could be too flush the irradiated cells with medium, pouring it off and adding new medium. This would remove any such background colonies if present. It could also be attempted to take the medium from an irradiated cell dish with freshly added medium, and add the medium to a new dish and see if colony formation occurs. To see if there are actually cells surviving irradiation, or if the cells are shielded, it would be possible to irradiate cells with doses around 20 Gy or higher, where any survival would be unlikely unless there is a shielding effect.

More experiments in the area from 0-5 Gy would also be relevant in order to find the curvature and shape for the low doses, aiding in the identification of an α value to be used in the LQ-model. Adding dose levels of 1 and 3 Gy would also be recommended.

6 Conclusion

A setup for cell irradiation at OCL was successfully made. A monitor chamber was added in the setup to achieve better dosimetry, and a method for monitoring beam homogeneity using Gafchromic EBT3 dosimetry films was found. Solutions have been found to proton beam homogeneity dose corrections in front of the Bragg-Peak, and suggestions have been made to improve distal edge BP homogeneity corrections as well.

The reason for the “tail” observed at high doses in the survival plot for cells irradiated with high LET protons was most likely due to an un-irradiated population of cells. The latest data showed that the Parafilm, used as an absorber and as a lid during irradiation, had an elastic structure similar to that of an accordion, resulting in an inhomogeneous dose distribution. As irradiations were performed at the distal edge of the Bragg-Peak, a small additional thickness in the absorber may have been enough to keep the protons from reaching some of the cells, shielding them from the radiation.

RBE values of 2.3 where found in front of the Bragg-Peak, and in the distal edge of the Bragg-Peak values between 4 and 10 were found. This indicates that the applied RBE of 1.1 may be insufficient, and care should be taken in radiotherapy with placing the end of proton track in the edge of the target volume. The use of LET dependent RBE values in radiotherapy could be used for optimization of the dose planning to obtain better tumour control.

References

ALBERTS, B. 2008. Molecular biology of the cell. 5th ed. New York: Garland,.

ATTIX, F. H. 1986. *Introduction to radiological physics and radiation dosimetry,* New York, Wiley.

BALL, M. P. 2016. DNA chemical structure. *In:* STRUCTURE.SVG, D. C. (ed.). Wikipedia: Wikipedia.

BELLI, M., BETTEGA, D., CALZOLARI, P., CERA, F., CHERUBINI, R., DALLA VECCHIA, M., DURANTE, M., FAVARETTO, S., GIALANELLA, G., GROSSI, G., MARCHESINI, R., MOSCHINI, G., PIAZZOLA, A., POLI, G., PUGLIESE, M., SAPORA, O., SCAMPOLI, P., SIMONE, G., SORRENTINO, E., TABOCCHINI, M. A., TALLONE, L. & TIVERON, P. 2000. Inactivation of human normal and tumour cells irradiated with low energy protons. *Int J Radiat Biol,* 76**,** 831-9.

BURDAK-ROTHKAMM, S., ROTHKAMM, K. & PRISE, K. M. 2008. ATM acts downstream of ATR in the DNA damage response signaling of bystander cells. *Cancer Res,* 68**,** 7059-65.

CASANOVA BORCA, V., PASQUINO, M., RUSSO, G., GROSSO, P., CANTE, D., SCIACERO, P., GIRELLI, G., LA PORTA, M. R. & TOFANI, S. 2013. Dosimetric characterization and use of GAFCHROMIC EBT3 film for IMRT dose verification. *J Appl Clin Med Phys,* 14**,** 4111.

CATTIN, P. 2016. Basics of X-ray: Principles of Medical Imaging. MIAC, University of Basel.

CHAUDHARY, P., MARSHALL, T. I., PEROZZIELLO, F. M., MANTI, L., CURRELL, F. J., HANTON, F., MCMAHON, S. J., KAVANAGH, J. N., CIRRONE, G. A., ROMANO, F., PRISE, K. M. & SCHETTINO, G. 2014. Relative biological effectiveness variation along monoenergetic and modulated Bragg peaks of a 62-MeV therapeutic proton beam: a preclinical assessment. *Int J Radiat Oncol Biol Phys,* 90**,** 27-35.

COLEY, B. D. & CAFFEY, J. 2013. Caffey's pediatric diagnostic imaging. 12th ed. Philadelphia, Pa.: Saunders,.

DAHLE, T. J., RYKKELID, A. M., STOKKEVAG, C. H., MAIRANI, A., GORGEN, A., EDIN, N. J., RORVIK, E., FJAERA, L. F., MALINEN, E. & YTRE-HAUGE, K. S. 2017. Monte Carlo simulations of a low energy proton beamline for radiobiological experiments. *Acta Oncol,* 56**,** 779-786.

FRAME, P. 1999. coolidgedrawing. Oak Ridge Associated Universities.

GAFCHROMIC 2014. Gafchromic EBT3 Scan Handling Guide. *In:* GAFCHROMIC (ed.) 12/14 ed.

GUAN, F., BRONK, L., TITT, U., LIN, S. H., MIRKOVIC, D., KERR, M. D., ZHU, X. R., DINH, J., SOBIESKI, M., STEPHAN, C., PEELER, C. R., TALEEI, R., MOHAN, R. & GROSSHANS, D. R. 2015. Spatial mapping of the biologic effectiveness of scanned particle beams: towards biologically optimized particle therapy. *Sci Rep,* 5**,** 9850.

HALL, E. J. & GIACCIA, A. J. 2012. *Radiobiology for the radiologist,* Philadelphia, USA, LIPPINCOTT WILLIAMS & WILKINS.

JOINER, M. & KOGEL, A. V. D. 2009. *Basic clinical radiobiology,* London, Hodder Arnold.

KHAN, F. M., GIBBONS, J. P., PINE, J. W., MOYER, E., JACKSON, A., CLEMENTS, J., WENDT, J. & EBRARY INC. 2014. Khan's the physics of radiation therapy. Fifth edition. ed.

KRANE, K. S. & HALLIDAY, D. 1988. *Introductory nuclear physics,* New York, Wiley.

LYMAN, J. T., AWSCHALOM, M., BERARDO, P., BICCHSE, H., CHEN, G. T. Y., DICELLO, J., FESSENDEN, P., GOITEIN, M., LAM, G., MCDONALD, J. C., SMITH, A. F., HAKEN, R. T., VERHEY, L. & ZINK, S. 1986. Protocol for Heavy Charged-Particle Therapy Beam Dosimetry. USA: the American Association of Physicists in Medicine.

M.J. BERGER, J. S. C., M.A. ZUCKER AND J. CHANG 2017. PSTAR: Computer program for Calculating Stopping-Power and Range Tables for Protons. 1.10.1998 ed.: National Institute of Standards and Technology, Gaithersburg, MD.

MA, C. M., COFFEY, C. W., DEWERD, L. A., LIU, C., NATH, R., SELTZER, S. M., SEUNTJENS, J. P. & AMERICAN ASSOCIATION OF PHYSICISTS IN, M. 2001. AAPM protocol for 40-300 kV x-ray beam dosimetry in radiotherapy and radiobiology. *Med Phys,* 28**,** 868-93.

PAGANETTI, H. 2014. Relative biological effectiveness (RBE) values for proton beam therapy. Variations as a function of biological endpoint, dose, and linear energy transfer. *Phys Med Biol,* 59**,** R419-72.

PAUL, H. 2009. Depth Dose Curves. *In:* CURVES.JPG, D. D. (ed.).

PODGORŠAK, E. B. 2005. *Radiation oncology physics : a handbook for teachers and students,* Vienna, International Atomic Energy Agency.

ROSSER, K. E. 1996. Measurement of absorbed dose to water for medium energy x rays. *Medical Physics,* 23**,** 2093-2093.

SORENSEN, B. S., BASSLER, N., NIELSEN, S., HORSMAN, M. R., GRZANKA, L., SPEJLBORG, H., SWAKON, J., OLKO, P. & OVERGAARD, J. 2017. Relative biological effectiveness (RBE) and distal edge effects of proton radiation on early damage in vivo. *Acta Oncol***,** 1-5.

STEIN, G. H. 1979. T98G: an anchorage-independent human tumor cell line that exhibits stationary phase G1 arrest in vitro. *J Cell Physiol,* 99**,** 43-54.

WALDELAND, E., HOLE, E. O., SAGSTUEN, E. & MALINEN, E. 2010. The energy dependence of lithium formate and alanine EPR dosimeters for medium energy x rays. *Med Phys,* 37**,** 3569-75.

ZHANG, R. & NEWHAUSER, W. D. 2009. Calculation of water equivalent thickness of materials of arbitrary density, elemental composition and thickness in proton beam irradiation. *Phys Med Biol,* 54**,** 1383-95.

Appendix A

Gafchromic EBT3 Film Dosimetry

Listed in Table 25 is settings for scanning of Gafchromic, using an Epson Perfection V850 Pro flatbed scanner. Further is doses delivered with corresponding monitor units (MU) or irradiation time, for calibration of the films to electrons, x-rays, ^{60}Co, and protons listed in Table 26, Table 27 and Table 28 and Table 29 respectively. All film measurement for positions and depths with protons are listed in Table 30.

TABLE 25. OVERVIEW OF SETTINGS REQUIRED FOR SCANNING EBT3 FILMS.

SETTINGS	
Document type	Transparency
Film Type	Positive film
Image Type	48-bit Colour
Resolution	150 ppt
Colour correction	Off

TABLE 26. DOSES WITH EQUIVALENT MUS DELIVERED FOR ELECTRON CALIBRATION OF TO GAFCHROMIC EBT3 FILMS.

Dose (Gy)	Monitor Units (MU)	# Films
0	0	3
0,5	54	3
1,5	161	3
3,0	321	3
5,0	535	3
7,5	803	3
10,5	1124	3
14	1498	3

TABLE 27. IRRADIATION DOSES FOR X-RAY CALIBRATION OF GAFCHROMIC EBT3 FILMS.

Dose (Gy)	Time	# Films
0	0 min 0 sek	2
1	2 min 18 sek	2
2	4 min 36 sek	2
5	11 min 30 sek	2
10	23 min 0 sek	2

TABLE 28. IRRADIATION DOSES FOR ^{60}CO CALIBRATION OF GAFCHROMIC EBT3 FILMS.

Dose (Gy)	Time (min)	# Films
0	0	2
2	4,92	4
5	12,31	4
10	24,62	4

TABLE 29. IRRADIATION DOSES FOR PROTON CALIBRATION OF GAFCHROMIC EBT3 FILMS.

Target dose (Gy)	Monitor Chamber output (µC)	Dose delivered (Gy)
2	1.178	1.84
2	1.115	1.75
3	1.716	2.69
3	1.644	2.57
5	2.621	4.11
5	2.17	3.40
10	5.212	8.16
10	5.392	8.45
14	8.123	12.72
14	8.208	12.86

TABLE 30. ALL POSITIONS FOR IRRADIATION OF DOSIMETRY FILMS WITH PROTONS. POSITIONING IN REFERENCE TO THE BEAM EXIT WINDOW, IF THE FILM HAS BEEN IRRADIATED AS A SQUARE IN FRONT OF THE IONIZATION CHAMBER OR AS A CIRCLE IN THE PETRI DISH IN THE CELL CONTAINER, DEPTH COMPONENTS, AND THE WATER EQUIVALENT DEPTH IS LISTED. IN THE WATER EQUIVALENT DEPTH, ABOUT HALF OF THE FILM THICKNESS IS INCLUDED (THE WHOLE ACTIVE LAYER).

		Film placement			
Experiment	**Position (cm)**	**In front of IC**	**In petri dish**	**Depth components**	**Water eq.depth (mm)**
SETUP 1					
1	106	x		0	0.1910
	106		x	1 Parafilm	0.3186
	106.1		x	2 Parafilm + 1 petri dish bottom	1.3195
2	88	x		0	0.1910
	88		x	1 Parafilm	0.3186
	88.1		x	2 Parafilm + 1 petri dish bottom + 1 EBT3	1.6669
3	88	x		0	0.1910
	88.1		x	2 Parafilm + 1 petri dish bottom	1.3195
	88		x	1 Parafilm	0.3186
	88	x		0	0.1910

	88	x		2 N6	1.3640
SETUP 2					
initial	88	x		1 N6	0.7775
	88		x	1 Parafilm	0.3186
	88		x	1 N6 + 2 Parafilm	1.0326
1	88		x	1 N6 + 2 Parafilm	1.0326
	88		x	1 Parafilm	0.3186
2	88	x	x	1 N6 + 2 Parafilm	1.0326
	88	x	x	1 Parafilm	0.3186
3		x		0	0.1910
	88	x	x	1 N6 + 2 Parafilm	1.0326
	88	x	x	1 Parafilm	0.3186
SETUP 3					
initial	85	x		0	0.1910
	75	x		0	0.1910
1	78	x		0	0.1910
	78	x		1 N6 + 2 Parafilm	1.0326
	78	x		1 N6 + 1 Parafilm	0.9051
SETUP 4					
initial	78	x		0	0.1910
	78	x		1 N6 + 1 Parafilm	0.9051
	78	x		1 N6 + 2 Parafilm	1.0326
1	81	x		0	0.1910

Ionization Chamber Measurements, Protons

All dosimetry performed at the cyclotron with different absorber depths, with and without the Monitor Chamber, and in different distances from the beam exit window is listed in Table 31.

TABLE 31. ALL DOSIMETRY MEASUREMENT POINTS DONE WITH AN IONIZATION CHAMBER WITH ALL FOUR SETUPS. IC POSITIONS ARE ALL IONIZATION CHAMBER POSITIONS WERE MEASUREMENTS WERE CONDUCTED. MC POSITIONS ARE POSITION THE MONITOR CHAMBER WAS AT DURING MEASUREMENT. THE X NOTES THAT THE MEASUREMENT WAS DONE WITHOUT THE MONITOR CHAMBER (MC) IN THE BEAM LINE.

SETUP 1 Experiment	Depth components	Water eqv. Depth	IC positions (cm)			MC positions (cm)	
1	0	0	88	108	128	x	
	1 Parafilm	0.1275	88			x	
	2 Parafilm	0.2550	88			x	
	2 Parafilm + dish bottom	1.1284	88			x	
	1 N6	0.5865	88	108	128	x	
	2 N6	1.173	88	108	128	x	
	3 N6	1.7595	88			x	
2	0	0	88			x	8
	1 Parafilm	0.1275	88			x	8
	2 Parafilm	0.2550	88			x	8
	2 Parafilm + dish bottom	1.1284	88			x	8
	1 N6	0.5865	88			x	8
	2 N6	1.1730	88			x	8
3	0	0	88			x	

SETUP 2 Experiment	Depth components	Water eqv. Depth	IC positions (cm)					MC positions (cm
1	0	0	48	68	88	108	128	8
	2 Parafilm	0.2550	48	68	88	108	128	8
	1 N6	0.5865			88			8
	1 N6 + 1 Parafilm	0.7140			88			8
	1 N6 + 2 Parafilm	0.8415			88		128	8
	1 N6 + 3 Parafilm	0.9690			88			8
	1 N6 + 4 Parafilm	1.0966			88			8
	2 N6	1.1730			88			8
	2 N6 + 1 Parafilm	1.3005			88			8
	1 EBT3	0.3473			88		128	8
	1 EBT3 + 1 Parafilm	0.4748						8
	1 N6 + 1 EBT3	0.9338			88			8
	1 N6 + 1 EBT3 + 2 Parafilm	1.1889			88			8
2	1 N6 + 2 Parafilm	0.84156			88			8
	1 EBT3 + 1 Parafilm	0.47489			88			8
3	1 N6 + 2 Parafilm	0.84156			88			8

	1 EBT3 + 1 Parafilm	0.47489	88	8

SETUP 3 Experiment	Depth components	Water eqv. Depth	IC positions (cm)	MC position (cm)
initial	0	0.0000	88	14
	1 N6	0.5865	88	14
	1 N6 +1 Parafilm	0.7140	88	14
	1 N6 +2 Parafilm	0.8416	78 88	14
	1 N6 +3 Parafilm	0.9691	78 88	14
1	0	0.0000	78	14
	1 Parafilm	0.1275	78	14
	1 N6	0.5865	78	14
	1 N6 +1 Parafilm	0.7140	78	14
	1 N6 +2 Parafilm	0.8416	78	14
	1 N6 +3 Parafilm	0.9691	78	14
	2 N6	1.1730	78	14
2	0	0.0000	78	14
	1 Parafilm	0.1275	78	14
	1 N6 +2 Parafilm	0.8416	78	14
	1 N6 +3 Parafilm	0.9691	77.5 77 78 79 78.5 77.8 77.9 78.1 78.2	14
3	1 Parafilm	0.1275	78	14
	1 N6 +3 Parafilm	0.9691	77.8 77.9 78 78.1 78.2	14

SETUP 4 Experiment	Depth components	Water eqv. Depth	IC positions (cm)	MC position (cm)
1	0	0.0000	81	14
	1 Parafilm	0.1275	81	14
	2 Parafilm	0.2551	81	14
	3 Parafilm	0.3826	81	14
	1 N6	0.5865	81	14

	1 N6 + 1 Parafilm	0.7140	81	14
	1 N6 + 2 Parafilm	0.8416	78 78.5 79 80 81 81.5	14
	1 N6 + 3 Parafilm	0.9691	78 81	14

Clonogenic Cell Survival Experiments

The number of seeded cells for target doses in all clonogenic cell survival experiments completed in this thesis is listed below. For x-rays these can be found in Table 32, and for ^{60}Co in Table 34. For the four different setup in proton experiments they are listed in Table 35, Table 36,

Table 37 and Table 38. For irradiation times corresponding to doses in x-ray experiments, these are listed in Table 33.

X-rays

TABLE 32. DELIVERED DOSES AND CELLS SEEDED FOR THE THREE CLONOGENIC SURVIVAL EXPERIMENTS WITH X-RAYS.

A

X-ray1		
Dose (Gy)	# cells	# dishes
0	100	10
1.74	150	5
4.35	400	5
8.7	15000	5

B

X-ray2		
Dose (Gy)	# cells	# flasks
0	250	10
2	500	5
5	2500	5
10	60000	5

C

X-ray3		
Dose (Gy)	# cells	# flasks
0	250	10
2	500	5
5	2500	5
10	60000	5

TABLE 33. X-RAY IRRADIATION TIME FOR EACH DOSE.

Dose (Gy)	Irradiation Time
1.74	4 min 0 sek
2	4 min 36 sek
4.35	10 min 0 sek
5	11 min 30 sek
8.7	20 min 0 sek
10	23 min 0 sek

^{60}Co

TABLE 34: NUMBER OF CELLS SEEDED IN ^{60}CO EXPERIMENTS C1-C3.

Dose (Gy)	# Cells	# Dishes
0	250	8
2	500	4
5	2500	4
10	60000	4

Protons

TABLE 35. TARGET IRRADIATION DOSES BEFORE DOSIMETRY IN THE THREE EXPERIMENTS USING SETUP 1. LISTED IS THE NUMBER OF CELLS SEEDED AND NUMBER OF DISHES IRRADIATED IN THE TWO POSITIONS.

Position 1		
Dose (Gy)	# cells	# dishes
0	100	4
2	100	4
5	500	4
10	10000	4

Position 2		
Dose (Gy)	# cells	# dishes
0	100	4
2	150	4
5	1000	4
10	20000	4

TABLE 36. TARGET IRRADIATION DOSES BEFORE DOSIMETRY IN THE THREE EXPERIMENTS USING SETUP 2. LISTED IS THE NUMBER OF CELLS SEEDED AND NUMBER OF DISHES IRRADIATED IN THE TWO POSITIONS.

A

Position 1		
Dose (Gy)	**# cells**	**# dishes**
0	100	4
2	100	4
5	500	4
10	8000	4

B

Position 2		
Dose (Gy)	**# cells**	**# dishes**
0	100	4
2	150	4
5	1000	4
10	20000	4

TABLE 37. TARGET DOSES, NUMBER OF CELLS SEEDED, AND NUMBER OF DISHES FOR ALL THREE EXPERIMENTS WITH SETUP 3.

	proton_setup3_1		proton_setup3_2		proton_setup3_3	
Dose	**# cells**	**# dishes**	**# cells**	**# dishes**	**# cells**	**# dishes**
0	250	6	250	6	250	6
2	500	3	500	6	500	6
5	2500	6	2500	6	2500	6
10	60000	3	60000	6	60000	6
14	93300	2	91800	4	120000	6

TABLE 38. TARGET DOSES, NUMBER OF SEEDED CELLS AND THE NUMBER OF DISHES IN THE EXPERIMENT WITH SETUP 4.

	proton_setup4_1	
Dose	**# cells**	**# dishes**
0	100	10
2	300	6
5	3000	6
10	30000	6
14	30000	6

Appendix B

Gafchromic EBT3 measurements, protons

All films irradiated with low-energy protons at OCL were analysed. Some films were irradiated as squares in a holder in front of the ionization chamber, indicated by the letter F in the name, and some were irradiated inside the 8.8 cm^2 circular petri dishes, indicated by the letter R in the name. The name of the film indicates which day using the setup it was irradiated (1 means day one using the setup etc.) and if it was irradiated in a holder (F) or in a petri dish (R). The last number, the one after the letter R or F, was simply to distinguish the films. Measured dose with standard deviation (σ), positioning and placement of the film, radiation time, water equivalent depth of the active layer in the film, and the dose rate is listed in the tables below. For setup 4, the films were only used to evaluate the homogeneity, as it was unclear as to how we could use the films for dosimetric purposes.

Setup 1

TABLE 39. RESULTS OF ANALYSIS OF IRRADIATED EBT3 FILMS ON SETUP 1.

					Film placement				
Film	**Dose (Gy)**	**σ dose (Gy)**	**Relative σ**	**Position (cm)**	**In front of IC**	**In petri dish**	**Radiation time (s)**	**water eq.depth (mm)**	**Dose rate (Gy/min)**
1_F01	*								
1_F02	10.93	1.84	17%	106	x		10.38	0.19	63.2
1_F03	1.32	0.24	18%	106	x		30	0.19	2.6
1_R01	4.10	0.63	15%	106		x	80.75	0.32	3.0
1_R02	6.29	1.00	16%	106.1		x	80.75	1.32	4.7
1_R03	3.57	0.52	15%	106		x	80.73	0.32	2.7
1_R04	4.26	1.50	35%	106.1		x	80.73	1.32	3.2
2_F01	2.92	0.38	13%	88	x		50	0.19	3.5
2_R01	4.42	1.26	29%	88		x	80.43	0.32	3.3
2_R02	7.68	2.15	28%	88.1		x	80.43	1.67	5.7
3_F01	2.88	0.48	17%	88	x		32.15	0.19	5.4
3_F02	2.76	0.53	19%	88	x		80.63	0.19	2.0
3_F03	2.76	0.49	18%	88	x		32.62	1.36	5.0
3_F04	6.97	1.19	17%	88	x		32.3	1.36	13.0
3_F05	7.13	1.33	19%	88	x		32.2	1.36	13.3
3_F06	7.19	1.33	18%	88	x		80.36	1.36	5.4
3_F07	13.63	2.79	20%	88	x		80.62	1.36	10.1
3_F08	14.60	2.90	20%	88	x		80.65	1.36	10.9

3_F09	13.33	2.65	20%	88	x		160.54	1.36	5.0
3_F10	2.50	0.39	15%	88	x		160.6	1.36	0.9
3_F11	4.02	0.70	17%	88	x		160.37	1.36	1.5
3_R01	7.15	1.12	16%	88.1		x	80.54	1.32	5.3
3_R02	7.08	1.05	15%	88.1		x	80.59	1.32	5.3
3_R03	4.53	0.64	14%	88		x	80.57	0.32	3.4
3_R04	4.72	0.77	16%	88		x	80.56	0.32	3.5

* Overexposed film, unable to correspond optical density to a dose.

Setup 2

TABLE 40. RESULTS OF ANALYSIS OF IRRADIATED EBT3 FILMS ON SETUP 2.

Film	Dose (Gy)	σdose (Gy)	Relative σ	Position (cm)	Film placement		Monitor Chamber (nC)	water eq.depth (mm)	Dose rate (Gy/µC)
					In front of IC	In petri dish			
1_F01	16.66	4.15	25%	28	x		1756	0.19	9.49
1_F02	4.42	0.91	21%	28	x		511.7	0.19	8.64
1_F03	5.23	0.28	5%	88	x		4006	0.19	1.30
1_F04	5.22	0.27	5%	88	x		3945	0.19	1.32
1_F05	7.65	0.41	5%	88	x		4006	0.78	1.91
1_F06	12.96	0.66	5%	88	x		4016	1.03	3.23
1_F07	4.58	0.20	4%	128	x		6036	0.19	0.76
1_R01	6.19	0.43	7%	88		x	1996	1.03	3.10
1_R02	5.61	0.35	6%	88		x	2002	1.03	2.80
1_R03	2.78	0.20	7%	88		x	2003	0.32	1.39
1_R04	2.45	0.19	8%	88		x	2006	0.32	1.22
2_F01	6.18	0.32	5%	88	x		2621	0.91	2.36
2_F02	8.44	0.62	7%	88	x		2622	1.03	3.22
2_F03	3.57	0.25	7%	88	x		2687	0.32	1.33
2_R01	8.12	0.66	8%	88		x	2665	1.03	3.05
2_R02	3.15	0.41	13%	88		x	2652	0.32	1.19
3_F01	1.47	0.15	10%	88	x			0.19	
3_F02	1.50	0.11	7%	88	x			0.19	
3_F03	2.26	0.09	4%	88	x			0.19	
3_F04	3.19	0.13	4%	88	x		2260	0.32	1.41
3_F05	6.68	0.24	4%	88	x		2231	1.03	2.99
3_R01	6.97	0.32	5%	88		x	2259	1.03	3.08
3_R02	6.26	0.60	10%	88		x	2205	1.03	2.84
3_R03	2.82	0.16	6%	88		x	2252	0.32	1.25
3_R04	2.76	0.13	5%	88		x	2232	0.32	1.24

Setup 3

TABLE 41. RESULTS OF ANALYSIS OF IRRADIATED EBT3 FILMS ON SETUP 3.

					Film placement	

Film	Dose (Gy)	σ dose (Gy)	Relative σ	Position (cm)	In front of IC	In petri dish	Monitor Chamber (nC)	water eq.depth (mm)	Dose rate (Gy/μC)
initial_F01	3.52	0.16	5%	85	x			0.1910	
1_F01	1.83	0.10	5%	78	x		1178	0.1910	1.56
1_F02	1.58	0.10	6%	78	x		1115	0.1910	1.42
1_F03	3.95	0.14	4%	78	x		2621	0.1910	1.51
1_F04	3.47	0.12	3%	78	x		2170	0.1910	1.60
1_F05	8.15	0.24	3%	78	x		5212	0.1910	1.56
1_F06	8.19	0.28	3%	78	x		5392	0.1910	1.52
1_F07	12.48	0.39	3%	78	x		8123	0.1910	1.54
1_F08	12.56	0.43	3%	78	x		8208	0.1910	1.53
1_F09	2.66	0.10	4%	78	x		1716	0.1910	1.55
1_F10	2.48	0.10	4%	78	x		1644	0.1910	1.51
1_F11	1.50	0.29	19%	78	x		2446	1.0326	0.61
1_F12	9.00	0.32	4%	78	x		2403	0.9051	3.75

Setup 4

TABLE 42. RESULTS OF ANALYSIS OF IRRADIATED EBT3 FILMS ON SETUP 4.

Film	Dose (Gy)	σ dose (Gy)	Relative σ	Position (cm)	Film placement: In front of IC	Film placement: In petri dish	Monitor Chamber (nC)	water eq.depth (mm)	Dose rate (Gy/uC)
initial_F01	3.71	0.13	3%	78	x		2624	0.1910	1.414
initial_F02	3.91	0.16	4%	78	x		1250	0.9051	3.129
initial_F03	0.15	0.05	33%	78	x		5114	1.0326	0.030
1_F01	2.98	0.15	5%	81	x		2265	0.1910	1.315

Cell survival curve for ^{60}Co

In Figure 62 the surviving fraction of T98G cells is plotted as a function of dose. The cells were irradiated without the medium, and due to long irradiation times they suffered elevated pH levels for periods up to 30 minutes. This was more than twice as long as the cells irradiated with low-energy protons, and the data was therefore not optimal as a reference in RBE calculations.

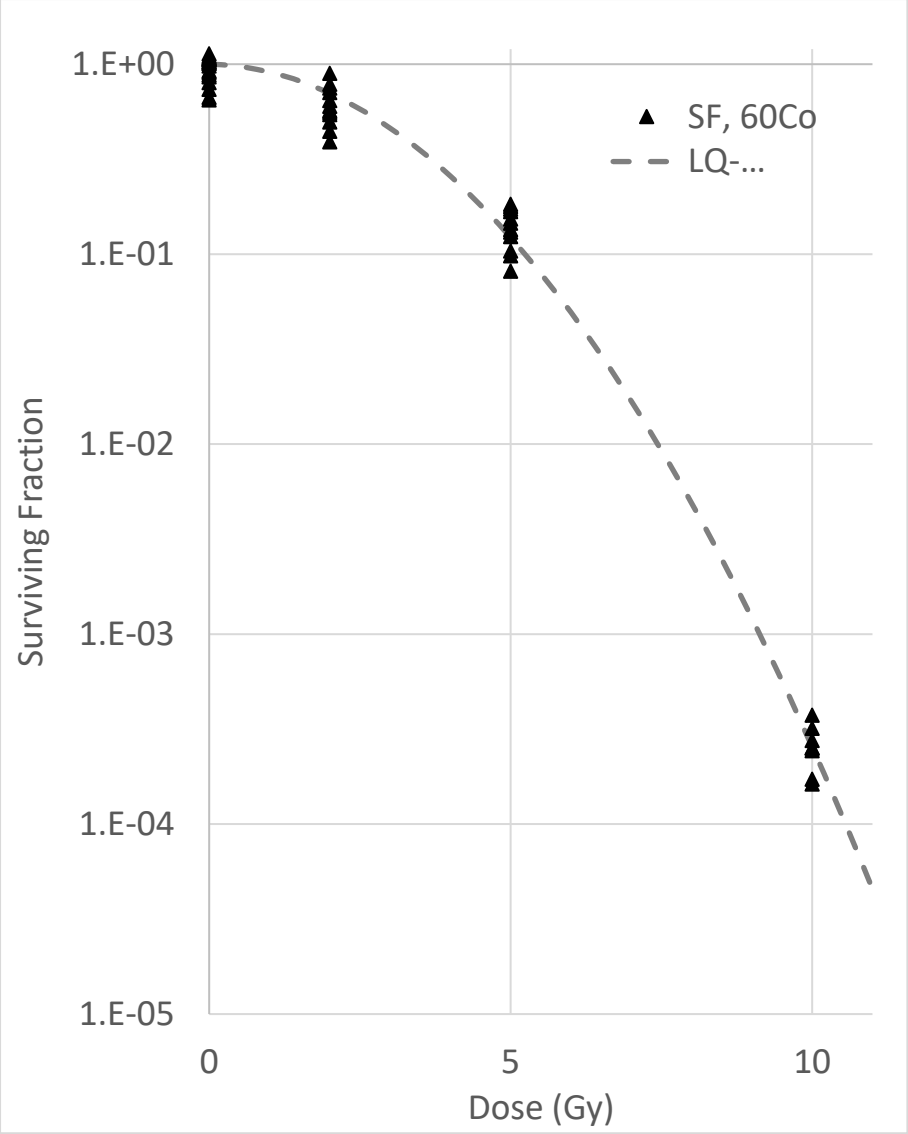

FIGURE 62. SURVIVING FRACTION AS A FUNCTION OF DOSE FOR T98G CELLS WITH GAMMA-RAYS FROM ^{60}CO. MEDIUM WAS REMOVED PRIOR TO IRRADIATION.

RBE

The RBE values for the modelled uncorrected survival data obtained from proton irradiation is plotted as a function of survival in Figure 63, together with the corrected models.

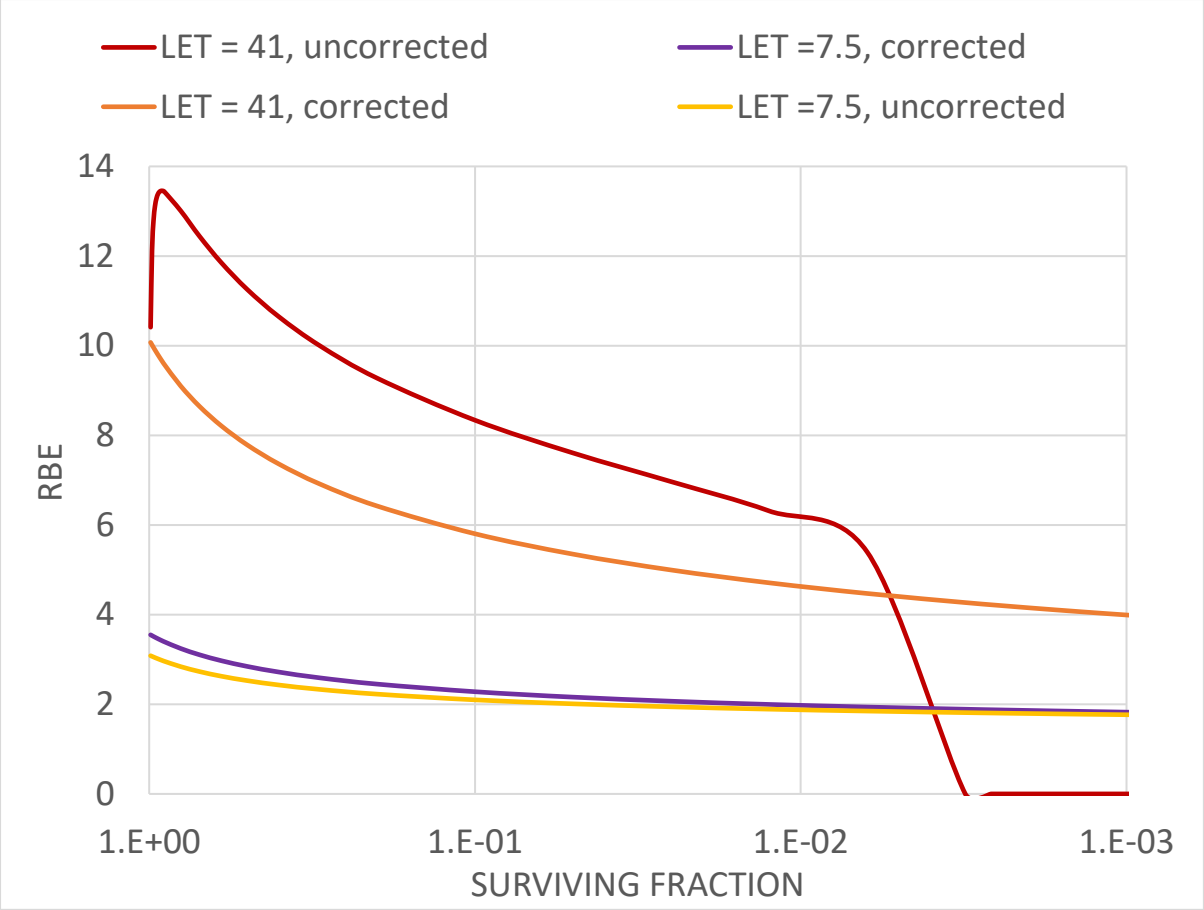

FIGURE 63. RBE VALUES ESTIMATED FOR BOTH CORRECTED CELL SURVIVAL MODELS, AND UNCORRECTED CELL SURVIVAL MODELS FOR GROUP 1 (LET = 7.5) AND GROUP 2 (LET=41).

Appendix C: IDL code

Calibration of Gafchromic EBT3 films

```
folder='\120516_Cobalt'
files = ['xray_0Gy_270916_001.bmp','xray_0Gy_270916_002.bmp','C-
60_2Gy001.bmp','C-60_2Gy002.bmp','C-60_2Gy003.bmp','C-60_2Gy004.bmp','C-
60_5Gy_001.bmp','C-60_5Gy_002.bmp','C-60_5Gy_003.bmp','C-
60_5Gy_004.bmp','C-60_10Gy_001.bmp','C-60_10Gy_002.bmp','C-
60_10Gy_003.bmp','C-60_10Gy_004.bmp']
centre =
[[160,160,165,159,166,156,163,159,154,166,170,163,164,159],[160,160,154,162
,163,168,157,161,163,164,157,161,161,153]]
doses = [0,0,2,2,2,2,5,5,5,5,10,10,10,10]

files = ['r_0gy_001.bmp','r_0gy_fargetavsola_001.bmp','C-60_2Gy001.bmp','C-
60_2Gy002.bmp','C-60_2Gy003.bmp','C-60_2Gy004.bmp','C-60_5Gy_001.bmp','C-
60_5Gy_002.bmp','C-60_5Gy_003.bmp','C-60_5Gy_004.bmp','C-
60_10Gy_001.bmp','C-60_10Gy_002.bmp','C-60_10Gy_003.bmp','C-
60_10Gy_004.bmp']
centre =
[[162,163,165,159,166,156,163,159,154,166,170,163,164,159],[157,147,154,162
,163,168,157,161,163,164,157,161,161,153]]
doses = [0,0,2,2,2,2,5,5,5,5,10,10,10,10]

;returns
result_RGB = calibration(folder,files,doses,centre,'cobalt60')

;Fitting to model myfunc
A = [0.5,5.0,0.3]
coef_RGB = LMFIT(result_RGB[*,0], result_RGB[*,1], A,
MEASURE_ERRORS=result_RGB[*,2], FITA=FITA, FUNCTION_NAME = 'myfunc',
/DOUBLE,SIGMA=sigma_cobalt)
A_RGB = A
print,'cobalt60', A
print,' sigma', sigma_cobalt ; returns error in model coefficients


;testing model on data
title = 'Calibration curve for Cobalt-60(red), 15 MeV protons(green), and 6
MeV electrons(blue)'
plot1 = ERRORPLOT( result_RGB[*,1], result_RGB[*,0],
result_RGB[*,2],result_RGB[*,2]*0,XTITLE='netOD',YTITLE=
'Dose(Gy)',TITLE=title,NAME='Cobalt-
60','r2X',OVERPLOT=1);,YRANGE=[0,13],XRANGE=[0,0.4])
; Overplot the fitted data:
X = INDGEN(100)*0.11
Z = MYFUNC(X,A_RGB)
Y = Z[*,0]
model1= PLOT(Y, X, OVERPLOT=1, 'r2--',NAME='Calibration curve, 60-Co')


folder='\240117_cyclotron_P8'
files =
['P8_calibration_240117_001.bmp','P8_calibration_240117_002.bmp','P8_calibr
ation_240117_003.bmp',$
```

```
'P8_calibration_240117_004.bmp','P8_calibration_240117_005.bmp','P8_calibra
tion_240117_006.bmp','P8_calibration_240117_007.bmp',$

'P8_calibration_240117_008.bmp','P8_calibration_240117_009.bmp','xray_0Gy_2
70916_001.bmp'];,'xray_0Gy_270916_002.bmp']

centre =
[[230,223,220,232,219,227,225,214,220,223,223],[206,204,212,220,205,203,207
,205,209,202,202]]
doses =
[1.84449442,1.745849982,4.103921795,3.397752879,8.160870048,8.442711301,12.
71886942,12.85196112,2.686886608,0];,0]

;returns
result_RGB = calibration(folder,files,doses,centre,'proton')
result_RGB[9,1]= 0
;Fitting to model myfunc
A = [0.5,5.0,0.3]

coef_RGB = LMFIT(result_RGB[*,0], result_RGB[*,1], A, FITA=FITA,
FUNCTION_NAME = 'myfunc', /DOUBLE, SIGMA=sigma_protons)
A_RGB = A
print,'proton', A
print, '  sigma', sigma_protons

;testing model on data

plot2 = ERRORPLOT(result_RGB[*,1], result_RGB[*,0],
result_RGB[*,2],XTITLE='netOD',YTITLE=
'Dose(Gy)',TITLE=title,NAME='Protons',
'g2X',OVERPLOT=1);XRANGE=[0,0.4],YRANGE=[0,13]
; Overplot the fitted data:
X = INDGEN(130)*0.11
Z = MYFUNC(X,A_RGB)
Y = Z[*,0]
model2= PLOT(Y, X, OVERPLOT=1, 'g2--',NAME='Calibration curve, protons')

folder='\Kalibrering_gaf_scan1'

files=
['kalibrering_000_001.bmp','kalibrering_000_002.bmp','kalibrering_000_003.b
mp','kalibrering_000_004.bmp',$

'kalibrering_005_001.bmp','kalibrering_005_002.bmp','kalibrering_005_003.bm
p',$

'kalibrering_015_001.bmp','kalibrering_015_002.bmp','kalibrering_015_003.bm
p',$

'kalibrering_030_001.bmp','kalibrering_030_002.bmp','kalibrering_030_003.bm
p',$

'kalibrering_050_001.bmp','kalibrering_050_002.bmp','kalibrering_050_003.bm
p',$

'kalibrering_075_001.bmp','kalibrering_075_002.bmp','kalibrering_075_003.bm
p',$

'kalibrering_105_001.bmp','kalibrering_105_002.bmp','kalibrering_105_003.bm
p',$
```

```
'kalibrering_140_001.bmp','kalibrering_140_002.bmp','kalibrering_140_003.bm
p']


doses =
[0.0,0.0,0.0,0.0,0.5,0.5,0.5,1.5,1.5,1.5,3.0,3.0,3.0,5.0,5.0,5.0,7.5,7.5,7.
5,10.5,10.5,10.5,14.0,14.0,14.0]
xlist = MAKE_ARRAY(25,value=218)
ylist = MAKE_ARRAY(25,value=218)
centre =  [[xlist],[ylist]] ;[xlist,ylist]

;returns
result_RGB = calibration(folder,files,doses,centre,'6 MeV electrons')

;Fitting to model myfunc
A = [5,0.,5.5]

coef_RGB = LMFIT(result_RGB[*,0], result_RGB[*,1], A,
MEASURE_ERRORS=result_RGB[*,2], FITA=FITA, FUNCTION_NAME = 'myfunc',
/DOUBLE, SIGMA=sigma_electron)
A_RGB = A
print,'electrons', A
print,' sigma', sigma_electron; returns error in model coefficients

;testing model on data

plot3 = ERRORPLOT( result_RGB[*,1], result_RGB[*,0],
result_RGB[*,2],result_RGB[*,2]*0,YTITLE='Dose [Gy]',XTITLE=
'netOD',TITLE=title,NAME='Electrons',
'b2X',OVERPLOT=1);,XRANGE=[0.0,0.4],YRANGE=[0,13]
; Overplot the fitted data:
X = INDGEN(130)*0.11
Z = MYFUNC(X,A_RGB)
Y = Z[*,0]
model3= PLOT(Y, X, OVERPLOT=1, 'b2--',NAME='Calibration curve, electrons')
folder='\xray_calibration_210317'
Xray_cal =
['xray_calibration_210317_001.bmp','xray_calibration_210317_002.bmp','xray_
calibration_210317_003.bmp','xray_calibration_210317_004.bmp','xray_calibra
tion_210317_005.bmp','xray_calibration_210317_006.bmp','xray_calibration_21
0317_007.bmp','xray_calibration_210317_008.bmp','xray_calibration_210317_00
9.bmp','xray_calibration_210317_010.bmp']
xray_doses = [0,0,1,1,2,2,5,5,10,10]
centre =
[[217,214,216,214,211,220,210,220,220,220],[220,210,226,229,235,217,222,220
,220,220]] ;[xlist,ylist]

;returns
result_RGB = calibration(folder,xray_cal,xray_doses,centre,'x-ray')

;Fitting to model myfunc
A = [5,0.,5.5]
coef_RGB = LMFIT(result_RGB[*,0], result_RGB[*,1], A,
MEASURE_ERRORS=result_RGB[*,2], FITA=FITA, FUNCTION_NAME = 'myfunc',
/DOUBLE,SIGMA=sigma_xray)
A_RGB = A
print, 'x-ray', A ; returns model coefficients
print,' sigma', sigma_xray ; returns error in model coefficients

;testing model on data
```

```
plot4 = ERRORPLOT( result_RGB[*,1], result_RGB[*,0],
result_RGB[*,2],result_RGB[*,2]*0,XTITLE='netOD',YTITLE=
'Dose(Gy)',TITLE=title,NAME='X-rays',
'k2X',XRANGE=[0,0.4],YRANGE=[0,13],overplot=1)
; Overplot the fitted data:
X = INDGEN(57)*0.25
Z = MYFUNC(X,A_RGB)
Y = Z[*,0]
model4= PLOT(Y, X, OVERPLOT=1, 'k2--',NAME='Calibration curve, x-rays')
leg = LEGEND(TARGET = [model1,model2,model3,model4], POSITION =
[0.05,12],/DATA, /AUTO_TEXT_COLOR)
end
```

```
FUNCTION calibration, folder, files, doses, centre, modality
; folder - TYPE=STRING, contains folder name containing wanted calibration
files
; files - TYPE=LIST OF STRINGS, contains a list of names of files used for
calibration
; doses - TYPE=LIST OF NUMBERS, doses given to each film, same order and
size as files
; centre - TYPE=2D, ARRAY OF INTEGERS, contains x and y coordinates of
centre of each file [[x1,x2,..],[y1,y2,..]
; modality - TYPE=STRING,
disk='C:\'
path='\Users\Rykkelid\Pictures'

cd, disk+path+folder


files = files
xcm_list=centre[*,0]
ycm_list= centre[*,1]

;seperating different colour channels into different arrays, preparing
empty arrays of right size to be filled
average_red = MAKE_ARRAY(N_ELEMENTS(files),1,/FLOAT, VALUE=0)
average_green = MAKE_ARRAY(N_ELEMENTS(files),1,/FLOAT, VALUE=0)
average_blue = MAKE_ARRAY(N_ELEMENTS(files),1,/FLOAT, VALUE=0)
average_RGB = MAKE_ARRAY(N_ELEMENTS(files),1,/FLOAT, VALUE=0)
netOD_RGB = MAKE_ARRAY(N_ELEMENTS(files),1,/FLOAT, VALUE=0)
;Geometrical centre of films, found manually



;Looping through list of exposed films, analyzing one and one and placing
the result in a list
i = 0 ; index in list of images to be analyzed
FOREACH file, files DO BEGIN

  img = read_bmp(file)

  img_red=reform(img(0, *,*)) ;chaning format of --- channel image
  img_green=reform(img(1, *,*))
  img_blue=reform(img(2, *,*))


  dim = size(img);dim is varaible containing the size of the image
  x = dim[2] ;dim[2] corresponds to the length of the image array
```

```
  ;print, total(img_RGB)

  ;watch = IMAGE(img,title=file) ; shows current image

  piksel = 0.01694382022 ;pixle size in [cm]
  radius = 1.6  ;radius used to calculate average transmission T[cm]
  r = FIX(radius/piksel)


  T_red = img_red
  T_green = img_green
  T_blue = img_blue

  ;print,total(T_RGB)/3
  x = dim[2]

  ; sentrum i bildet på runde filmer (manuelt funnet)
  xcm=xcm_list[i]
  ycm=ycm_list[i]
  OD_red = -ALOG10(T_red)
  OD_blue = -ALOG10(T_blue)
  OD_green = -ALOG10(T_green)
  OD_RGB = (OD_Red+OD_blue+OD_green)/float(3)

  ;average_red[i] = Average_optical_density(OD_red, xcm, ycm, r)
  ;average_green[i] = Average_optical_density(OD_green, xcm, ycm, r)
  ;average_blue[i] = Average_optical_density(OD_blue, xcm, ycm, r)
  average_RGB[i] = Average_optical_density(OD_RGB, xcm, ycm, 60)
  netOD_RGB[i] = average_RGB[i] ;adding the unexposed
  IF modality EQ '6 MeV electrons' THEN BEGIN
    netOD_RGB[i] = netOD_RGB[i]
  ENDIF

  IF modality EQ 'proton' THEN BEGIN
    netOD_RGB[i] = netOD_RGB[i]+ 2.098258 ; average zero level for films
used in proton calibration
  endif
  IF modality EQ 'x-ray' THEN BEGIN
    netOD_RGB[i] = netOD_RGB[i]+ 2.0951293 ; average zetro level for film
in x-ray calibration
  endif
  IF modality EQ '6 MeV electrons' THEN BEGIN
    netOD_RGB[i] = netOD_RGB[i]+2.1097457 ; average zetro level for film in
electron calibration
  endif
  IF modality EQ 'cobalt60' THEN BEGIN
    netOD_RGB[i] = netOD_RGB[i] + 2.10977 ;average zetro level for film in
cobalt60 calibration
  endif
;  titlex='Profil plot i x-retning, gjennom sentrum,'+files[i]
;  titley='Profil plot i y-retning, gjennom sentrum,'+files[i]
;  xnamex = 'x [cm]'
;  xnamey='y [cm]'
;  yname = 'Dose [Gy]'
;  style = 'r' + '-1'


  i++
ENDFOREACH

result_RGB = compute_OD(netOD_RGB,Doses,'x-ray calibration, RGB','k2X')
```

```
return, result_RGB
end
```

```
FUNCTION Average_optical_density, OD, x_cm,y_cm,r
  ;Calculates average value of a 2D array inside radius r
  total = 0
  counter = 0

  r_square = r^2

  FOR X=x_cm-r,x_cm+r , 1 DO BEGIN
    FOR Y=y_cm-r,y_cm+r , 1 DO BEGIN

      A = (X-x_cm)^2 + (Y-y_cm)^2

      IF (A LT r_square) THEN BEGIN
          total = total + OD[X,Y]
          counter++
      ENDIF
    ENDFOR
   ENDFOR

   average = (float(total)/float(counter))
   RETURN, average
END
```

```
FUNCTION myfunc, X,A

  f= A[0] + A[1]*X
  g= A[2] + X
  RETURN, [[-ALOG(f/g)], [-1/f], [-X/f],[1/g]]
End
```

```
FUNCTION compute_OD, measurements, dose, title, style

levels = dose[UNIQ(dose)]
optical_density = make_array(n_elements(levels), /FLOAT, VALUE=0)
standard_deviation = make_array(n_elements(levels), /FLOAT, VALUE=0)
i=0
FOREACH level, levels DO BEGIN
  index = WHERE(dose EQ level)
  Y = measurements[index]
  optical_density[i]=mean(Y)
  standard_deviation[i] = stddev(Y)
  i++
ENDFOREACH
RETURN, [[levels], [optical_density], [standard_deviation]]
END
```

```
disk='C:\'
path='\Users\Rykkelid\Pictures'
folder = '\All_setups_cyclotron'

cd, disk+path+folder

files=['setup1_1_F001.bmp','setup1_1_F002.bmp','setup1_1_F003.bmp','setup1_
1_R001.bmp','setup1_1_R002.bmp','setup1_1_R003.bmp','setup1_1_R004.bmp',$
  'setup1_2_F001.bmp','setup1_2_R001.bmp','setup1_2_R002.bmp'  ,$

'setup1_3_F001.bmp','setup1_3_F002.bmp','setup1_3_F003.bmp','setup1_3_F004.
bmp','setup1_3_F005.bmp','setup1_3_F006.bmp','setup1_3_F007.bmp','setup1_3_
F008.bmp','setup1_3_F009.bmp','setup1_3_F010.bmp','setup1_3_F011.bmp',$

'setup1_3_R001.bmp','setup1_3_R002.bmp','setup1_3_R003.bmp','setup1_3_R004.
bmp',$

'setup2_1_F001.bmp','setup2_1_F002.bmp','setup2_1_F003.bmp','setup2_1_F004.
bmp','setup2_1_F005.bmp','setup2_1_F006.bmp','setup2_1_F007.bmp',$

'setup2_1_R001.bmp','setup2_1_R002.bmp','setup2_1_R003.bmp','setup2_1_R004.
bmp',$

'setup2_2_F001.bmp','setup2_2_F002.bmp','setup2_2_F003.bmp','setup2_2_R001.
bmp','setup2_2_R002.bmp',$

'setup2_3_F001.bmp','setup2_3_F002.bmp','setup2_3_F003.bmp','setup2_3_F004.
bmp','setup2_3_F005.bmp','setup2_3_R001.bmp','setup2_3_R002.bmp','setup2_3_
R003.bmp','setup2_3_R004.bmp',$

'setup3_1_F001.bmp','setup3_1_F002.bmp','setup3_1_F003.bmp','setup3_1_F004.
bmp','setup3_1_F005.bmp','setup3_1_F006.bmp','setup3_1_F007.bmp','setup3_1_
F008.bmp','setup3_1_F009.bmp','setup3_1_F010.bmp','setup3_1_F011.bmp','setu
p3_1_F012.bmp',$
  'setup3_initial_F001.bmp','setup4_1_F001.bmp','setup4_initial_F001.bmp'
,'setup4_initial_F002.bmp','setup4_initial_F003.bmp']


; a,b,c for protons
A=[10.249,0.457,10.235]
; give each file a x-coordinate and y-coordinate idicating centre, and one
zero level of the OD[xcm,ycm,zero_level]
centers=HASH()

centers('setup1_1_F001.bmp')=[164,151,2.11] ;overexposed
centers('setup1_1_F002.bmp')=[170,159,2.12]&
centers('setup1_1_F003.bmp')=[154,156,2.113]
centers('setup1_1_R001.bmp')=[161,167,2.117]&
centers('setup1_1_R002.bmp')=[166,170,2.117]
centers('setup1_1_R003.bmp')=[158,166,2.117]&
centers('setup1_1_R004.bmp')=[162,157,2.117]

centers('setup1_2_F001.bmp')=[163,160,2.113]&
centers('setup1_2_R001.bmp')=[157,164,2.113]&
centers('setup1_2_R002.bmp')=[166,170,2.113]

centers('setup1_3_F001.bmp')=[160,167,2.11]&
centers('setup1_3_F002.bmp')=[157,164,2.1118]
```

```
centers('setup1_3_F003.bmp')=[165,164,2.11]&
centers('setup1_3_F004.bmp')=[160,163,2.1109]
centers('setup1_3_F005.bmp')=[160,166,2.1076]&
centers('setup1_3_F006.bmp')=[163,162,2.1095]
centers('setup1_3_F007.bmp')=[158,158,2.0994]&
centers('setup1_3_F008.bmp')=[152,153,2.0945]
centers('setup1_3_F009.bmp')=[160,161,2.1075]&
centers('setup1_3_F010.bmp')=[160,167,2.11]&
centers('setup1_3_F011.bmp')=[154,163,2.1069]
centers('setup1_3_R001.bmp')=[156,151,2.113]&
centers('setup1_3_R002.bmp')=[155,153,2.113]
centers('setup1_3_R003.bmp')=[154,159,2.113]&
centers('setup1_3_R004.bmp')=[152,160,2.113]

centers('setup2_1_F001.bmp')=[216,211,2.09552]&
centers('setup2_1_F002.bmp')=[219,207,2.09418]
centers('setup2_1_F003.bmp')=[214,208,2.08797]&
centers('setup2_1_F004.bmp')=[224,213,2.08878]
centers('setup2_1_F005.bmp')=[227,220,2.09405]&
centers('setup2_1_F006.bmp')=[223,215,2.09815]&
centers('setup2_1_F007.bmp')=[215,215,2.0839]
centers('setup2_1_R001.bmp')=[164,162,2.113]&
centers('setup2_1_R002.bmp')=[163,160,2.113]
centers('setup2_1_R003.bmp')=[169,154,2.113]&
centers('setup2_1_R004.bmp')=[164,162,2.113]

centers('setup2_2_F001.bmp')=[222,228,2.0938]&
centers('setup2_2_F002.bmp')=[220,207,2.0943]&
centers('setup2_2_F003.bmp')=[221,216,2.10625]
centers('setup2_2_R001.bmp')=[174,171,2.10515]&
centers('setup2_2_R002.bmp')=[173,169,2.10515]

centers('setup2_3_F001.bmp')=[219,214,2.0917]&
centers('setup2_3_F002.bmp')=[222,218,2.0949]
centers('setup2_3_F003.bmp')=[220,209,2.0922]&
centers('setup2_3_F004.bmp')=[219,210,2.0962]&
centers('setup2_3_F005.bmp')=[222,212,2.09542]
centers('setup2_3_R001.bmp')=[229,237,2.113]&
centers('setup2_3_R002.bmp')=[222,224,2.113]
centers('setup2_3_R003.bmp')=[223,219,2.113]&
centers('setup2_3_R004.bmp')=[232,241,2.113]

centers('setup3_1_F001.bmp')=[230,206,2.098258]&
centers('setup3_1_F002.bmp')=[223,204,2.098258]
centers('setup3_1_F003.bmp')=[220,212,2.098258]&
centers('setup3_1_F004.bmp')=[232,220,2.098258]
centers('setup3_1_F005.bmp')=[219,205,2.098258]&
centers('setup3_1_F006.bmp')=[227,203,2.098258]
centers('setup3_1_F007.bmp')=[225,207,2.098258]&
centers('setup3_1_F008.bmp')=[214,205,2.098258]
centers('setup3_1_F009.bmp')=[220,209,2.098258]&
centers('setup3_1_F010.bmp')=[218,216,2.098258]
centers('setup3_1_F011.bmp')=[214,200,2.098258]&
centers('setup3_1_F012.bmp')=[228,197,2.098258]

centers('setup3_initial_F001.bmp')=[228,213,2.098258333]
centers('setup4_1_F001.bmp')=[227,214,2.11]
centers('setup4_initial_F001.bmp')=[232,227,2.10275]
centers('setup4_initial_F002.bmp')=[228,209,2.1025]
centers('setup4_initial_F003.bmp')=[225,227,2.102625]
```

```
centers("proton_081117001.bmp")=[223,213,2.10059]
centers("proton_081117002.bmp")=[244,215,2.10059]
centers("proton_081117003.bmp")=[229,219,2.10059]
centers("proton_081117004.bmp")=[229,217,2.10059]
centers("proton_081117005.bmp")=[235,218,2.10059]
centers("proton_081117006.bmp")=[242,210,2.10059]
centers("proton_081117007.bmp")=[229,220,2.10059]
centers("proton_081117008.bmp")=[235,213,2.10059]
centers("proton_081117009.bmp")=[203,208,2.10059]
centers("proton_081117010.bmp")=[208,210,2.10059]
centers("proton_081117011.bmp")=[228,212,2.10059]
centers("proton_081117012.bmp")=[219,212,2.10059]
centers("proton_081117013.bmp")=[224,210,2.10059]
centers("proton_081117014.bmp")=[207,211,2.10059]
centers("proton_081117015.bmp")=[192,203,2.10059]



h = ORDEREDHASH()
h('files')='DOSE_r(Gy)    sigmaDOSE_r(Gy) '
i=0
foreach file, files DO BEGIN

  img = file
  dim = size(img)
  img = read_bmp(img)

  img_red=reform(img(0, *,*))
  img_green=reform(img(1, *,*))
  img_blue=reform(img(2, *,*))

  x = dim[2]
  ;watch = IMAGE(img,title=file)

  xcm=centers(file,0)
  ycm=centers(file,1)
  piksel = 0.01694382022 ;pixle size in [cm]
  r = 150 ;radius in pixles


  T_red = img_red
  T_green = img_green
  T_blue = img_blue

  x = dim[2]


  OD_red = -ALOG10(T_red)
  OD_blue = -ALOG10(T_blue)
  OD_green = -ALOG10(T_green)
  OD_RGB = (OD_Red+OD_blue+OD_green)/float(3)

  OD_RGB_corrected = OD_RGB + centers(file,2)

  Dose = give_dose_from_OD(OD_RGB_corrected,A)

  p = plot(OD_RGB_corrected, title=file)
  length = size(img_blue[*,1])
  length = length[1] ;number of elements in x and y direction
```

```
  x_distance = FINDGEN(length)
  x_distance = (x_distance-xcm)*piksel

  y_distance = FINDGEN(length)
  y_distance=(y_distance-ycm)*piksel


  ;px =plot(x_distance[xcm-130:xcm+130],Dose[xcm-130:xcm+130,ycm],
title='x'+file,xrange=[-3,3],yrange=[0,10]) ; plotting dose against
distance from center
  ;py =plot(y_distance[ycm-130:ycm+130],Dose[xcm,ycm-130:ycm+130],title='y
'+file,xrange=[-3,3],yrange=[0,10]) ; plotting dose against distance from
center


  Dose_r= Average_of_array_with_stddev(Dose,xcm,ycm,r)


  h(file) = [mean(Dose_r), stddev(Dose_r)]

  i+=1
endforeach
print, h


end
-------------------------------------------------------------------------------------------------------------------

FUNCTION give_dose_from_OD, OD, A

  f = exp(OD)*A[0] - A[2]
  g = 1-exp(OD)*A[1]
  D= f/g
  return, D
 end

FUNCTION Average_of_array_with_stddev, array, x_cm,y_cm,r
  ;Calculates average value of a 2D array inside radius r
  total = 0
  counter = 0

  r_square = float(r^2)
  result = LIST()
  FOR X=x_cm-r,x_cm+r , 1 DO BEGIN
    FOR Y=y_cm-r,y_cm+r , 1 DO BEGIN

      A = (X-x_cm)^2 + (Y-y_cm)^2

      IF (A LT r_square) THEN BEGIN
        total = total + array[X,Y]
        result.add,array[X,Y]
        counter+=1
      ENDIF
    ENDFOR
  ENDFOR

  average = (float(total)/float(counter))

  result = result.toarray()
  RETURN, result
END
```